1-1-2012

Supersonic Windtunnel Noise Attenuation

William Wai Lim Wong
Ryerson University

SUPERSONIC WINDTUNNEL NOISE ATTENUATION

by

William Wai Lim Wong

BASc, University of Waterloo, 2009

A thesis

presented to Ryerson University

in partial fulfillment of the

requirements for the degree of

Master of Applied Science

in the Program of

Aerospace Engineering

Toronto, Ontario, Canada, 2012

I hereby declare that I am the sole author of this thesis. This is a true copy of the thesis including any required final revisions, as accepted by my examiners.

I authorize Ryerson University to lend this thesis to other institutions or individuals for the purpose of scholarly research

I further authorize Ryerson University to reproduce this thesis by photocopying or by other means, in total or in part, at the request of other institutions or individuals for the purpose of scholarly research.

I understand that my thesis may be made electronically available to the public.

Abstract

Supersonic Wind Tunnel Noise Attenuation

Master of Applied Science, 2012

William Wai Lim Wong

Aerospace Engineering

Ryerson University

The aerodynamic generated noise in the supersonic wind tunnel during operation at Ryerson University has exceeded the threshold of hearing damage. An acoustic silencer was to be designed and added to the wind tunnel to reduce the noise level.

The main sources of noise generated from the wind tunnel with the silencer were identified to be located at the convergent divergent nozzle and the turbulent region downstream of the shock wave at the diffuser with the maximum acoustic power level of the entire wind tunnel at 161.09 dB. The designed silencer provided an overall sound pressure level reduction of 21.41 db which was considered as acceptable.

Refinement to the mesh size and changes to the geometry of the mixing chamber was suggested for a more accurate result in noise output as well as flow conditions would match up to the physical flow. Additional acoustic treatment should be applied to the wind tunnel to further reduce sound pressure level since the noise level still exceeded the threshold of hearing loss.

Acknowledgement

I would like to thank Dr. Paul Walsh for his insight and suggestions during the development of this thesis. I would also thank Dr. Jason Lassaline and Dr. Jeffrey Yokota on the examination committee for their recommendations on the thesis. I would also acknowledge the computational resources provided by SHARCNET.

Table of Contents

List of Tables

List of Figures

List of Appendices

Nomenclature

Symbols

a	porous material fibre diameter
A	cross section area of duct
α	absorption coefficient
α_1	viscous resistance coefficient
B	dimensionless permeability
$c\infty$	far field speed of sound
c_o	speed of sound of air
d	hydraulic diameter of diffuser
d_i	thickness of ith porous layer
δ	Rschevkin end correction factor for resonator neck
δ_{ij}	Kronecker symbol
ε	absolute roughness
ε_o	perforated plate open area percentage
f	frequency (Hz)
fr	friction factor
g	gravity
h_f	head loss
k	wavenumber
k_{xi}	wavenumber of ith layer
L	duct length
μ	dynamic viscosity
ν	kinematic viscosity
ω	angular frequency
P	perimeter of duct
P_b	Back Pressure
P_o	Reservoir total pressure
Ψ	incidence angle
R	pressure reflection coefficient
Re	Reynolds number
r_{helm}	surface resistance of resonant absorber plate
ρ	density
ρ_o	density of air
t	perforated plate thickness
T	temperature
σ	flow resistivity of porous material
τ_{ij}	Lighthill stress tensor
u_i	velocity in i^{th} direction
V	flow velocity
X	dimensionless quantity of Delany and Bazley
x_i	length in i^{th} direction
z_{helm}	impedance of resonant absorber plate
z_i	characteristic impedance of ith layer
z_{si}	impedance of ith layer

Abbreviations

APL	Acoustic Power Level
CAA	Computational Aero Acoustics
CFD	Computational Fluid Dynamics
DES	Detached Eddy Simulation
FW&H	Ffowcs- Williams & Hawking
SPL	Sound Pressure Level

Glossary

Absorption coefficient	Ratio of absorbed to incident energy on striking any surface (1)
Acoustic impedance	Sound absorption in a medium (2)
Acoustic power level	A measure of acoustic power of the source and is location independent
Back pressure	Pressure of the region downstream of the tunnel exit (3)
Insertion loss	The difference in sound power level or intensity measured at the same location before and after acoustic treatment
Overall sound pressure level	The sum of sound pressure level across a range of frequencies
Pressure reflection coefficient	The fraction of acoustic energy reflected off a boundary (4)
Sound pressure level	A measure of acoustic pressure that is location dependent.
Surface impedance	The ratio of sound pressure amplitude to acoustic wave particle velocity amplitude that impinges on the surface (5)

1 Introduction

Supersonic wind tunnels have been used for decades in research facilities and are still used due to limitations in the use of computational fluid dynamics (CFD). The first supersonic wind tunnel was located in Peenemünde Army Research Center in Germany in 1936 (6). Most of the supersonic wind tunnels used were for military applications such as the development of missiles, fighter jets, and space vehicles.

There are multiple configurations of supersonic wind tunnels. The supersonic wind tunnel in Ryerson University is an open circuit blowdown type. This type of supersonic wind tunnel is used for transonic and supersonic flow tests. Gas is stored in a high pressure storage tank. When in operation, the gas is released into a settling chamber then through an expansion nozzle to accelerate the flow to supersonic in the test section and past a diffuser to release into the atmosphere. The test section Mach number is dependent on the area ratio of the nozzle and the temperature and pressure of the gas. The advantages of a blowdown wind tunnel are lower capital cost and ease of start up. The disadvantages are short run times and noisy operation (7).

Noise is major problem for the operation of supersonic wind tunnel. Excessive noise can cause hearing loss. Noise is also considered a nuisance to the surrounding community and is subject to city regulations. The Ryerson University campus is located in the downtown of a major city and is susceptible to noise complaints which could place limitations on the use of the wind tunnel. At the moment, without any acoustic treatment applied to the wind tunnel, the noise is perceived to be intolerable. As a result, a simple and effective acoustic treatment is needed to minimize the impact to the occupants of the building as well as the surrounding community.

There have been research and publications about noise reduction for supersonic wind tunnel test section. Much of the research focused on the expansion nozzle wall design and treatment. The focus of this research was to design an acoustic treatment aft of the diffuser. Commercial CFD package was used to determine the optimal configuration of this treatment and estimate the resulting sound pressure level of the wind tunnel.

2 Background

2.1 Source of Noise

The main source of noise in supersonic wind tunnels is generated from the turbulent boundary layer along the jet nozzle wall, which is difficult to control (8). Aerodynamic noise is associated with high speed and or unsteady gas flow interaction with solid object. There are three main sources of aerodynamic noise. A monopole is present when heat or mass is added to a fluid flow at an unsteady rate. The generated pulse spreads in a spherical pattern. A dipole is present when a flow interacts with a solid body. This creates two poles close to one another, less than a wavelength apart and in different phase. A quadrupole occurs due to the viscous stress in the flow that exists in pairs to cancel out the forces. Quadrupoles are the main source of noise in high speed, turbulent, subsonic flow and have a great strength in regions with high mean-velocity and turbulent gradients.

The flow in the wind tunnel becomes supersonic when the ratio of the stagnation pressure to the outlet pressure is 1.89. The noise source is from turbulent mixing in the shear layer. High frequency noise radiates near the nozzle wall where eddies are small and lower frequency noise is radiated further downstream where the size of the eddy increases.

Morkovin identified that noise is generated from the quadrupole and dipole radiation from the turbulent boundary layer and the fluctuation in position of the Mach waves generated from surface finishes (9). Factors identified that would affect the boundary layer transition near the nozzle wall include wall roughness, wall temperature, upstream suction, and settling chamber disturbances. The generated noise travels along the Mach line in supersonic flow which propagats towards the diffuser and exhausts into the atmosphere (10). Additional noise can be originated from the compressor if no noise control is present before the compressed gas is fed into the expansion jet nozzle.

2.2 Solutions to Noise Reduction

The only solution to eliminate the noise source at the nozzle wall is to maintain a laminar boundary layer along the whole wind tunnel wall. However, this has yet to be achieved. Many solutions to control the noise in high speed flow have been proposed in journal papers and some are used in practise. They are divided into two categories: active and passive. Active control generally involves injection of external energy to the flow while passive control generally controls the flow via alterations in the geometry of the duct.

2.2.1 Benchmark

The University of Toronto has an undergraduate supersonic laboratory that is also in an open circuit and operates at Mach 1.6. In the wind tunnel layout, the diffuser is placed in an acoustic enclosure separated by a wall in another room as seen in Figure 1. There is a 20 hp 3 phase motor driving a vacuum pump that increases the pressure aft of the diffuser to minimize back pressure due to pressure head. The gas goes through a muffler with a series of baffles and then exhausted to outdoors.

The supersonic wind tunnel at University of Texas at Arlington has the flow exhaust into a large sphere from the diffuser as seen in Figure 2. A large tube is connected with the sphere which leads the flow into a large silencer.

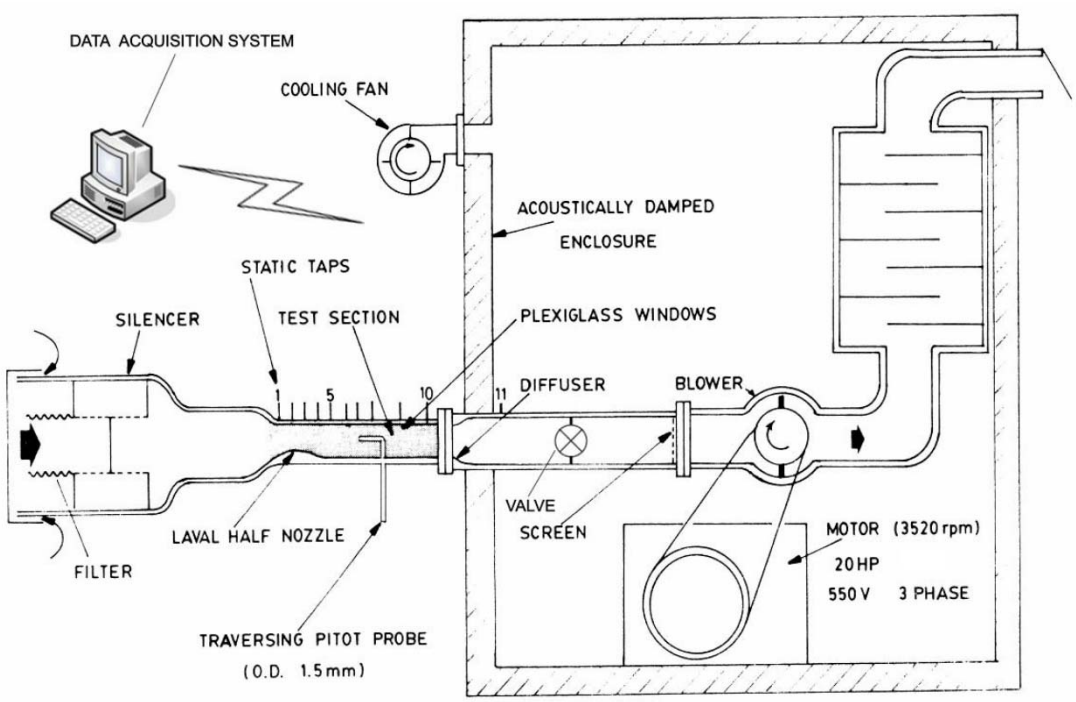

Figure 1: University of Toronto supersonic facility (11).

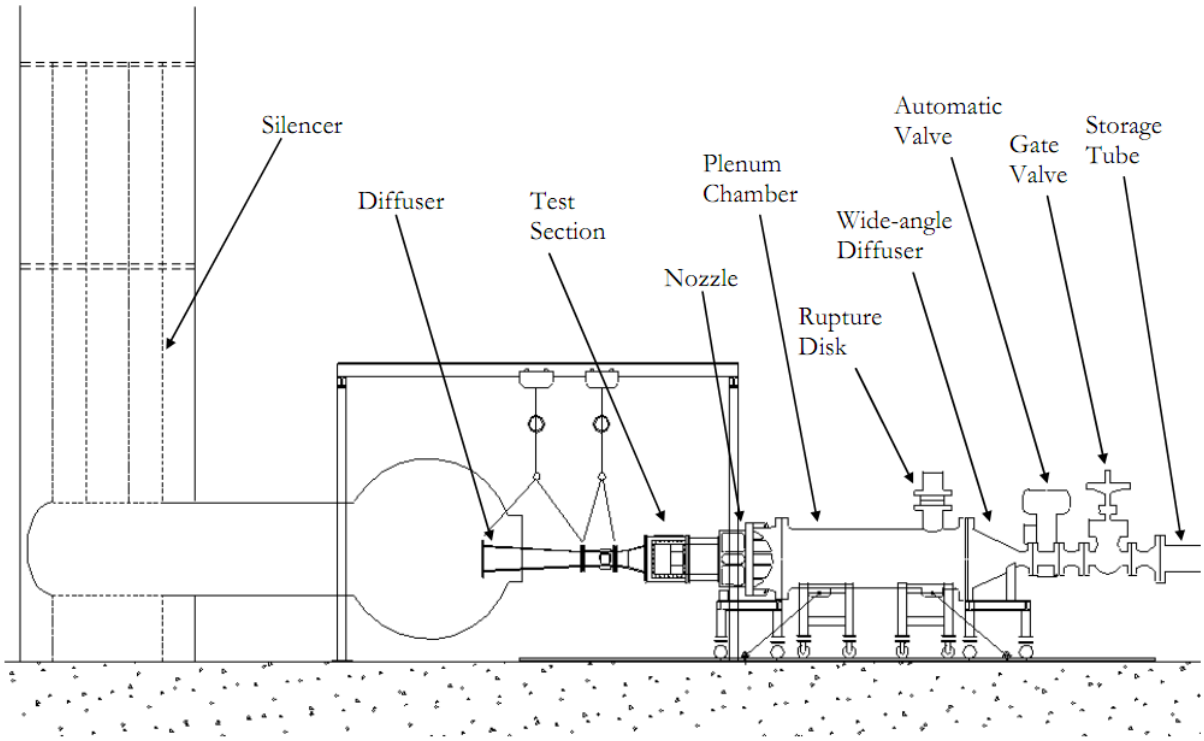

Figure 2: Supersonic wind tunnel layout at University of Texas at Arlington (12).

The NASA Glenn 8 by 6 foot supersonic wind tunnel in Cleveland had a muffler installed after noise complaints from the surrounding community. The Glenn wind tunnel consists of 5 Helmholtz resonators at the diffuser to absorb noise in the 5 to 11Hz band as seen in Figure 3. In the muffler region, there are 6 parallel ducts with each having a 62 feet resonator used to attenuate the 12 to 20 Hz noise band. The resonator is then followed by a 90 feet section of 6 inch thick fibreglass panel in a 2 feet cavity that was designed to attenuate the 20 to 800 Hz band(13).

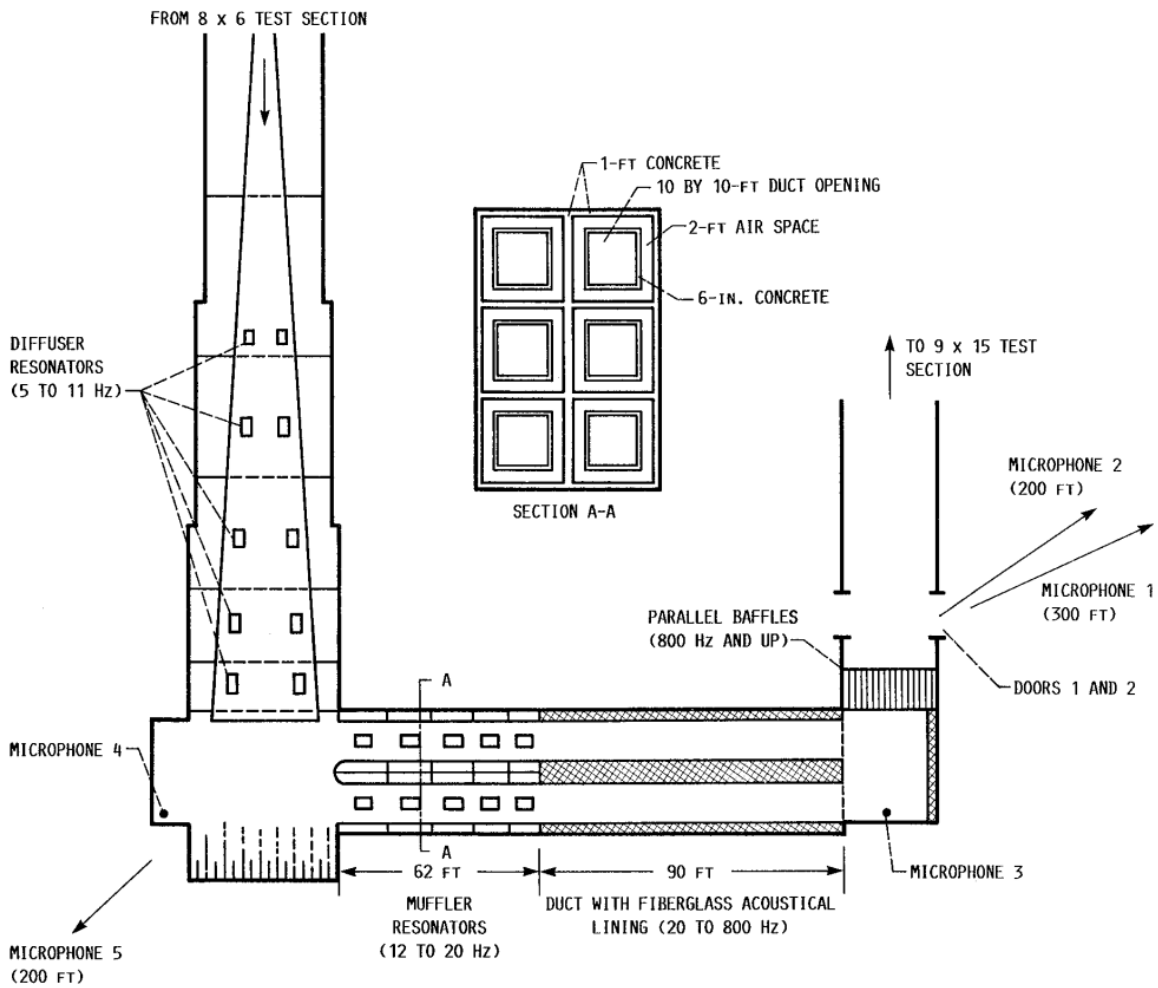

Figure 3: Acoustic treatment of the supersonic wind tunnel at NASA Glenn Research Center (13).

2.2.2 Nozzle Wall Treatment

One of the methods to reduce noise is to reduce or eliminate the source. Multiple papers had been published on the development of quiet supersonic and hypersonic wind tunnel at NASA for reducing test section noise. The focus of these papers had been on the expansion nozzle wall design in an attempt to delay the transition of the boundary layer from laminar to turbulent.

2.2.2.1 Suction Port

One technique is to create a suction port in the convergent section of the nozzle before the thrat. The suction port would remove the turbulent boundary layer from the settling chamber near the wall so that a new laminar boundary layer would be formed further downstream at the nozzle wall right after the throat. Research found disturbances from the settling chamber upstream would travel through the nozzle and enter into the test section. The disturbances would increase the Reynold's number downstream and a turbulent boundary layer along the nozzle wall would develop sooner which would

generate more noise (8). In theory, the suction port had great potential, however, in physical application, it was hindered by nonuniform suction as well as surface roughness. As a result, Langley had abandoned this approach in the 1970s (9).

2.2.2.2 Maintain Surface Finish of Nozzle

Anders et al. also discussed about the surface finish of the convergent divergent nozzle. Since the free-stream unit Reynold's number decreases as the Mach number increases, the stagnation pressure must increase in order to increase the unit Reynold's number in the test section. However, since the thickness of the boundary layer is inversely proportional to the square root of the unit Reynold's number, the boundary layer at the throat wall would be thin (14). As a result, the boundary layer would be sensitive to the surface finish. The surface finish should have a tolerance in the range of 0.001 – 0.002 inches (14). A polished nozzle wall has an increase of 30% in the transitional Reynold's number, when turbulent eddies begin to form. However, cleaning and polishing of the nozzle wall would be required in order to maintain the performance. An increase in temperature of the nozzle wall also increass the transition Reynold's number by 20% compared to a nozzle wall at room temperature. The boundary layer thickness would increase while the flow's sensitivity to the wall roughness would decrease (8).

2.2.3 Silencer

Other approach to reduce noise impact by the supersonic wind tunnel is to apply a silencer to the exhaust of the wind tunnel. The most common types of silencer are dissipative silencer and resonators. Dissipative silencers use sound absorptive material that converts sound energy into heat. The resonator reflects sound waves back to the source to create a destructive interference like a Helmholtz resonator. Resonators are designed to supress noise at a particular frequency so that it is only effective for narrow frequency band. Dissipative silencer on the other hand can attenuate noise in a broader frequency range but it is more effective in the mid to high frequency ranges. As a result, most silencers and like the one employed at the NASA Glenn research facility have a combination of the two silencer types to reduce noise across the whole hearing frequency range.

2.2.4 Curved Baffle

Curved baffles in the duct as seen in Figure 4 would be one of the more effective techniques to decrease sound pressure level by blocking the line of sight (15). An insertion loss of 5 dB in the low frequency and 10 dB in the high frequency band could be achieved with a curved baffle as seen in Figure 5.

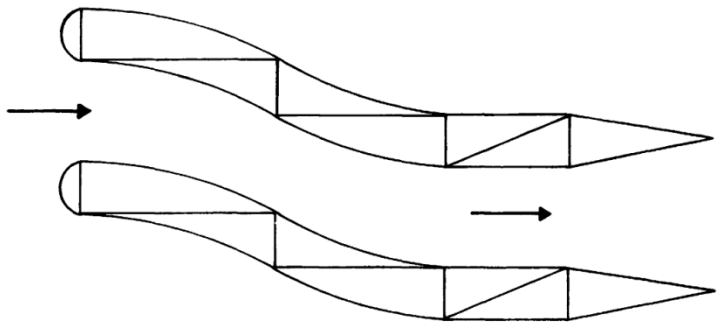

Figure 4: Curved baffle configuration (15).

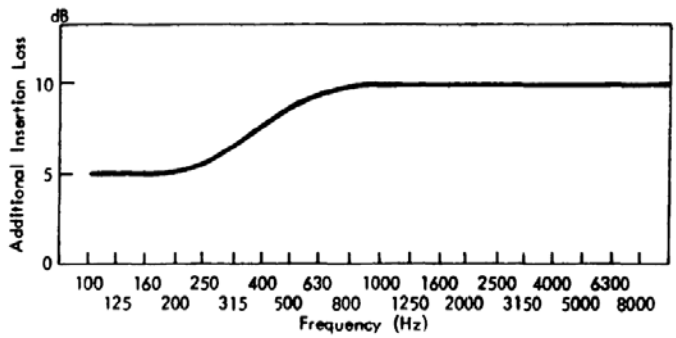

Figure 5: Insertion loss due to curved baffle (15).

2.2.5 Plasma Actuators

The use of electric discharge plasma has been studied but some mechanisms may not be practical for high speed flows. Samimy et al. studied the thermal effects of high-temperature, high-current, near-wall arc discharge (16). They found a sudden temperature change created a spike in local pressure in which generated a shock wave that altered the supersonic flow. The application of plasma discharge in the study showed a slight noise reduction in the range of 0.6dB to 1 dB measured 30°-90° from the flow axis over a range of Strouhal numbers (16).

2.2.6 Tangential Jet

A tangential jet injected into a supersonic flow to alter the shear layer structure has been experimented. Luff et al studied the noise generation of flow with tangential flow injection through eight 4mm ports upstream of the nozzle exit and eight 1.5mm diameter blowing jets at the nozzle exit. For the injectors placed upstream of the nozzle, a 44% mass flow ratio resulted in the lowest sound pressure level measured at angles between 60°-90° from the flow axis with the greatest noise reduction of 3dB at 90°. Between 15°-60° from the flow axis, a mass flow ratio of 65% from the injectors provided the greatest sound pressure level reduction. For the tangential jets at the nozzle exit, a mass flow ratio of greater than 1.1% resulted in an increase of sound pressure level starting from 50° of the jet flow axis up to 90°. A 11% mass flow ratio resulted in an average sound pressure level reduction of 2 dB. However, the

drawback of this method would decrease the flow speed of the jet due to the acceleration of the flow in the tangential direction agitated by the injection of tangential jet (17).

2.2.7 Vacuum Bubbles

There was a research on the potential use of vacuum bubbles for noise and vibration attenuation. The concept was developed by Dr. Bschorr (18). The vacuum bubbles were made of a thin metallic shell with a cavity that was in vacuum as seen in Figure 6. The vacuum bubbles were designed as an alternative to the Helmholtz resonator and one of its advantages was taking up less space than a resonator of equivalent performance. The drawback of vacuum bubble was it would be expensive to acquire and the bubbles would require precision during manufacturing due to sensitivity in performance from material to static pressure. The function of the vacuum bubble was to act as a spring where the shell must be statically stiff and yet dynamically soft. The shell profile of the bubble would be in the form of an arc. When exposed to pressure load, the shell would deform and push in but strong enough from fracture (18) as seen in Figure 6.

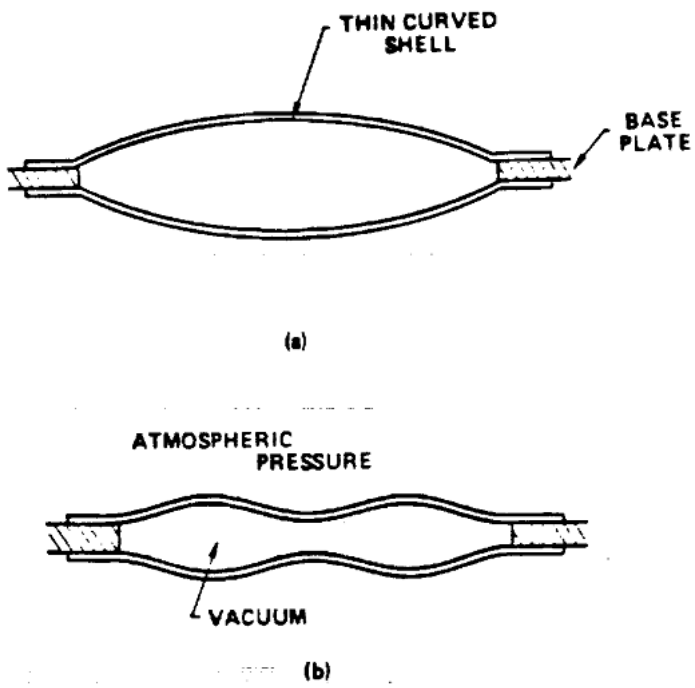

Figure 6: Diagram of vacuum bubble (a) at rest and (b) under pressure (18).

2.2.8 Perforated Liners

Perforated liners with an array of opening equally spaced apart have been applied for noise reduction in many applications such as automotive muffler and turbofan engine. The moving air in the duct and the still air in the resonator generate a shear layer (19). Studies have found that the acoustic resistance,

where the acoustic energy is transformed into other form of energy, increases linearly with the main flow speed. However, for low speed flow from 0 – 24 m/s, the shear layer would grow exponentially due to Kelvin-Helmholtz instabilities and oscillate. This in effect creates a source of noise increasing the sound pressure level in the duct. Studies have concluded perforated liners suppress noise by two mechanisms depending on the acoustic intensity. Viscous dissipation as a result of wall friction due to the presence of the holes is responsible for the suppression of lower sound pressure level up to 140dB (20). The vortex shed from the upstream circumference of the holes is the main mechanism for suppression of high sound pressure level. The acoustic energy is transferred into the kinetic energy of the vortices.

2.2.9 Oblique Perforation

The acoustic performance of several oblique perforate pattern at different oblique angles, porosity, and hole diameter were studied by Khan et al. for applications to high thrust turbojet engine (21). The experiments revealed a forward facing angle oblique perforated pattern had better acoustic performance compared to normal angle and backward facing angle. The forward facing angle pattern showed via high speed video camera that the shock structures from the outlet of the base tube without perforated pattern had been eliminated. This reduced the broadband noise from the jet and eliminated jet screech. However at low pressure ratio between two and three when measured at 90° to the flow axis, the forward facing angle pattern displayed a discrete tone where the overall sound pressure level was greater than the other perforated patterns. This was resolved by trimming the inner sharp edge of each hole as seen in Figure 7 but would result in decrease in acoustic performance for pressure ratio of 4 and higher.

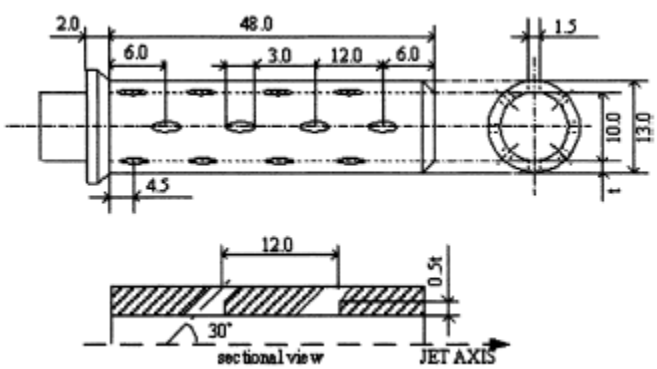

Figure 7: Forward facing perforate pattern with inner edge trimmed (21).

2.2.10 Tabs

Broadband associated noise and jet screech are caused by unstable waves interacting with shock-cell structure. Jet screech occurs in under expanded supersonic condition and result in a spike in sound pressure level for a discrete tone over a certain range of pressure ratio. As the sonic flow is exhausted, it expands and then contracts back to its original size over a specific distance depending on the pressure ratio. During the contraction, conical shock waves are formed growing upstream towards the exit nozzle. This phenomenon is repeated several times forming a cellular pattern, as seen in Figure 8, until the repetition is halted due to turbulent mixing with the ambient air (22). Jet screech has the potential to weaken an object structurally (23).

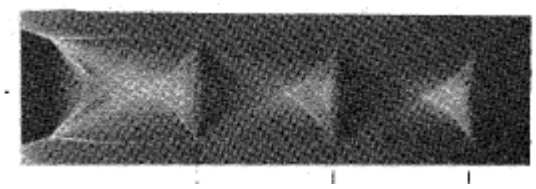

Figure 8: Shock structure downstream of nozzle without tabs (24).

Experiments have found the placement of small intrusion of rectangular tabs at the end of the nozzle exits suppressed the screech and hence reduced the jet noise due to the alteration in the shock wave structure downstream of the exit as seen in Figure 9.

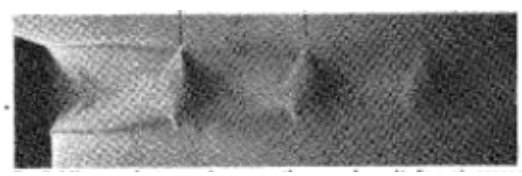

Figure 9: Shock structure downstream of nozzle with rectangular tabs (24).

However, the centreline velocity decreased as a result of the attachment of tabs to the nozzle (25). Later studies revealed triangular or delta shaped tabs tilted downstream provided better performance than their rectangular shaped counterparts.

2.3 Computational Aeroacoustics

The use of computational simulation to calculate acoustic performance is a relatively new development due to computational hardware limits in the past. The two main source of aerodynamic noise are impulsive and turbulence. Impulsive noise occurs due to a moving body in a fluid flow or unsteady aerodynamic loads acting on a stationary surface. The unsteady aerodynamic loads create pressure fluctuations that radiate sound. Impulsive noise can be easily predicted with numerical simulation. The

other noise source is from turbulence which occurs in many scenarios. Noise from turbulence has a broad band spectrum and turbulent energy converts most efficiently into acoustic energy at sharp edges. Like turbulent aerodynamic simulations in CFD, noise from turbulence is difficult to simulate accurately. The most common techniques include direct numerical simulation (DNS), Reynolds-averaged Navier-Stokes (RANS), or large-eddy simulation (LES). Since CFD modelling of turbulence is not perfect, accurate modelling would require specific setup for each individual case. There is a large disparity in the energy, length, and time scales between aeroacoustics and aerodynamics. The acoustical energy is 4 to 9 magnitudes smaller than mechanical energy. As a result, the damping techniques in CFD to supress any numerical noise would cancel out the acoustic energy in the simulation. Aeroacoustics is a time dependent problem. For flows with a high Reynolds number, the turbulent eddy will be smaller and as a result, a fine grid will be required. A large simulation domain is required since sound travels over a distance. As a result, the simulation would require greater computer resource that is available to small number of organizations.

Fluent in Ansys 13.0 was the commercial CFD package used for this research. There are two acoustics model available within Fluent: Segregated Source-propagation Method, which is the Ffowcs-Williams & Hawking (FW&H) Model, and Stochastic Noise Generation and Radiation, which is the Broadband Noise Model. The physics behind the acoustics code used in Fluent is based on Lighthill's acoustic analogy. Lighthill's analogy solves the acoustic problem in two parts. The first part is the noise generation from the fluid flow. The second part is the noise propagation in a medium at rest due to external fluctuations (26).

Lighthill's equation of aerodynamic noise is based on Navier Stokes and continuity equations without the gravitational source term (26).

$$\frac{\partial \rho}{\partial t} + \nabla \cdot (\rho u) = 0 \tag{2.1}$$

$$\frac{\partial \rho u}{\partial t} + \nabla \cdot (\rho u u) + \nabla p = \nabla \cdot \tau \tag{2.2}$$

$$c_\infty^2 \nabla^2 \rho = c_\infty^2 \nabla^2 \rho \tag{2.3}$$

$$\rho' = \rho - \rho_\infty \tag{2.4}$$

$$p' = p - p_\infty \tag{2.5}$$

Subtracting the divergence of equation 2.2 from the time derivative of equation 2.1 and add the identity of equation 2.3 and the relations of equations 2.4 and 2.5 would yield (26):

$$\frac{\partial^2 \rho'}{\partial t^2} - c_\infty^2 \nabla^2 \rho' = \frac{\partial^2 T_{ij}}{\partial x_i \partial x_j} \tag{2.6}$$

$$T_{ij} = \rho u_i u_j + (p' - c_\infty^2 \rho')\delta_{ij} - \tau_{ij} \tag{2.7}$$

Lighthill has transformed the governing equation of the fluid flow into a wave equation format.

A third method exists in Fluent to simulate the generation and propagation of noise using the CAA method, essentially the same concept as DNS. As mentioned above, this would require a fine spatial grid and small time step size for which the hardware resources are unavailable and thus cannot be done.

The FW&H model is used to predict noise transmitted into the far field using an integral method. The aerodynamics of the flow is solved using one of the viscous models in Fluent and the flow field variables are then used to predict the noise generated from the flow. The sound pressure history at a receiver location would be computed using surface and volume integrals. The Broadband Noise Source Model is used for turbulent flows where there is no distinct tone across the entire frequency band. This model uses turbulence quantities from turbulence model, semi-empirical correlations, and Lighthill's analogy for analysis of the noise source. This model is mainly used to determine the prominent noise generating region and also compare different design in noise generation. This model can be used in steady state and thus is less hardware intensive of the two models available. However, unlike FW&H, this model cannot calculate noise propagation. The FW&H model, according to the Fluent user guide, states it should only be used for propagation of sound to free space and should not be used in duct or enclosed space (27). It will not model sound reflection off solid boundary correctly and the source to the receiver must be in a straight line. This model is also only available in transient simulations.

Since the propagation of sound is important in the design, both methods would be used during the design process. Even though the Fluent user guide stated the FW&H model is not applicable to internal flows, a validation study was conducted to determine whether FW&H model should be used.

3 Validation and Mesh Sensitivity Analysis

3.1 Mesh Sensitivity

A mesh analysis was performed to determine the appropriate cell size for the simulation of the final design based on the concept of Richardson extrapolation. The idea is that using a systematically refined mesh, the convergence rate of the mesh refinement discretization could be used to estimate the exact solution to the model (28). The model used for the mesh analysis included the supersonic tunnel with a silencer attached to the diffuser. The silencer in the model consisted of a 16 gauge perforated plate with 0.5 inch hole diameter and 48% area opening. Inside the silencer was a porous sound absorbent material of glass wool. Three simulations were required for Richardson extrapolation beginning with a coarse mesh. Each cell volume would be 1/8th of the previous mesh size for the remaining two simulations. The initial mesh size setting used was: minimum size 0.005m, maximum size 0.02m, and maximum face size of 0.04m. The total number of nodes with an adapted boundary was 142,843 nodes. The next case increased to 977,087 nodes and then 3,276,930. The physical model and boundary conditions in each case were the same. The area-weighted average absolute pressure, Mach number, and acoustic power level were measured at two locations downstream, at x=2.7m named plane-A, as seen in Figure 10, and at the outlet. The results are found in Table A-1 of Appendix A. The maximum acoustic power level (APL) was also measured for each case since that would be dominant measure of noise heard in the surrounding environment. The results are found in Table A-2 of Appendix A.

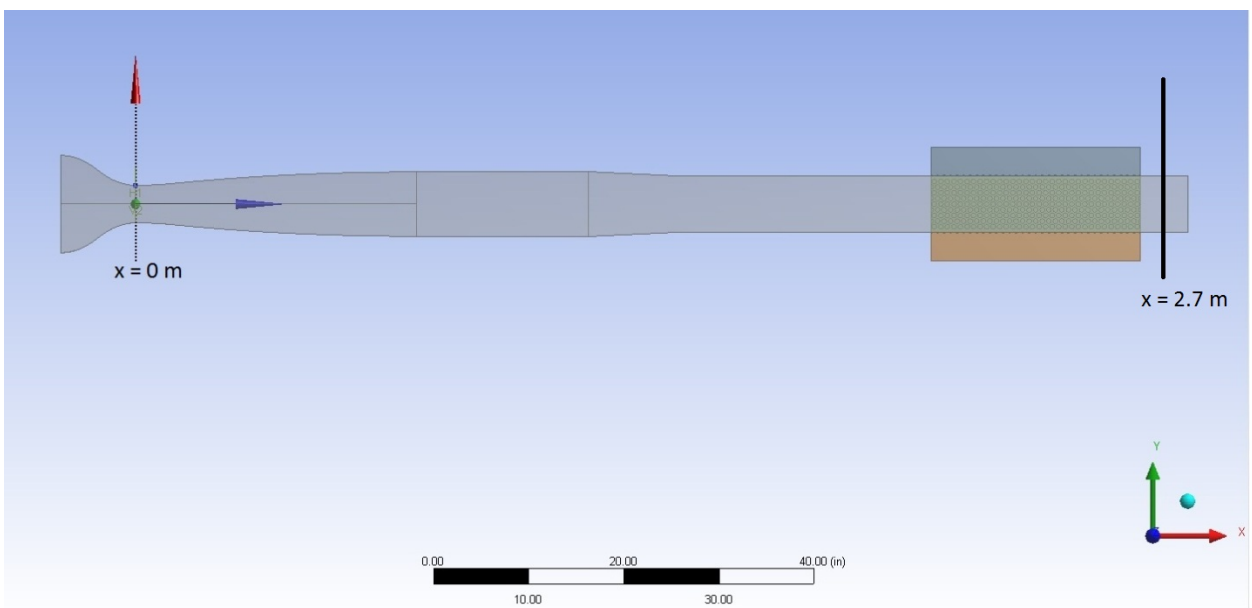

Figure 10: Location of plane-A along wind tunnel.

APL is a measure of acoustic power of the source and is location independent. When APL is expressed in dB, it is a ratio to a reference acoustic power of 10^{-12} watts. SPL on the other hand is location dependent and is a measure of acoustic pressure. When SPL is expressed in dB, it is a ratio to a reference acoustic pressure of $2x10^{-5}$ Pa.

Using a series of data with a systematically reduced mesh size and applying Richardson extrapolation, the APL of the wind tunnel configuration could be estimated to 3rd order accurate. The order of accuracy is directly related to the number of data points available such that results with a mesh volume 1/4096th of the initial size would be required for a 4th order accurate estimate. The simulation was conducted with Ansys Fluent 13.0 running on a Dell T5500 computer in the Ryerson University Kerr Hall West 71B computer lab. The 3rd order accurate estimation of area-weighted average APL at plane-A was calculated to be 118.17 dB and the maximum APL estimated was calculated to be 153.6269 dB. The calculations could be seen in Appendix B. The area-weighted average APL at plane-A with respect to the number of nodes was plotted and shown in Figure 11 and the maximum acoustic power level with respect to the number of nodes shown in Figure 12. Data from plane-A was chosen over data from the outlet for the extrapolation because the data from plane-A would not be affected by the boundary conditions.

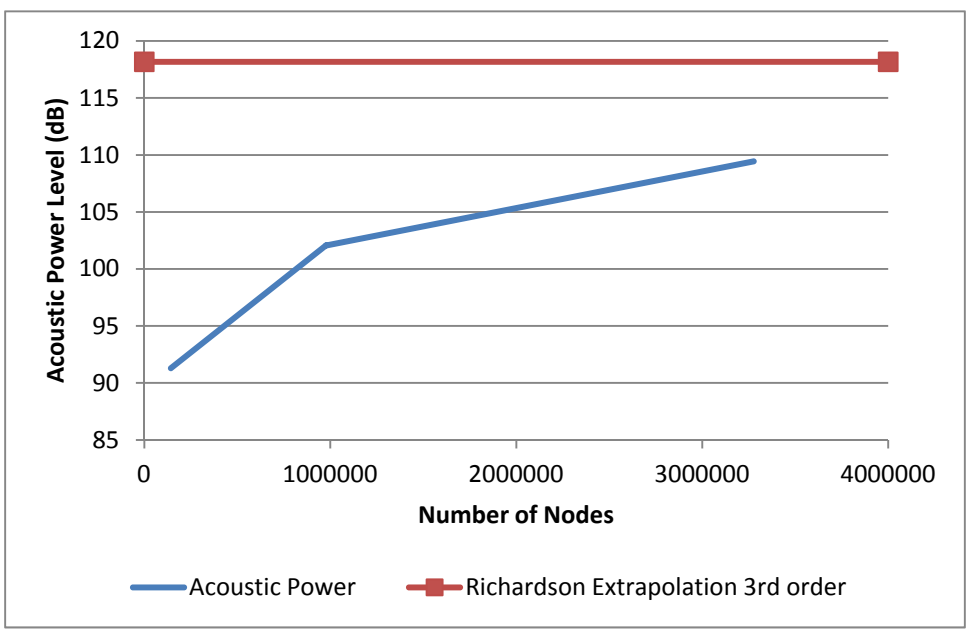

Figure 11: Acoustic power level trend with increasing node at plane-A.

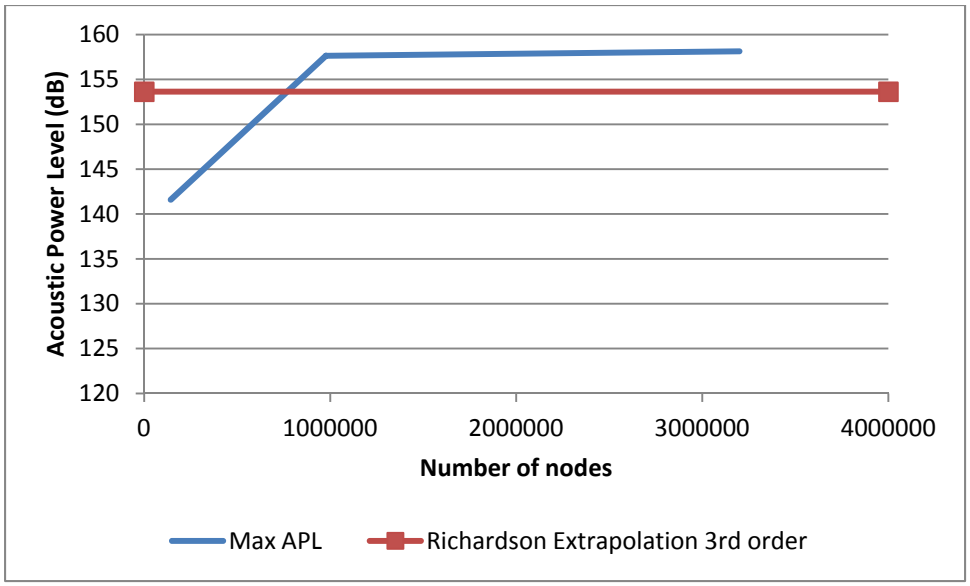

Figure 12: Maximum acoustic power level with increasing nodes.

The APL from CFD and 3rd order estimation at plane-A had a difference of 8.7219 dB or 7.38%. Looking at the maximum APL, the analysis has reached an asymptote of approximately 159 dB but the 3rd order estimate was lower at 153.35 dB. This was the result of one of the limitations of Richardson extrapolation where a significant difference should exist for the variable of interest in between mesh refinement. A further refinement was not pursued due to the number of mesh elements involved and the lack of computing resources. The result from the last simulation was close to the estimated exact solution of Richardson extrapolation.

3.2 Validation and time step

The second step was to validate the accuracy of the results provided by Fluent and the size of the mesh required for the latter simulations in the design process. This was accomplished by comparing with experimental results.

The benchmark problem was the M219 cavity case which was a transonic flow over a cavity. This benchmark problem had been used by multiple journal papers including the one by Li and Hamed (29). The computing geometry used for validation is shown in Figure 13 where D is 4 inches. The sound recorders were placed at locations indicated in Figure 14 at the mid-plane of the geometry.

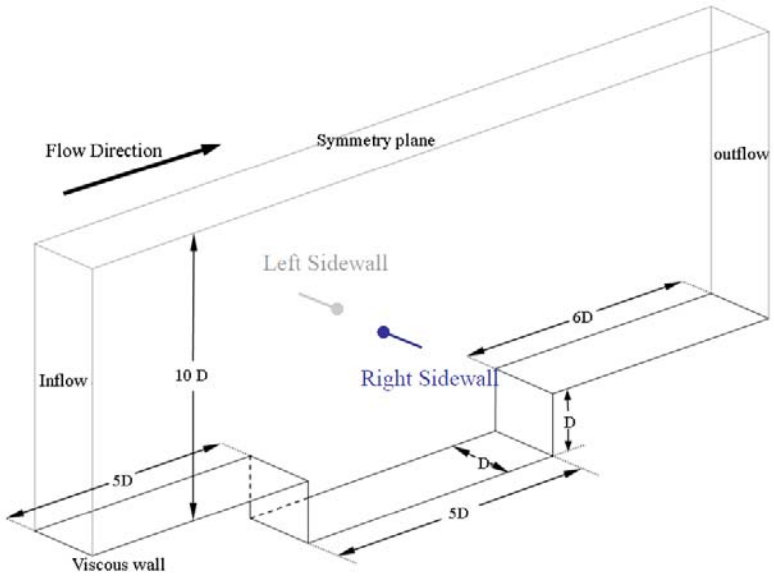

Figure 13: Computation geometry of transonic flow over cavity (29).

Figure 14: Location of sound receivers inside cavity (29).

This particular problem was chosen as the benchmark because it would test the accuracy of sound propagation and sound reflection off impermeable surfaces of the acoustics model available in Fluent. The transonic flow would be similar to the flow velocity expected in the diffuser region of the wind tunnel. Only the FW&H model could provide sound pressure level vs. frequency and thus it was used in conjunction with Detached-Eddy Simulation (DES) and realizable k-epsilon as the viscous model to determine the appropriate time step size that would yield results similar to the benchmark problem. The generated mesh used an element size of 0.005m with refinement over the region of the cavity and further refinement inside the cavity as seen in Figure 15.

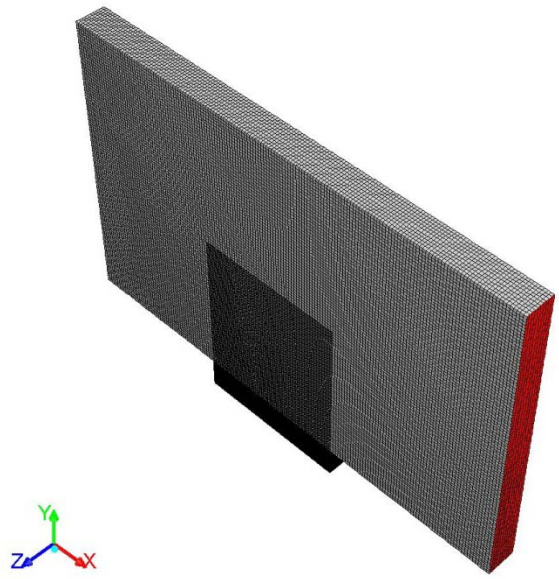

Figure 15: Generated mesh of validation case.

The boundary condition used for the inlet was far-field pressure inlet with a Mach number of 0.85 and the outlet was a pressure outlet with gauge pressure of 0 Pa. The model was simulated with 2nd order upwind spatial and temporal discretization and with a time step size of 0.00001 sec and 50,000 iterations. The acoustic data from the first 10,000 iterations were omitted due to the fluctuations during the starting of the simulation. The sound pressure level from the simulation at the three recorders as seen in Figure 16 to Figure 18 was compared with the experimental results in the blue coloured plot.

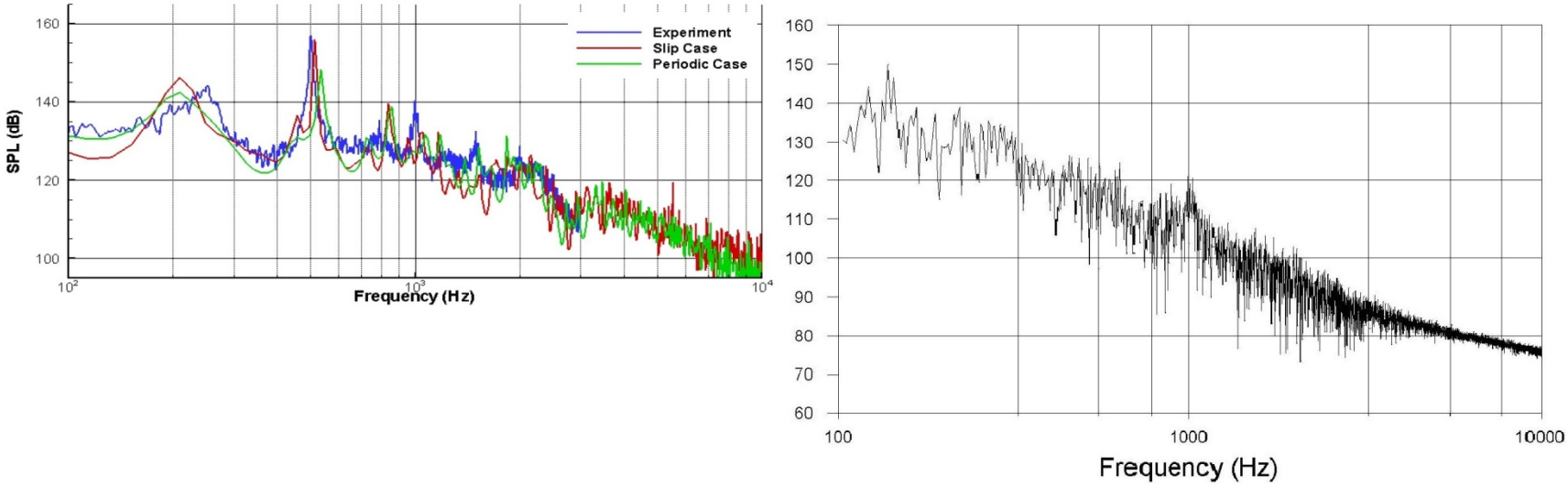

Figure 16: Experiment sound pressure level at point 1 (left, blue) (29) and simulated results (right).

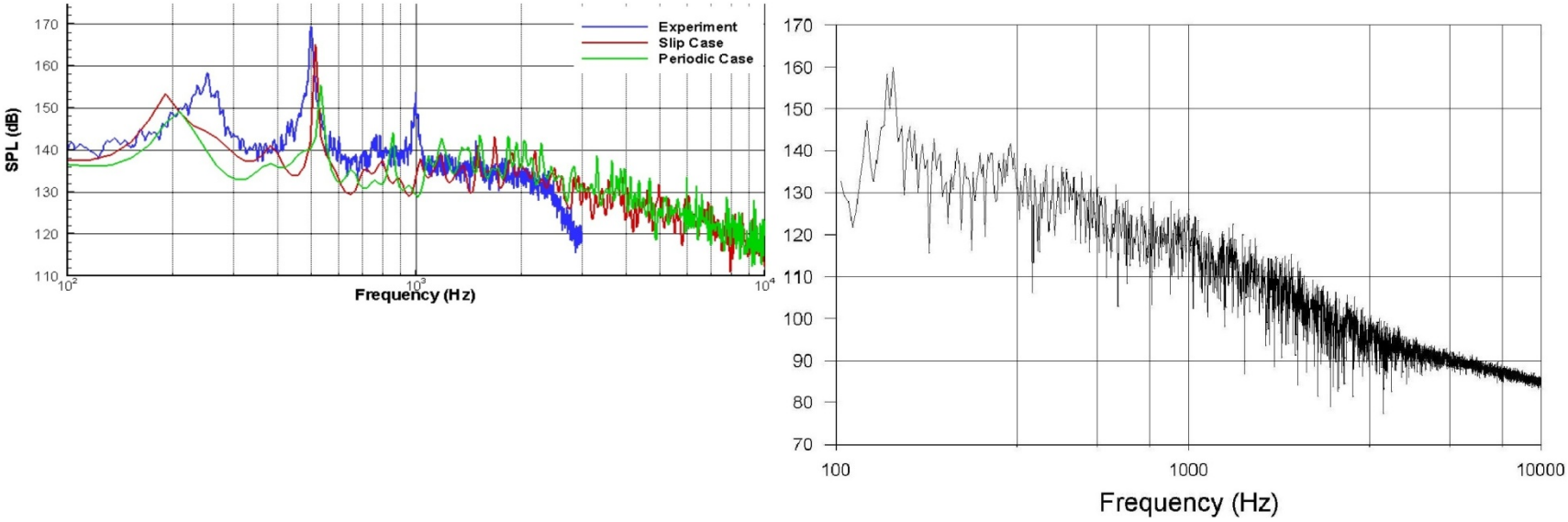

Figure 17: Experiment sound pressure level at point 2 (left, blue) (29) and simulated results (right).

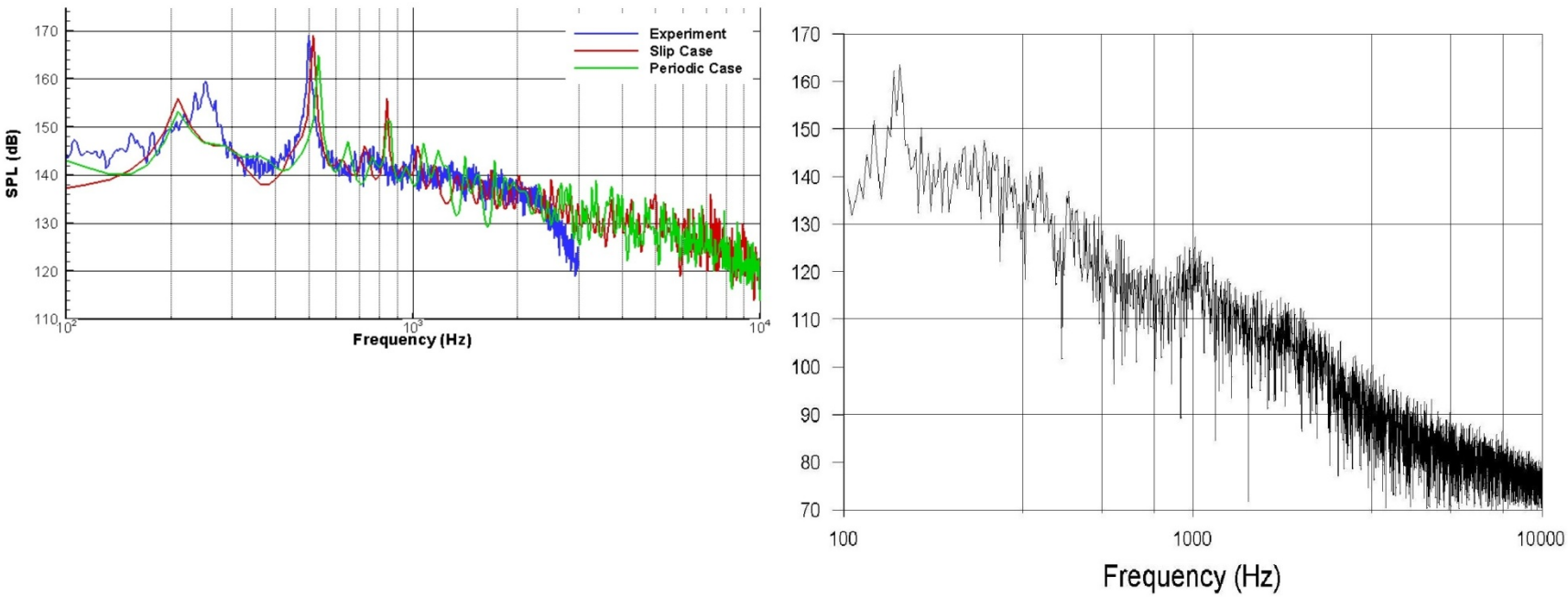

Figure 18: Experiment sound pressure level at point 3 (left, blue) (29) and simulated results (right).

Several observations were made from the results running on Fluent. The simulation did not replicate the tone at 500 Hz in the experimental results. For frequencies greater than 1000 Hz, the general trend was similar to the experimental data as well as the results of Li and Hamed. However, the result from Fluent was approximately 20-30 dB or 18-27% lower than the experiment and Li and Hamed. The simulations conducted by Li and Hamed (red and green plot in Figure 16-18) yield closer results to the experimental data using the WIND code from NASA. They also used a finer spatial grid size of 3.5 million grid points and time step size of $8x10^{-7}$ sec as well as a third order discretization scheme. Based on the current circumstances where only a low order discretization scheme is available, a computational resource limit on the refinement of the mesh size, and an acoustic package with limitation on internal flow, an error of 18-27% is considered acceptable for the purpose of this study. The FW&H model then would be used in the design process. The simulation results would be used for comparison to determine the noise attenuation achieved by the silencer so the sound pressure level from simulation versus the actual sound pressure level would not be relevant for comparison purposes.

4 Design of the Silencer

The design should consider eight aspects: space limitation, weight, exposure to people, need for cleaning, exposure to weather, contamination, gas temperature, flow velocity, and for intense cases linearity of response, and acoustic fatigue.

The three main design criteria chosen were: noise performance, cost, and minimize back pressure. The main objective was to attenuate noise to a sound pressure level that would not cause pain and hearing loss to the occupants of the building and community.

Cost is always a constraint in engineering design and in order to keep the cost down, the design should be simple. Any electromechanical devices such as a pump or actuators would be ruled out. The materials used to fabricate the silencer should be commonly available.

The compressed air storage tank was designed to contain gas at a specified pressure level that would allow the flow to become supersonic in the divergent section of the expansion nozzle and test section. The ratio of the pressure inside the storage tank, P_o, over the pressure downstream of the wind tunnel exit, referred to as back pressure, P_b, is used to determine the location of the normal shock wave inside the wind tunnel. The pressure in the storage tank is fixed, thus if the back pressure increases significantly, the location of the weak normal shock wave in the diffuser shifts upstream into the test section. When the value of back pressure approaches to the pressure level of the reservoir, the flow in the entire wind tunnel will be subsonic. Increase in back pressure due to the silencer geometry should be kept to a minimum to prevent the shock wave from moving upstream.

The noise reduction mechanisms from journal papers and benchmark were considered in all possible design. The design configuration of the silencer was divided into three categories: the main type of mechanism (active or passive), secondary passive mechanism, and the flow path of the duct. Three possible configurations were randomly created based on the three categories and summarized in Table 1 and shown in Figure 19, 20, and 21 respectively.

	Design/Configuration		
	1	2	3
Primary Mechanism	Active Tangential Jet	Active & Passive Vacuum pump & Reflective Silencer	Passive Perforated Liner
Secondary Mechanism	Tabs	Sound Shield	None
Flow Path	U-bend/2-90° bend	S-bend	Straight

Table 1: Summary of three design configurations.

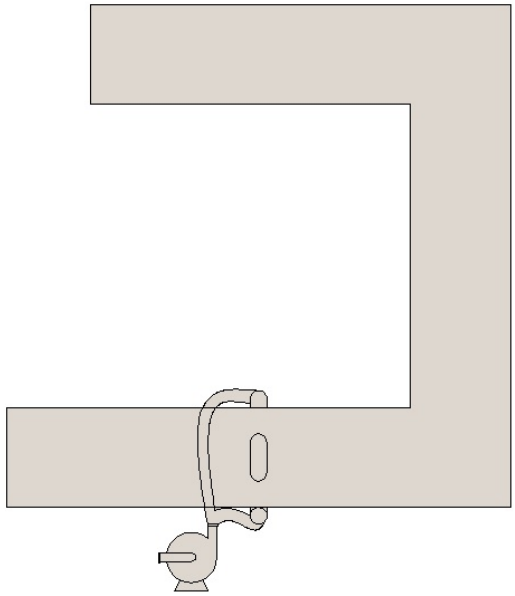

Figure 19: Design 1 layout.

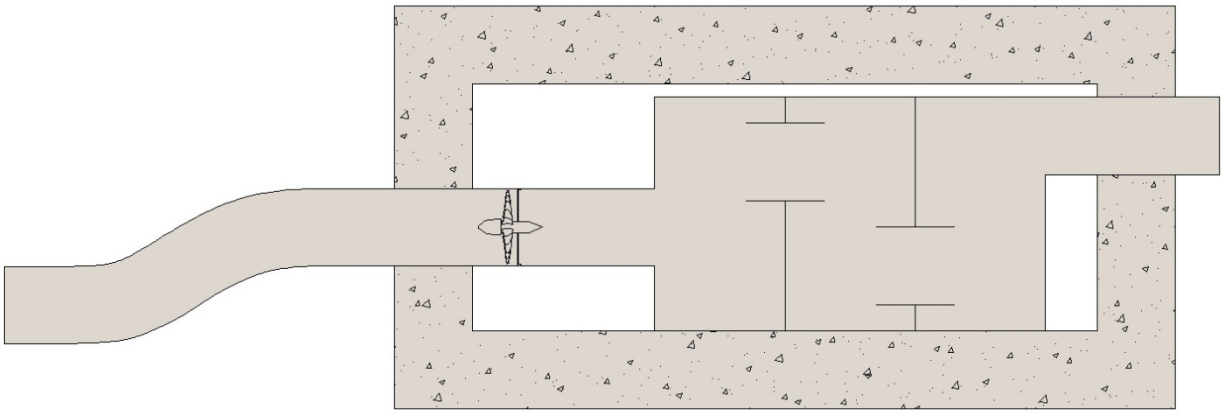

Figure 20: Design 2 layout.

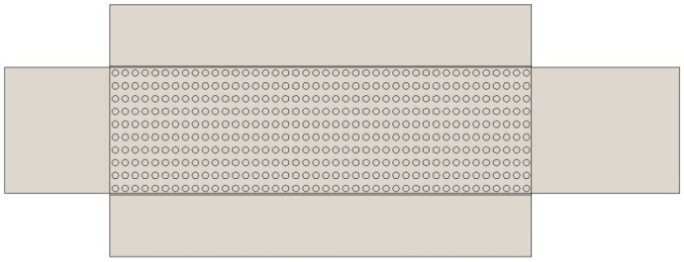

Figure 21: Design 3 layout.

The three chosen design configurations were then evaluated against the three criterions identified: Cost, back pressure, and noise performance. The evaluation of the design configurations along with the chosen design is shown in Table 2.

	Design		
Criteria	1	2	3
Cost (40%)	4	1	10
Pressure Loss (40%)	5	10	9
Noise Performance (20%)	5	10	1
Total Score	4.6	6.4	**7.8**

Table 2: Evaluation matrix of design configurations.

In regards to cost, Design 3 would be the lowest in both material and labour cost due to its simplicity, thus given a rating of 10. On the other end of the spectrum, design 2 would cost the most due to the number of components required. The axial pump for increasing pressure and the sound shield are expensive items. The reflective muffler is a labour intensive fabrication due to the placement of baffles so the huge expense would yield a rating of 1. Design 1 would cost substantially more than design 3 due to the tangential jet. The injection ports would likely take some time to fabricate and the pump would add to the total cost. The cost of Design 1 was estimated to be around the median of Design 2 and 3 and was given a rating of 4.

Design 1 would have the greatest back pressure in the tunnel because of the u-shaped bend generating recirculation. As a result, it was rated with a low score. The increased back pressure from the reflective silencer and s-shaped bend in Design 2 would be compensated with the axial pump, hence the design was given a score of 10. Design 3 would have low to moderate back pressure from the increased friction of the perforated liner. The back pressure magnitude should be comparable to Design 2 so it was given a rating of 9.

Based on the noise attenuation mechanisms in each design and the level of noise attenuation achieved for each mechanism from journal papers, Design 3 was given the lowest score for noise performance. Design 2 had the greatest potential for noise attenuation due to the s-shaped bend and the reflective silencer. The noise due to the axial pump and possible noise from vibration would be contained in the sound shield. The noise should be attenuated to an acceptable level as the air is exhausted out. It was rated the maximum score. For design 1, noise attenuation would be achieved via the tangential jet, tabs at the outlet, and from the corner bend due to sound reflection. The noise performance would be between Design 1 and 3, and therefore was given a score of 5.

Based on the evaluation from the design matrix, Design 3 was rated the highest with a score of 7.8. Consequently, further efforts were focused on Design 3 to refine the design by specifying the dimensions and type of perforated liner.

4.1 Silencer Configuration

The silencer configuration selected was a straight path with acoustic chambers on all four surfaces of the duct similar to Figure 22. Each chamber would have a perforated liner facing the flow and with the possibility of sound absorbing material added into the chamber. The perforated liner separating the chamber and the main flow in the duct serves two purposes. The holes act as a mechanism to attenuated noise. The perforated liner also protects the porous material, if applied, from the flow of gas. Without any screen or protection, the sound absorbing material would deteriorate due to the high speed flow which would require adding more sound absorbing material each time before operating the wind tunnel. If a rigid screen is not present, the flow entering the silencer could compact the absorbing material due to its porosity and fibrous nature and create a large turbulent region from the sudden expansion of the tunnel. As a result, it would generate another source of noise.

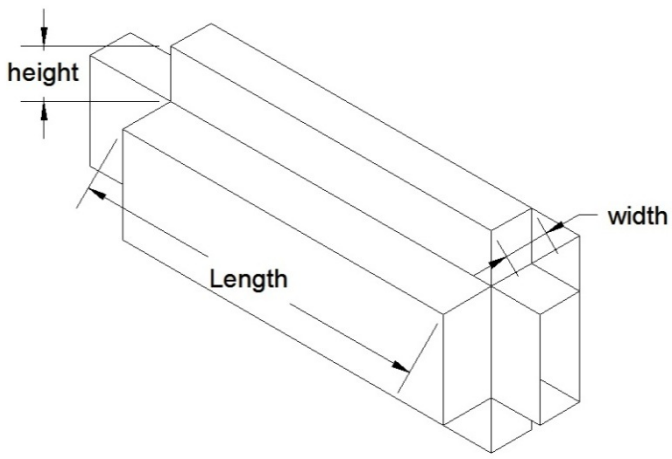

Figure 22: Definition of dimensions for acoustic chamber design.

4.1.1 Perforated Liner hole diameter and opening area

Four perforate liner with different hole diameter and opening area were selected initially as those were commonly used and could be purchased in retail. The hole diameter and opening percentage are summarized in Table 3.

Pattern	Hole Diameter	Opening percentage
1	0.1875”	33%
2	0.3125”	47%
3	0.5”	48%
4	0.75”	51%

Table 3: Perforated patterns studied.

The four patterns were modelled and simulated with the same physical dimensions and same boundary conditions. Changes to the Fluent default settings that were used throughout the entire study are summarized in Table A-18 of Appendix A. Based on the results, the area- weighted average APL at the outlet face decreased as the hole diameter decreased as seen in Figure 23. The results are found in Table A-3 of Appendix A. Naturally, the maximum APL would be the variable of interest but the meshing algorithm in Ansys created smaller mesh size for the patterns with smaller hole diameter. As seen from the mesh sensitivity analysis, a smaller mesh size would yield a higher maximum APL so a clear conclusion could not be drawn based on the maximum APL of all four patterns. The outlet was chosen as the location of comparison because the mesh size would be similar for all four pattern mesh model. The flow has gone past the acoustic treatment so the level of sound power should be comparable for all four patterns.

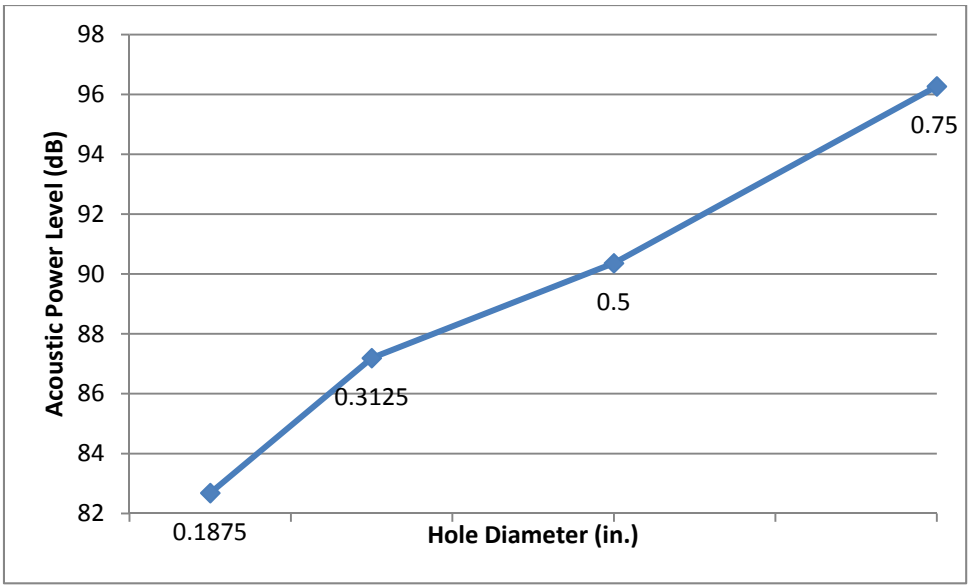

Figure 23: Hole pattern comparison in regards to acoustic power level.

Since the perforated liners also has different open area percentage, further simulations were performed with hole opening percentage of 10%, 30%, and 50% for hole diameters of 0.3125" and 0.5" and 10%, 20%, and 40% opening percentage for 0.1875" hole diameter. Again, the area-weighted average APL at the outlet was chosen as the basis of comparison over the maximum APL for the same reasons explained previously. The general trend based on the results as presented in Figure 24 shows the area-weighted average APL at the outlet decreases with greater hole opening percentage. Results for the other variables are found in Table A-4, Table A-5, and Table A-6 of Appendix A. It was evident hole diameter is a greater contributor than hole opening percentage in regards to noise attenuation.

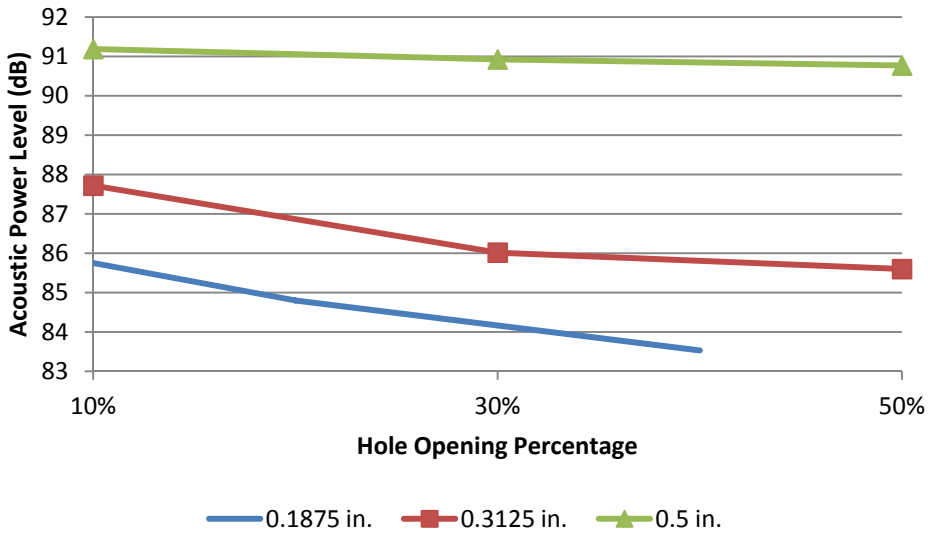

Figure 24: Acoustic power level results of different hole diameter and opening percentage.

The results were consistent with the findings of Tam and Ju where they found the acoustic impedance to increase when the opening was divided into multiple smaller openings (30). The hole pattern layout was also studied between aligned and staggered pattern as shown in Figure 25. The study focused only on hole diameter of 0.1875” since it provided the greatest noise attenuation. The hole spacing dimension is listed in Table 4.

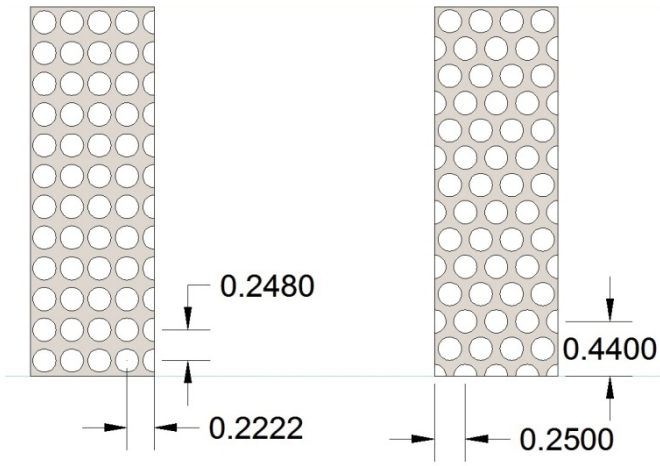

Figure 25: Aligned and staggered pattern of 50% opening perforated liner.

		Opening Area Percentage				
Diameter	Pattern	10%	20%	30%	40%	50%
0.1875”	Aligned	0.5625”	0.375”	0.296875”	0.25”	0.234375”
	Staggered	0.5625”	0.40625”	0.328125”	0.28125”	0.25”

Table 4: Hole spacing for opening area and pattern study.

The results were taken at a plane 0.75” offset inside the outlet plane defined as plane-A to avoid effects of boundary condition. Area-weighted average APL was used as the basis of comparison over maximum APL because the greater open area percentage required finer mesh size. As a result, the higher open area percentage would have a greater maximum APL as seen in Figure 26.

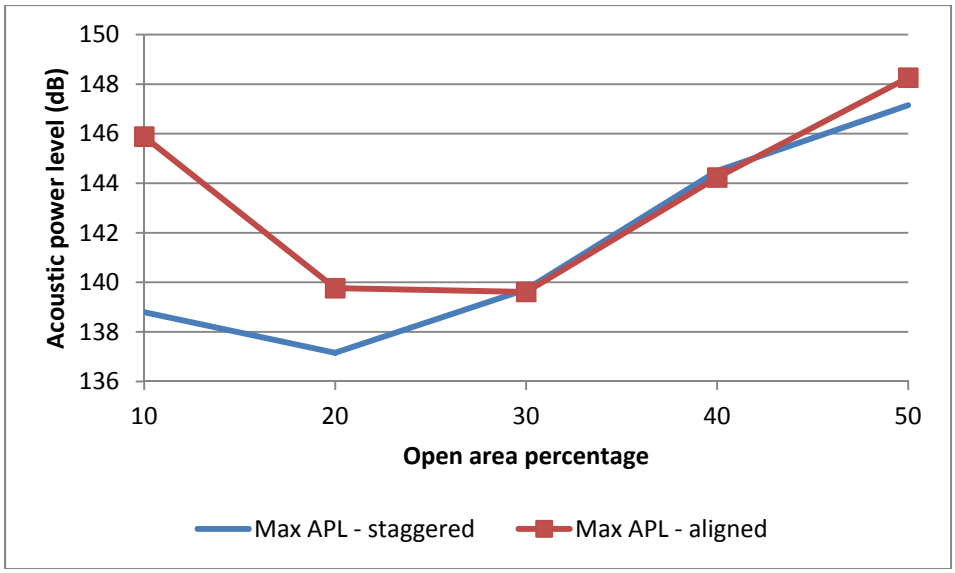

Figure 26: Maximum acoustic power level vs. open area for 0.1875" hole diameter.

The area-weighted average APL for 0.1875" hole diameter at plane-A is presented in Figure 27. The numerical results at the outlet and plane-A for both aligned and staggered pattern are found in Table A-7 to Table A-10 of Appendix A as well as the maximum APL in Table A-11. From the results, it was evident the staggered hole pattern yield a similar or lower APL depending on the hole opening percentage. As seen in Figure 27, the APL reduced between 3-4 dB when the hole opening percentage increased from 10% to 50%. The final design would incorporate a staggered 50% area open percentage perforated liner since both Figure 26 and 27 revealed the staggered pattern has better acoustic performance.

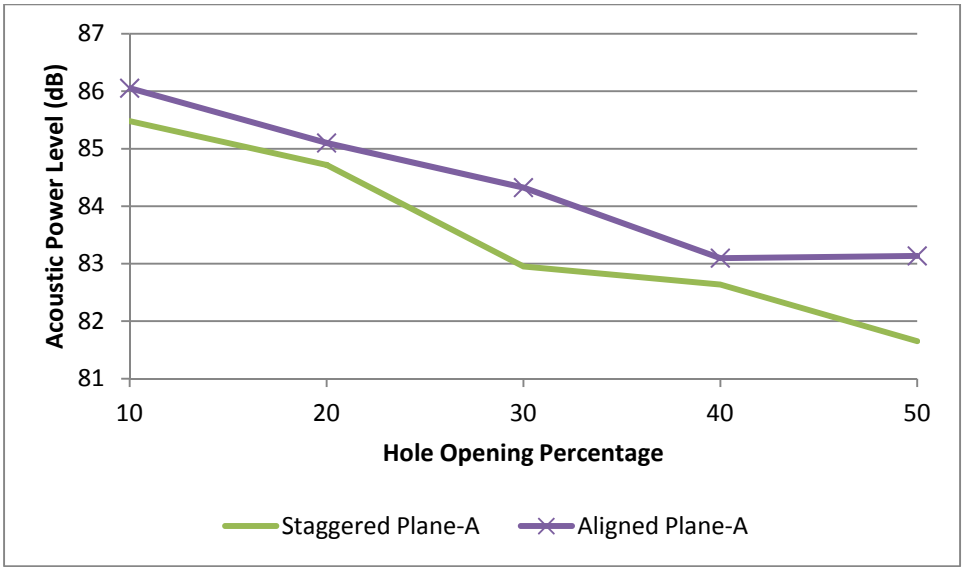

Figure 27: Hole pattern comparison for 0.1875" hole diameter.

4.1.2 Porous Material

Porous material transforms sound energy from mid to high frequencies into heat. Ideally, the silencer should have an absorption coefficient as close to unity across the whole frequency range so that it would attenuate the maximum sound pressure per unit length of the silencer possible. This low end frequency shortfall could be improved by increasing the thickness of the absorber or adding a perforated liner over the porous absorber. The perforated liner serves two functions; it acts as a Helmholtz resonator which could improve the absorption coefficient in the low frequency band and it acts as a protection for the porous absorber so that it does not deteriorate quickly due to the high speed flow in the tunnel. For a porous absorber of one or multiple layers with a perforated liner, the impedance at normal incidence can be calculated using the following transfer matrix (1).

$$z_{si+1} = \frac{-jz_{si}z_i \cot(k_{xi}d_i)+z_i^2}{z_{si}-jz_i \cot(k_{xi}d_i)} \tag{4.1}$$

Delany and Bazley has created an empirical model to predict the absorption of porous material. It is used to determine the characteristic impedance of the porous material based on the flow resistivity, σ, of the material. The characteristic impedance is defined in equation 4.2 and the variable X defined in equation 4.4 (1).

$$z_c = \rho_o c_o(1 + 0.0571X^{-0.754} - j0.087X^{-0.732}) \tag{4.2}$$

The wavenumber is defined as (1):

$$k = \frac{\omega}{c_o}(1 + 0.0978X^{-0.700} - j0.189X^{-0.595}) \tag{4.3}$$

$$X = \frac{\rho_o f}{\sigma} \tag{4.4}$$

The end correction factor developed by Rschevkin which can be applicable to all opening percentage of perforated liners is given as (1):

$$\delta = 0.8(1 - 1.47{\varepsilon_o}^{\frac{1}{2}} + 0.47{\varepsilon_o}^{\frac{3}{2}}) \tag{4.5}$$

The impedance of a Helmholtz resonator is given as (1):

$$z_{helm} = r_{helm} + j\omega m_{helm} \tag{4.6}$$

$$r_{helm} = \frac{\rho}{\varepsilon_o}\sqrt{8\nu\omega}(1+\frac{t}{2a}) \tag{4.7}$$

The surface impedance of the absorber can be used to calculate the pressure reflection coefficient. The equation is given as (1):

$$R = \frac{\frac{z_1}{\rho c}\cos(\varphi)-1}{\frac{z_1}{\rho c}\cos(\varphi)+1} \tag{4.8}$$

Where Ψ is the incidence angle and z_1 is the surface impedance. The ratio of the absorbed and incident energy, known as absorption coefficient, is calculated as (1):

$$\alpha = 1 - |R|^2. \tag{4.9}$$

Using equation 4.1, the absorption coefficient of various flow resistivity of porous material with a pattern 1 perforated liner was plotted in Figure 28.

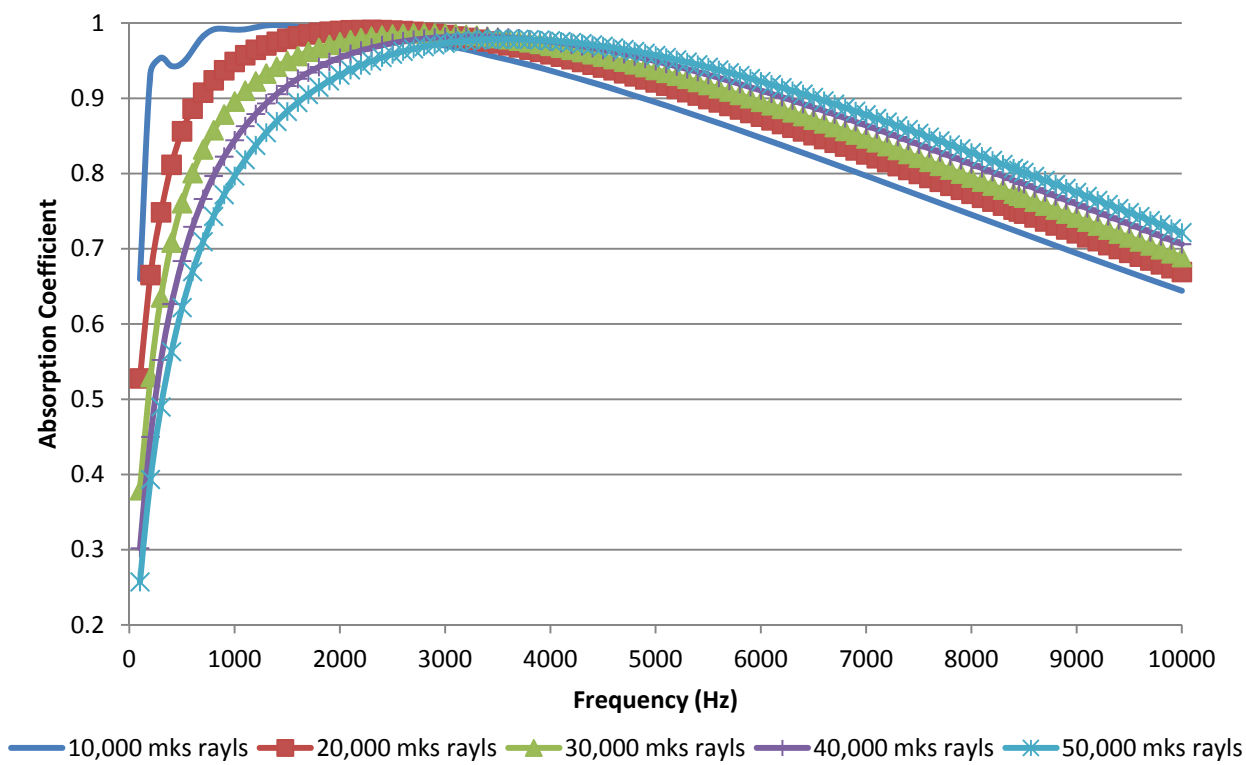

Figure 28: Absorption coefficient comparison of various flow resistivity.

Based on Figure 28, porous absorber with lower flow resistivity has a higher absorption coefficient for the low end frequency whereas absorber with higher flow resistivity would perform better at the high

end frequency. Since human hearing is more susceptible to low and mid frequency noise than high frequency, the lower flow resistivity sound absorbent material was chosen.

However, it was unknown how much of the sound energy dissipated was due to the function of the viscous friction from the acoustic liner and whether the porous material would provide any performance in noise attenuation for the case of high speed flow. From Meyer et al., they observed the attenuation decreased and the maximum attenuation shifted towards higher frequencies for a Helmholtz resonator with Rockwool backing as the flow velocity increased in a series of experiments (31). This could be compared by running a simulation between a silencer with porous material in the chamber and one with just air.

Glass wool was randomly chosen as the fibrous material placed in the chamber since it was a material commonly used for acoustic applications. For modelling randomly-oriented fibre in Fluent, experimental data of various materials from Jackson and James (32) was used to determine the proper inputs. The dimensionless permeability of glass wool with a volume fraction of 10% along with the fibre diameter used in the experiment was taken from the published table to calculate the viscous resistance coefficient. The equation given by Fluent user's guide is (33)

$$B = \frac{\alpha_1}{a^2} \tag{4.10}$$

The study was performed in conjunction with the chamber height study in the next section.

4.1.3 Chamber Height

Since the calculation in previous section was suited for still air situations, several simulations were performed to determine the effects of flow on the height of the chamber.

Five chamber heights were tested ranging from one to five inches in one inch increments and filled with glass wool. The results are shown in Table A-12 of Appendix A. Three chamber heights of one, three, and five inches were simulated without glass wool with the results shown in Table A-13 of Appendix A. The perforate sheet modelled was pattern 1 with a chamber length of 22.5 inches. The relation between chamber height and maximum APL of the entire wind tunnel is shown in Figure 29.

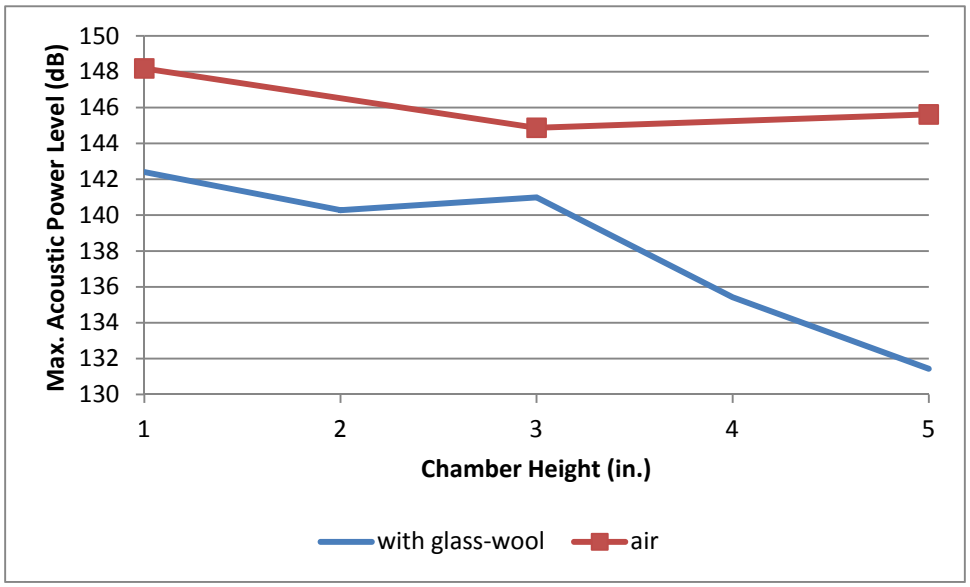

Figure 29: Maximum acoustic power level vs. chamber height.

Based on the trend seen from the simulations, it was seen the exit Mach number of the wind tunnel decreased as the dimension of the chamber increased in height.

In continuation of the previous section, the area-weighted average APL at the outlet revealed the chamber without glass wool was lower than with glass wool. However the maximum APL measured was the opposite as the maximum APL was lower for the chamber filled with glass wool. The trend also showed the maximum APL decreased as the height of the chamber increased. From the APL contour plot of the wind tunnel with the silencer height of 3" and 5" with glass wool as seen in Figure A-9 to Figure A-12 of Appendix A, and without glass wool as seen in Figure A-13 to Figure A-16 of Appendix A, it was clear that for the case without glass wool, the maximum APL was located inside the holes of the perforated liner. It was also the source of maximum APL of the entire wind tunnel. The final design would have a height of 5 inches and filled with glass wool.

4.1.4 Number of Chambers

The length of the chamber is usually decided to tune out distinct tones and the chamber length should be 1/8th the wavelength of the corresponding frequency of the tone. This however, would only be practical for the low end frequency due to longer wavelengths. In dealing with supersonic flow, the sound pressure level is fairly constant across the whole hearing frequency range. There is no specific frequency to be tuned so the chamber length can be arbitrary. The benefit of dividing the silencer into multiple chambers is to ensure sound does not travel inside the chamber from one end to the other. The number of chambers included with the silencer design was investigated. A silencer of length 60" was

studied with 3 configurations: 2-30” chamber, 3-20” chamber, and 6-10” chambers. The area-weighted average Mach number APL at the outlet surface and maximum APL of the entire wind tunnel was compared among the 3 configurations which is found in Table A-14 and Table A-15 of Appendix A. The APL contour plot of the various configurations is seen in Figure A-17 to Figure A-22 of Appendix A. Based on the results, the area-weighted average of absolute pressure and Mach number were similar at the outlet for all three configurations. The 3-20” chamber had the lowest area-weighted average APL of all but when compared to the maximum APL of the entire wind tunnel, the 6-10” chamber configuration was slightly lower as seen in Table A-15. However the 3-20” chamber was still the chosen configuration of design because the maximum APL at the silencer region and the area-weighted average at the outlet was the lowest of all. It would also save material cost in comparison to the 6-10” chambers.

4.1.5 Length of silencer

In theory, the longer the silencer, the more noise would be attenuated. However, there was a limit to how long the silencer could be due to the size restriction of the room in which the wind tunnel is located. The length of the silencer also had a trade off in increase of back pressure as the surface friction of the silencer was much greater than the rest of the duct due to the presence of the holes. A series of simulation was performed to study the average sound power on the outlet surface in relation to the length of the silencer. Silencer lengths of 20, 30, 40, 60, and 100 inches were simulated. The perforated sheet used was pattern 4. This particular pattern was chosen due to the fewer amount of nodes required for the model. The results are presented in Table A-16 of Appendix A.

From the results, it was evident that the area-weighted average APL and maximum APL did not decrease linearly with increasing silencer length. 60 inches would be the ideal length of the silencer as the trend of the acoustic power approached to an asymptote for lengths greater than 60 inches as seen in Figure 30. This phenomenon occurred because the increased number of holes also increased the number of noise generating sources.

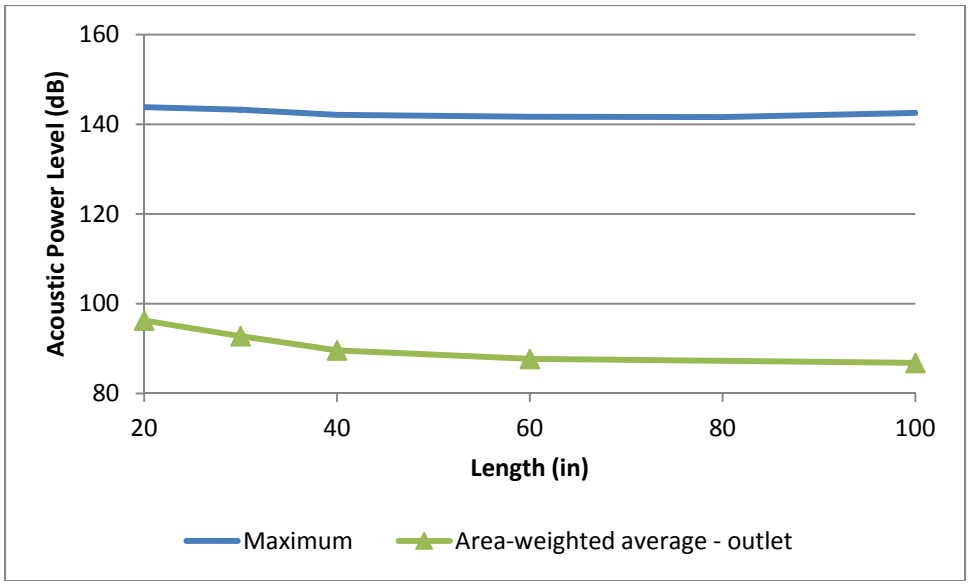

Figure 30: Acoustic power level vs. length for pattern 4.

The study was tested against pattern 1, as this pattern provided the greatest attenuation, to determine if it would yield similar results. Three silencer lengths of 22.5, 40, and 60 inches were tested with results presented in Table A-17 of Appendix A. The trend showed increasing noise attenuation with increase in length of the silencer as seen in Figure 31, while the Mach number decreased and back pressure increased. However, the odd data point was the absolute pressure at length of 60” having a lower pressure than that of 40” length.

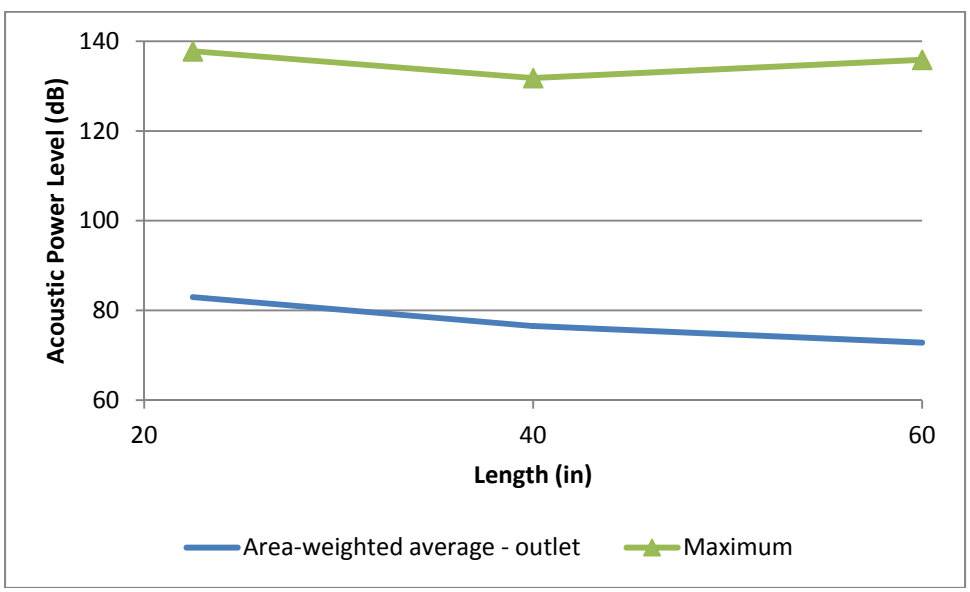

Figure 31: Acoustic power level vs. length for pattern 1.

However when the maximum APL of all three lengths of pattern 1 was compared, the 40” length yield the lowest level. This was probably because the 60” case required a slightly finer mesh than the other cases which might had resulted with greater the maximum APL. The selected length for the silencer was 60”.

4.1.6 Preliminary Configuration

The summary of the chosen silencer configuration is presented in Table 5.

Perforated Pattern	0.1875” hole diameter 0.06” sheet thickness 51% open area
Chamber Dimension	Length - 20” Height - 3” Width – same as tunnel diffuser dimension
Silencer Length	60”
Absorbent Material	glass wool

Table 5: Preliminary silencer configuration.

4.2 Simulation of Wind Tunnel without Acoustic Treatment

For comparison purposes, the existing wind tunnel was simulated to determine the maximum APL and SPL at the outlet.

4.2.1 Initial Baseline Simulation

The noise source generated inside the wind tunnel was identified to be in the expansion nozzle and along the walls as seen in Figure A-1. The maximum APL of the baseline wind tunnel was 141 dB. From Figure A-2, the baseline tunnel did not exhibit a shockwave in the diffuser section as the flow remained supersonic leaving the outlet. Three sound recorders were placed at different locations downstream of the tunnel exit. The first recorder was placed in the centre at the outlet, the second was placed at the corner of the diffuser at the outlet, and the third at the centreline, 30 cm away from the outlet. The sound pressure level plot of each recorder could be found in Figure A-3 to Figure A-5. The calculated overall sound pressure level by Fluent for recorders 1 to 3 were 150.88 dB, 143.85 dB, and 120.39 dB respectively.

Human hearing is limited to a specific range, as defined by the region inside of the red boundary in Figure 32.

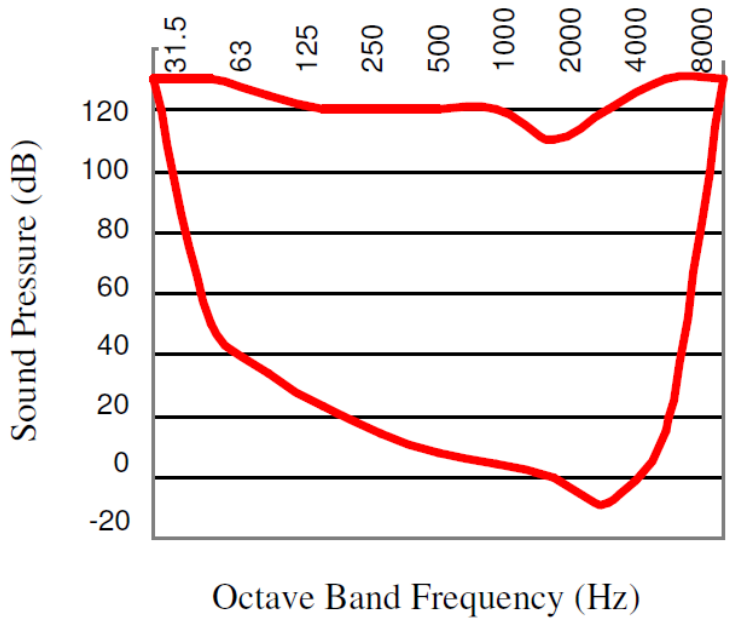

Figure 32: Range of human hearing (34)

A-weighting measurement scheme is normally used for sound pressure level measurements to reflect the human hearing range and this correction could be distinguished when the unit of measurement is displayed as dB(A). The A-weight sound pressure level plot for the three recorders is shown in Figure A-6 to Figure A-8.

A normal shock wave was expected in the diffuser of the existing tunnel, thus modification to the wind tunnel was required.

4.2.2 Revised Baseline Simulation

A normal shockwave was missing in the diffuser in the simulation without acoustic treatment. As a result, the noise output and sound pressure level at the outlet of the wind tunnel was underestimated.

The root of the problem could be explained with gas dynamics analysis. The schematic of a supersonic wind tunnel is shown in Figure 33.

Figure 33: Pressure layout of wind tunnel.

From one dimensional gas dynamics analysis and assuming a calorically perfect gas, using ratios from normal shock table of a test section of Mach 2.0, the downstream Mach number on the right hand side of the normal shock in the diffuser would be 0.5774. The throat area ratio of the diffuser to the expansion nozzle could be approximated using the ratio (3) in equation 4.10.

$$\frac{A_{t,2}}{A_{t,1}} = \frac{p_{0,1}}{p_{0,2}} \tag{4.10}$$

The height of the throat in the nozzle is 3.937 inches and the stagnation pressure ratio for Mach 2.0 is 1.3872. Therefore, the theoretical minimum diffuser throat height is 5.461 inches. However, the designed diffuser height is 5.954 inches. One of the reasons for a larger diffuser throat height is to avoid choking during the start up of the wind tunnel, so that the mass flow can flow past the diffuser. On the other hand, a larger diffuser throat area will not be able to decrease as much velocity than a smaller diffuser throat area.

The pressure ratio across the wind tunnel could be calculated with the following pressure ratios:

$$\frac{P_o}{P_b} = \frac{P_o}{P_1} \times \frac{P_1}{P_2} \times \frac{P_2}{P_{o,2}} \times \frac{P_{o,2}}{P_b} \tag{4.11}$$

The values of the ratios were taken from isentropic properties and normal shock tables for M 2.0 where:

$$\frac{P_o}{P_1} = 7.824 \quad , \quad \frac{P_1}{P_2} = \frac{1}{4.5} \quad , \quad \frac{P_2}{P_{o,2}} = \frac{1}{1.256} \quad , \quad \frac{P_{o,2}}{P_b} \approx 1$$

With the assumption of isentropic flow and a weak normal shock located in the diffuser, the theoretical pressure ratio P_o/P_b to run the tunnel was calculated to be 1.384. However, assuming atmospheric pressure for the back pressure, the CFD result showed there was a normal shock at the test section rather than in the diffuser. The one dimensional analysis assumed the flow velocity would be approximately zero at the exit of the diffuser which is not the case physically. For the simulation of the wind tunnel starting at the convergent divergent nozzle, the inlet total gauge pressure of 325,000 Pa would yield an area-weighted average of Mach 1.04 at the outlet and it was evident the flow was

decreasing to Mach 1.0 in the diffuser section as shown in Figure C-1. Based on the area-weighted average gauge pressure of 32033.61 Pa at the outlet surface, the ideal pressure ratio of the wind tunnel would be approximately 3.20.

Instead of spending time, due to the mesh size involved, on trial and error to determine the total reservoir pressure that would compensate for the pressure loss from the mixing chamber, the ratio P_o/P_b = 7.824 was used for all the simulations. As a result, this was also one of the reasons why the exit flow was supersonic.

Several methods could be applied to decrease the exit flow velocity. The area velocity ratio (3), equation 4.12,

$$\frac{dA}{A} = (M^2 - 1)\,\frac{du}{u} \tag{4.12}$$

shows that in order to decrease the velocity of a supersonic flow, the area would have to decrease as well. Another solution to decrease the velocity of the flow leaving the diffuser would be to extend the length of the diffuser.

The area-weighted average inlet total pressure at the convergent nozzle was 745095.4 Pa, which would equate to an overall pressure ratio of 3.87. Based on the ideal pressure ratio of 3.2, the absolute outlet pressure should then be 232842.3 Pa, a difference of 40,354 Pa. The total pressure drop across the mixing chamber was 46670 Pa so the ideal pressure ratio from the mixing chamber inlet to the wind tunnel outlet was 3.40.

The head loss due to friction from the tunnel wall and turbulence would dissipate the fluid energy. Based on the outlet conditions, the calculated length that would generate a pressure increase was approximately 1.54 m or 60 inches. The calculation for the necessary pressure increase is found in Appendix B.

The diffuser extension was added to the baseline wind tunnel model and simulated again. As shown in Figure C-2 and Figure C-3, a normal shock wave could be seen in the diffuser in the Mach number and pressure contour plot of steady state simulation with the extension. The acoustic power level plot was presented in Figure C-4 and a strong source of noise generation was located downstream of the normal

shock as seen in Figure C-5, which did not exist previously. This noise source was the result of the presence of turbulence along the walls as seen in the turbulent kinetic energy plot in Figure C-6 and Figure C-7. The area-weighted average Mach number and absolute pressure at the outlet was 1.02 and 217788.59 Pa respectively.

Four noise recorders were placed inside the diffuser at the centreline of the flow, where sound pressure level was the greatest, and each spaced 20 inches apart. The first recorder was placed at the location where the outlet would have been without the diffuser extension. Recorders 2, 3, and 4 were be placed downstream of recorder 1, with recorder 4 located at the outlet.

The A-weighted sound pressure level for all four recorders is shown in Figure C-8 to Figure C-11 of Appendix C. Recorder 1 was likely located upstream of the shock wave as the sound pressure level was the lowest of all four. The sound pressure level of recorders 2 to 4 increased along the diffuser towards the outlet. For receiver 4, the peak sound pressure level was between 161-162 dB(A) for the 500 and 1000Hz octave band. The overall sound pressure level calculated by Fluent for the recorders 1 to 4 was 175.6202, 186.6273, 189.8786, and 190.2349 dB respectively.

4.3 Simulation of Design

A half symmetric mesh of the wind tunnel, mixing chamber, and silencer was generated using the maximum and minimum mesh size deemed appropriate from the mesh sensitivity analysis. The mesh included 4,997,531 nodes. The operation of the wind tunnel was first simulated in steady state using the realizable k-epsilon model and applying same boundary conditions and discretization scheme throughout the whole report. The simulation was repeated in transient state. DES with realizable k-epsilon and FW&H acoustic model was used, same as what was used in the validation case. 50,000 time steps were simulated with a time step size of 0.00001 seconds. The computation was conducted on the Orca cluster of Sharcnet which uses AMD Opteron 6174 processor running on CentOS 5.x operating system.

4.4 Simulation Results

4.4.1 Steady State Results

The APL contour plot of the wind tunnel with silencer is shown in Figure D-3 of Appendix D. The 60” silencer had a maximum APL of 161.0928 dB. Figure D-3 shows the main sources of noise originate at

the convergent divergent nozzle and downstream of the shock wave where turbulence along the diffuser wall begin to develop.

Data was recorded at two planes, one at the outlet and another at 3.69 m downstream from the throat of the nozzle as shown in Figure 34, and identified as Plane B.

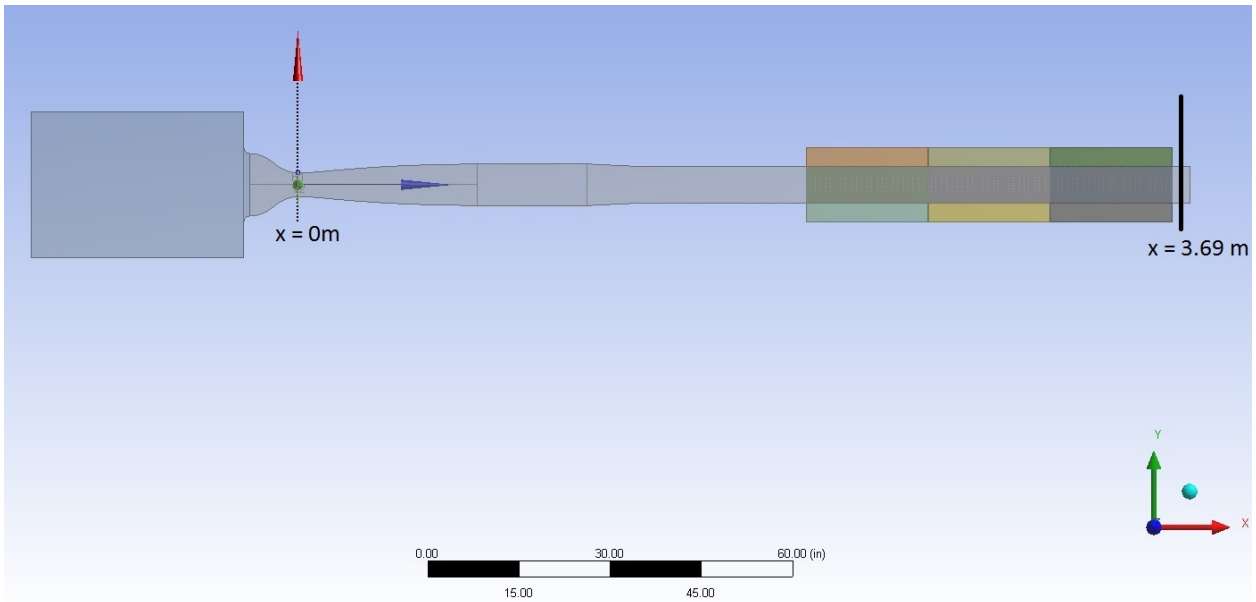

Figure 34: Location of plane for data collection.

The area-weighted average data recorded is presented in Table 6 along with the simulation results of the baseline wind tunnel without sound treatment.

	Outlet	Plane B	Baseline outlet
Absolute Pressure (Pa)	234779.55	243944.16	217788.59
Mach Number	0.98349512	0.95171911	1.0224875
Acoustic Power Level (dB)	74.568367	77.332588	115.81006

Table 6: Area-weighted average results from preliminary design.

The maximum APL of the entire wind tunnel was 161.09 dB, in the silencer region, the maximum APL was 133.73 dB, and at the outlet, the maximum APL was 114.99 dB. In comparison, the maximum APL of the entire wind tunnel and at the outlet without the silencer was 140.07 dB and 124.95 dB respectively.

The silencer generated a strong normal shock wave inside the tunnel in the diffuser region. From **Error! Reference source not found.**, the turbulence generated downstream of the shockwave was another noise source that reached up to 153 dB of acoustic power level.

As seen in Table 6, there was a 16,991 Pa difference in pressure at the outlet as a result of the silencer addition. From the Mach number contour plot in Figure D-1 of Appendix D, the Mach number in the test section was 1.95, close to the design Mach number of 2.0. An area of concern would be the size of the supersonic region has decreased as the normal shock wave shifted upstream into the test section. The contour plot results for the final design, Figure D-1 to D-3 in Appendix D, could be compared with the baseline tunnel without acoustic treatment, Figure C-2 to Figure C-4 of Appendix C. This meant the silencer has created a significant amount of back pressure. From the length study of 60 inch silencer, the Mach number contour plot in Figure A-24 and pressure contour plot in Figure A-25 of Appendix A showed the shock wave was further downstream in the diffuser section without the mixing chamber in the model. This had brought out a concern with the geometric model of the mixing chamber created for the simulation. Further investigation is required to identify the difference in the normal shock location.

4.4.2 Transient Results

Five sound recorders were inserted in the simulation. Two were located inside the tunnel at 3.69 m from the throat, one at the centreline and one at the corner. Another two were placed at the outlet 3.72 m from the throat, one at the centreline and the other at the corner. The fifth was placed at the centreline, 0.3 m away from the outlet of the tunnel. The sound pressure level vs. frequency plots of the five recorder s are shown in Figure D-5 to Figure D-9 of Appendix D. The overall sound pressure level calculated by Fluent for recorders 1 to 5 were 170.595 dB, 160.0783 dB, 168.8203 dB, 141.9525 dB, and 125.7462 dB respectively. Overall sound pressure level is the sum of sound pressure level across a range of frequencies.

The A-weighted sound pressure level measurements of the five receivers are shown in Figure D-10 - Figure D-14 of Appendix D. The highest A-weighted sound pressure level would be at the 500 and 1000 Hz octave band with a peak of approximately 142.5 dB(A) for recorder 1 and 141 dB(A) for recorder 3. In comparison to the sound output of wind tunnel without acoustic treatment, the overall sound pressure level at the outlet saw a reduction of 21.4 dB.

The reduction sound pressure level at the outlet was due to the dissipation of the turbulent region along the diffuser. The presence of the holes in the perforated liner prevented the development turbulent boundary layer. From this finding, it would also be ideal to have the silencer located immediately

downstream to the normal shock wave in the diffuser. Turbulent boundary layer would form downstream next to the normal shock, thus the silencer would dissipate the turbulent kinetic energy and eliminate a major noise source.

5 Conclusion

A straight silencer, made of staggered perforated plain steel liner forming the tunnel wall, and surrounded by four chambers of 60 inch length and 5 inch height, was designed to attenuate noise generated from the turbulent boundary layer upstream at the expansion nozzle and diffuser wall. Noise energy is transformed into vortex energy due to the presence of circular holes increasing the friction in the flow. Noise energy is also transformed to heat due to the sound absorbent material. The physical dimension of the silencer was optimized individually based on comparison of APL data from a series of steady state simulations.

Two CFD simulation of the wind tunnel with the silencer was conducted where the broadband noise model was applied for the steady state simulation and the FW&H model was used for the transient simulation. The results from the steady state broadband noise model showed the silencer reduced the noise generated from the diffuser walls. At the outlet surface, the maximum APL for the wind tunnel with and without acoustic treatment was 114.99 dB and 124.95 dB respectively.

The transient simulation using the FW&H method showed the highest A-weighted sound pressure level was approximately 142.5 dB(A) located in the octave band of 500 and 1000 Hz. Sound measurement recorders placed at the corner and the centre of the wind tunnel showed sound pressure level was greatest at the centre. This meant most of the noise attenuation would occur near the solid boundary.

Compared to the result of the acoustic treatment, there was a reduction of 21.4 dB in overall sound pressure level at the outlet centre. For a design with a single noise attenuation mechanism, it would be considered as acceptable since the reduction was close to the upper range of theoretical noise attenuation level of similar silencer design (35). Some proposed noise attenuation mechanisms found in journal papers only resulted in single digit noise reduction in dB. The design also met the design criteria in which cost was minimize due to the simple geometry of the silencer. The back pressure did not increase significantly, thus the desired Mach number was achieved in the test section. However, further investigation would be required to determine the location of the normal shock wave.

The sound pressure level measured from the wind tunnel with acoustic treatment exceeded the 120-130 dB threshold of damage to hearing. The level of attenuation fell short of the design objective with

regards to noise. In order to attenuate sound to below 120 dB, additional sound reduction mechanisms is required in the silencer design. The designers of the benchmark cases may have arrived to a similar conclusion and thus, their noise control solution included multiple sound attenuation mechanisms. Based on this finding, further work on the design is necessary for greater increase in sound attenuation level. As a result, the cost of the silencer would increase from the additional hours of analysis and increase in complexity of the design.

6 Recommendations

1. Before on making the decision to fabricate the silencer, simulate the model with a finer mesh, smaller time step size, and higher order discretization scheme if computing resource is available. The computing resources were limited in this study and the acoustic result from CFD simulation thus far was under predicted due to dissipation in the numerical scheme. A suitable CFD package for internal noise transmission with a higher than 2nd order discretization scheme would lead to a reduction in numerical error and would likely predict the actual sound pressure level. This would provide a more accurate result on noise attenuation provided by the silencer.

2. Conduct experiments on various sound absorbent materials on the silencer when built. The study of various sound absorbing materials was not conducted in the design process due to the lack of input variables in Fluent for sound absorbent porous material. A trial would determine the appropriate material for this particular application.

3. In order to reduce the sound pressure level below the threshold of hearing loss, additional sound attenuation mechanism would have to be explored in combination with the existing design. A continuation to this study would be recommended to explore the impact on additional sound attenuation features added to the wind tunnel.

Appendix A – CFD results

	Plane @ 2.7m from nozzle throat			Outlet Plane		
# of Nodes	Abs. Pres.	Mach	Acoustic	Abs. Pres.	Mach	Acoustic
142843	284200.44	0.92608804	91.28521	269513.34	0.96776444	88.089211
977087	283322.5	0.94207031	102.0563	261826.52	1.0068388	99.033379
3276930	278406.19	0.96151018	109.4437	260447.44	1.0165315	106.74712

Table A-1: Summary of area-weighted average results from mesh analysis measured at two locations.

# of Nodes	Maximum Acoustic Power Level (dB)	
	tunnel	silencer
142843	141.5895	128.9472
977087	157.6376	135.6537
3276930	158.1396	143.1274

Table A-2: Maximum acoustic power level results from mesh analysis.

Pattern	Absolute Pressure (Pa)	Mach number	Acoustic Power Level (dB)	
			At Outlet	Maximum - tunnel
1	266514.66	0.96368277	82.683746	137.782
2	254419.69	1.003338	87.194679	145.7575
3	264582.44	0.96614093	90.357536	144.608
4	277450.3	0.9293918	96.269028	143.8082
No pattern	190622.38	1.2775635	105.47455	

Table A-3: Area-weighted averages at outlet plane of the 4 perforated patterns.

Opening %	Absolute Pressure (Pa)	Mach number	Acoustic Power Level (dB)
10%	269143.34	0.958743	85.754211
20%	270172.47	0.96130759	84.80127
40%	268458.44	0.96184313	83.532608

Table A-4: Pattern 1 hole study area-weighted average results at outlet.

Opening %	Absolute Pressure (Pa)	Mach number	Acoustic Power Level (dB)
10%	269475.66	0.95840758	87.718285
30%	261340.33	0.98261136	86.016418
50%	269976.63	0.95780277	85.59893

Table A-5: Pattern 2 hole study area-weighted average results at outlet.

Opening %	Absolute Pressure (Pa)	Mach number	Acoustic Power Level (dB)
10%	272967	0.94371939	91.188828
30%	273898.25	0.95365912	90.923752
50%	272572.28	0.94299179	90.770988

Table A-6: Pattern 3 hole study area-weighted average results at outlet.

Opening %	Absolute Pressure (Pa)	Mach number	Acoustic Power Level (dB)
10%	270197.4	0.956293	86.33084
20%	267601.5	0.955684	85.62624
30%	265536.1	0.967785	84.49599
40%	262190.6	0.978268	83.85095
50%	266239.4	0.970113	84.0992

Table A-7: Pattern 1 aligned and uniform spacing area-weighted average results at outlet.

Opening %	Absolute Pressure (Pa)	Mach number	Acoustic Power Level (dB)
10%	272388.9	0.949966	86.0528
20%	269095.1	0.951435	85.10048
30%	266782.4	0.965046	84.32387
40%	266849.1	0.962736	83.09707
50%	270372.3	0.956913	83.13616

Table A-8: Pattern 1 aligned and uniform spacing area-weighted average results at plane-A.

Opening %	Absolute Pressure (Pa)	Mach number	Acoustic Power Level (dB)
10%	273190.8	0.943941	85.70383
20%	269422.7	0.964245	85.03443
30%	265789.5	0.963717	83.58167
40%	263026.4	0.975287	83.27297
50%	261236.6	0.981889	82.76492

Table A-9: Pattern 1 staggered and uniform spacing area-weighted average results at outlet.

Opening %	Absolute Pressure (Pa)	Mach number	Acoustic Power Level (dB)
10%	275254.7	0.938438	85.47968
20%	273196.8	0.953053	84.719
30%	270795.1	0.948052	82.95054
40%	267239.2	0.961461	82.63612
50%	265713.5	0.967913	81.65205

Table A-10: Pattern 1 staggered and uniform spacing area-weighted average results at plane-A.

Maximum Acoustic Power Level (dB)				
	Staggered		Aligned	
Opening %	tunnel	silencer	tunnel	silencer
10%	138.7968	130.3153	145.8824	145.8824
20%	137.157	130.3654	139.7637	138.5099
30%	139.7158	136.1153	139.6132	132.9965
40%	144.4967	144.4967	144.2308	144.2308
50%	147.1515	137.0463	148.2621	145.8924

Table A-11: Maximum acoustic power level of pattern 1 for staggered and aligned spacing.

Height (in)	Absolute Pressure (Pa)	Mach number	Acoustic Power Level (dB)	
			At Outlet	Maximum - tunnel
1	219466.89	1.1297535	84.767776	142.4061
2	238120.19	1.0587856	84.274567	140.2764
3	267113.28	0.96292168	82.948975	140.9915
4	267671.28	0.95387375	84.697914	135.4175
5	266113.38	0.9560051	85.4729	131.4333

Table A-12: Area-weighted average at outlet face of simulated results of various chamber depths filled with glass wool.

Height (in)	Absolute Pressure (Pa)	Mach number	Acoustic Power Level (dB)	
			At Outlet	Maximum - tunnel
1	220768.89	1.099982	83.955597	148.1822
3	241534.48	1.0237164	82.429207	144.8726
5	256143.63	0.97888529	83.030983	145.6186

Table A-13: Area-weighted average at outlet face of simulated results of various chamber depths filled with air.

	Absolute Pressure (Pa)	Mach number	Acoustic Power Level (dB)
6 x 10” chamber	269550.13	0.90330601	88.137199
3 x 20” chamber	269972.91	0.90262413	87.707069
2 x 30” chamber	270183.38	0.90285635	89.420479

Table A-14: Area-weighted average results at outlet for various number of baffles of a 60" chamber.

Maximum Acoustic Power Level (dB)		
	Tunnel	Silencer
6 x 10” chamber	141.7685	131.4702
3 x 20” chamber	142.109	130.919
2 x 30” chamber	143.4077	133.5512

Table A-15: Maximum acoustic power level of various length configurations of a 60" silencer.

Length	Absolute Pressure (Pa)	Mach number	Acoustic Power Level (dB)	
			At Outlet	Maximum - tunnel
20”	277295.84	0.929392	96.269028	143.8082
30”	278398.25	0.915792	92.77626	143.2466
40”	276257.59	0.910491	89.600182	142.109
60”	269972.91	0.902624	87.707069	141.6912
100”	258928.53	0.901071	86.803322	142.5258

Table A-16: Outlet face area-weighted average results of length study from pattern 4.

Length	Absolute Pressure (Pa)	Mach number	Acoustic Power Level (dB)	
			At Outlet	Maximum - tunnel
22.5	269215.25	0.956744	82.94898	137.782
40	272056.16	0.936953	76.51759	131.7979
60	271361.56	0.921266	72.7953	135.8785

Table A-17: Area-weighted average at outlet face results from length study using pattern 1.

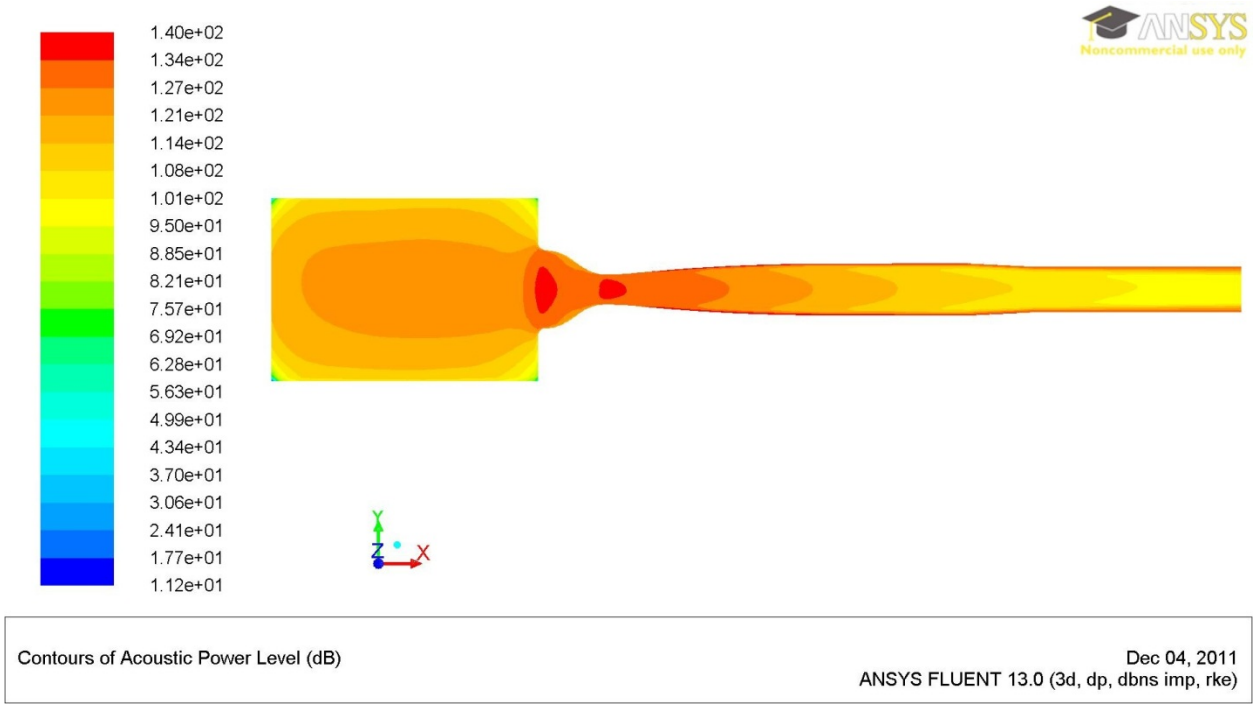

Figure A-1: Acoustic power level contour at midplane of existing wind tunnel.

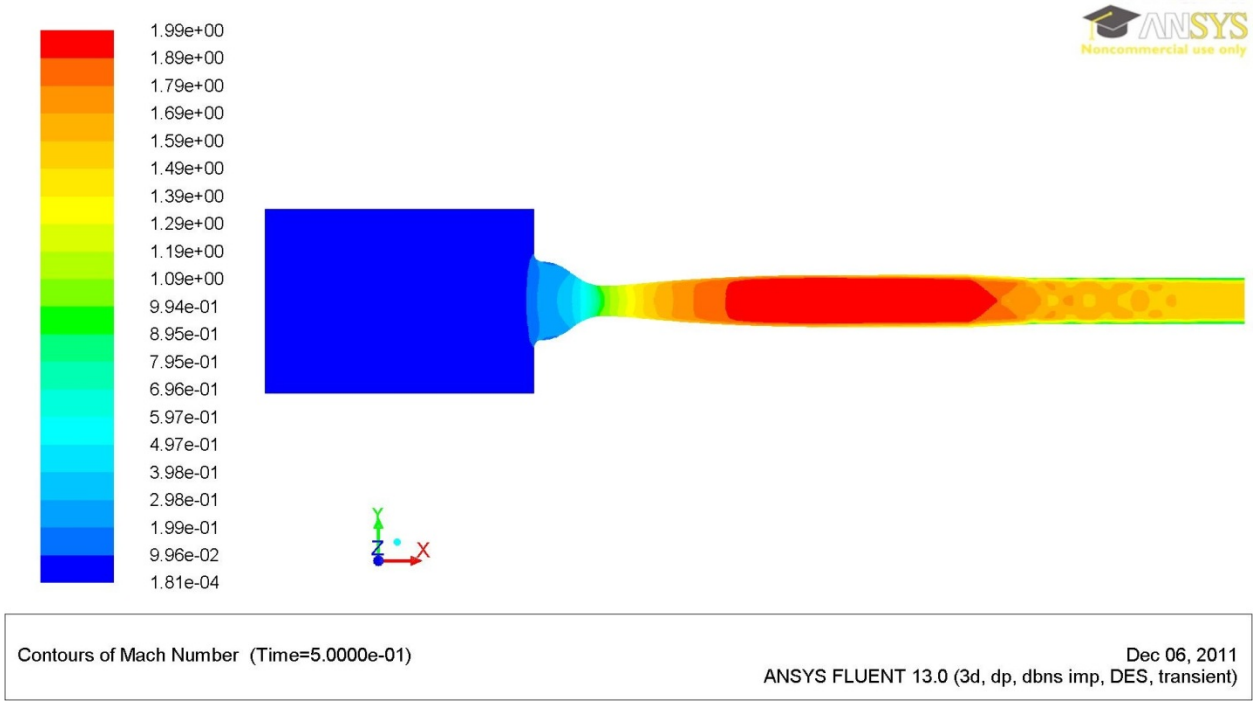

Figure A-2: Mach number contour at midplane of existing wind tunnel.

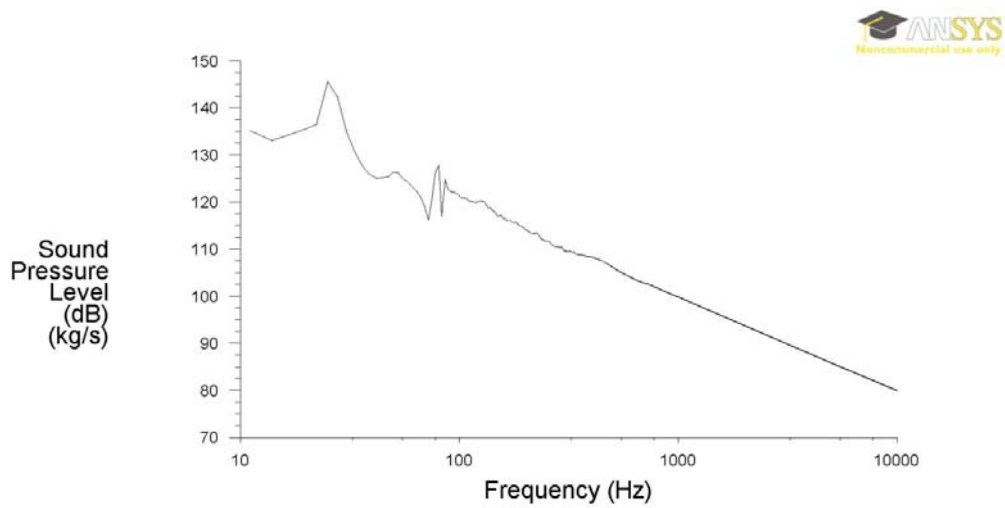

Figure A-3: Sound pressure level at receiver 1 of existing wind tunnel.

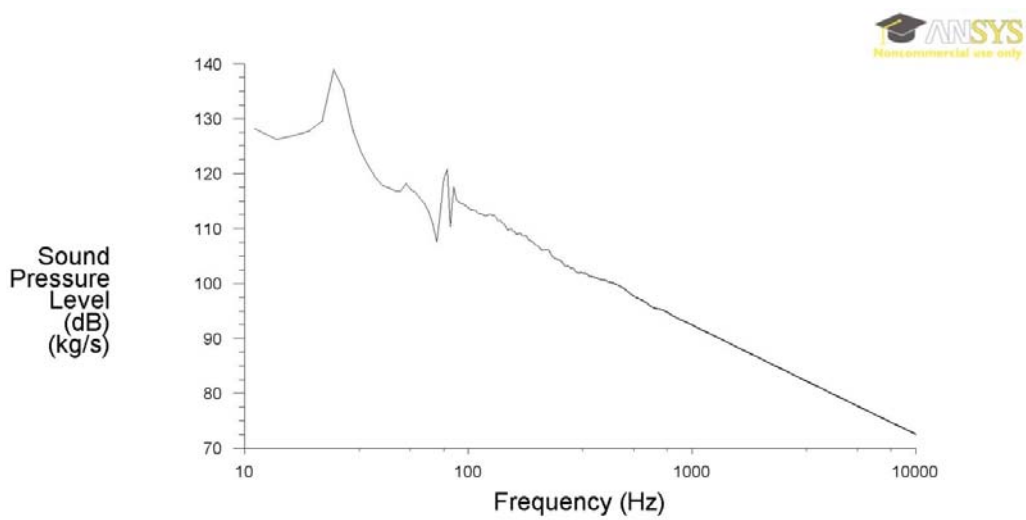

Figure A-4: Sound pressure level at receiver 2 of existing wind tunnel.

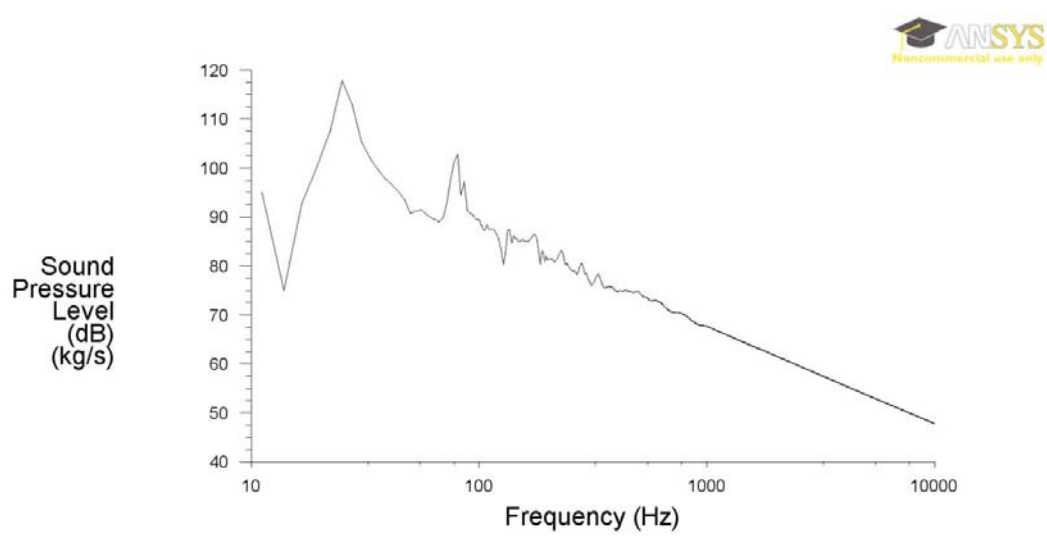

Figure A-5: Sound pressure level at receiver 3 of existing wind tunnel.

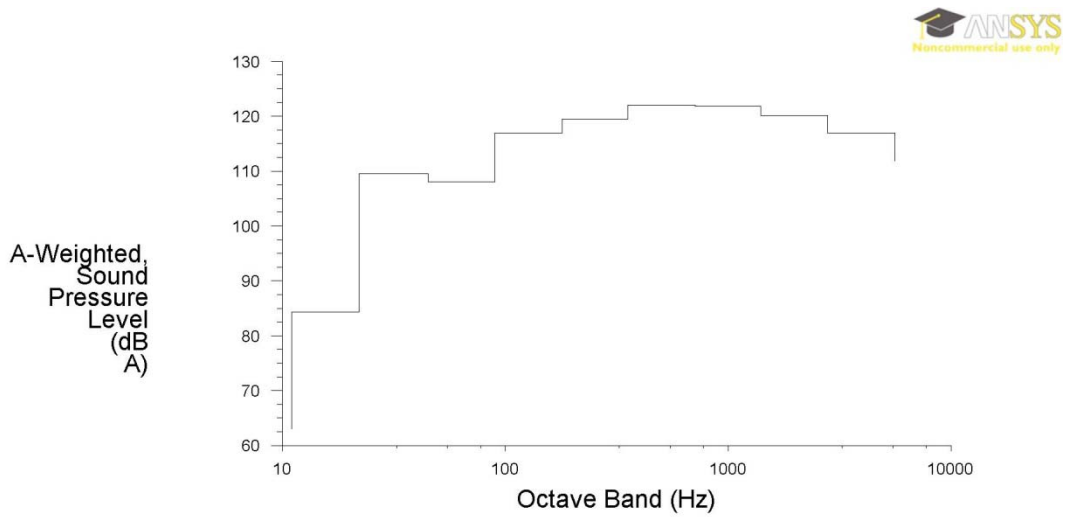

Figure A-6: A-weighted sound pressure level at receiver 1 of existing wind tunnel.

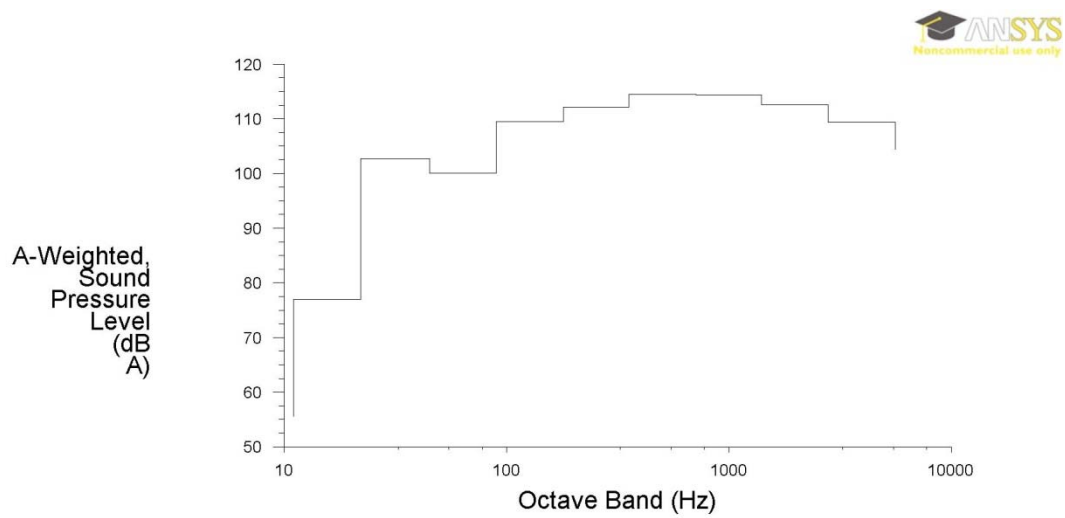

Figure A-7: A-weighted sound pressure level at receiver 2 of existing wind tunnel.

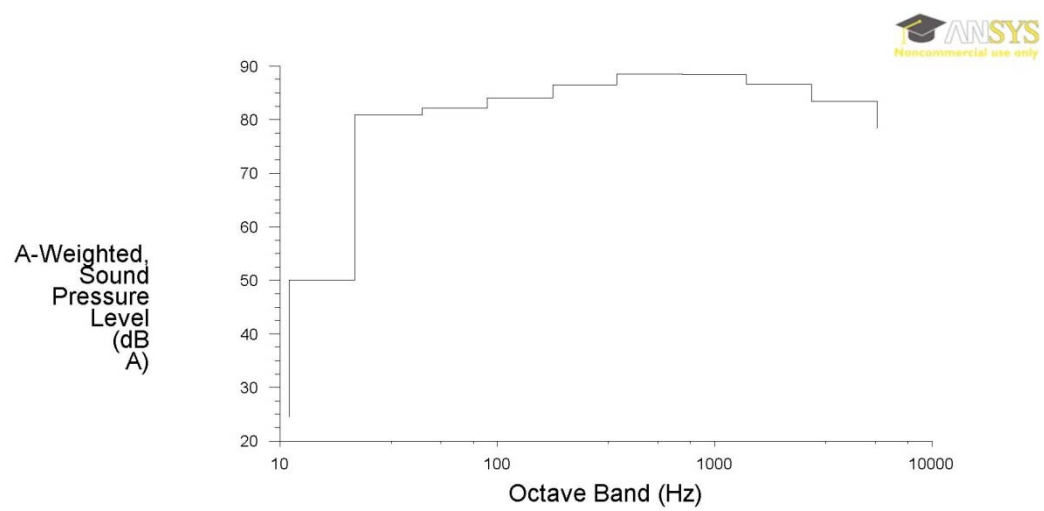

Figure A-8: A-weighted sound pressure level at receiver 3 of existing wind tunnel.

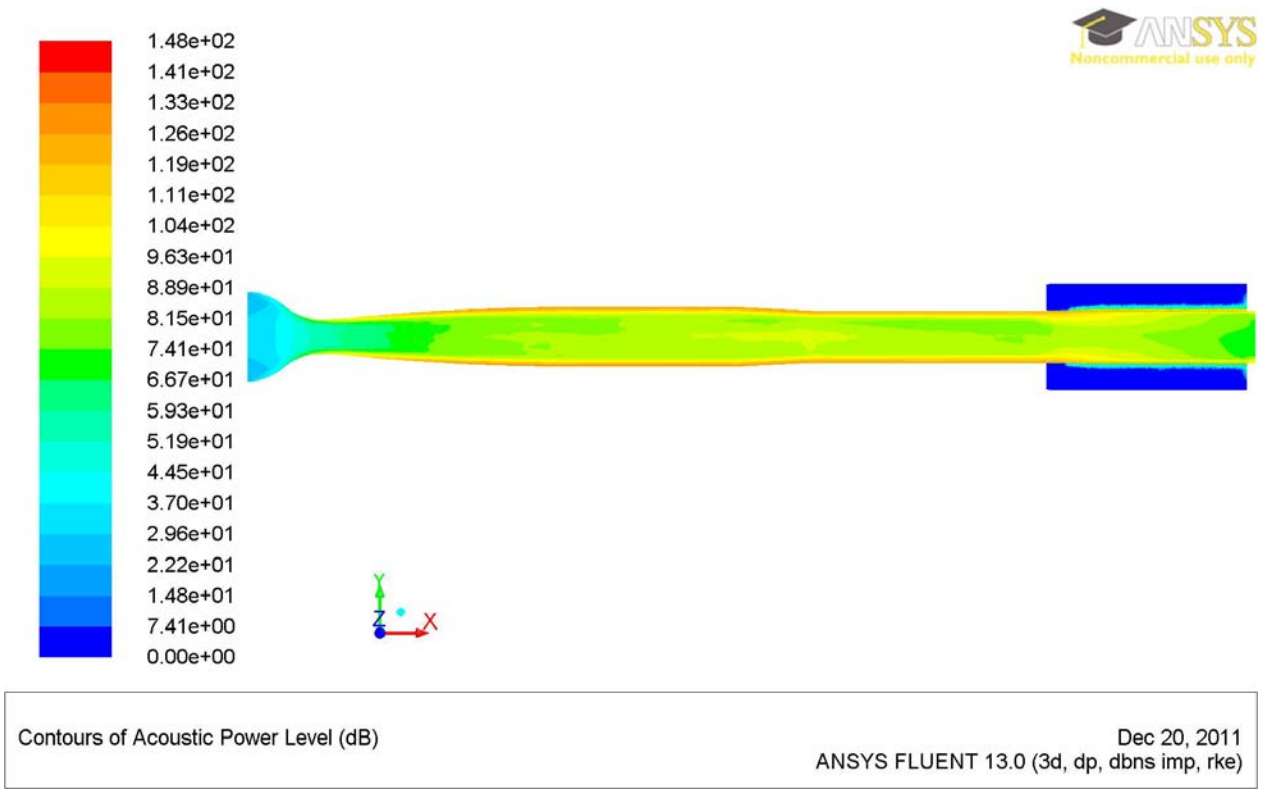

Figure A-9: Acoustic power level contour of tunnel with 3" silencer height and glass wool.

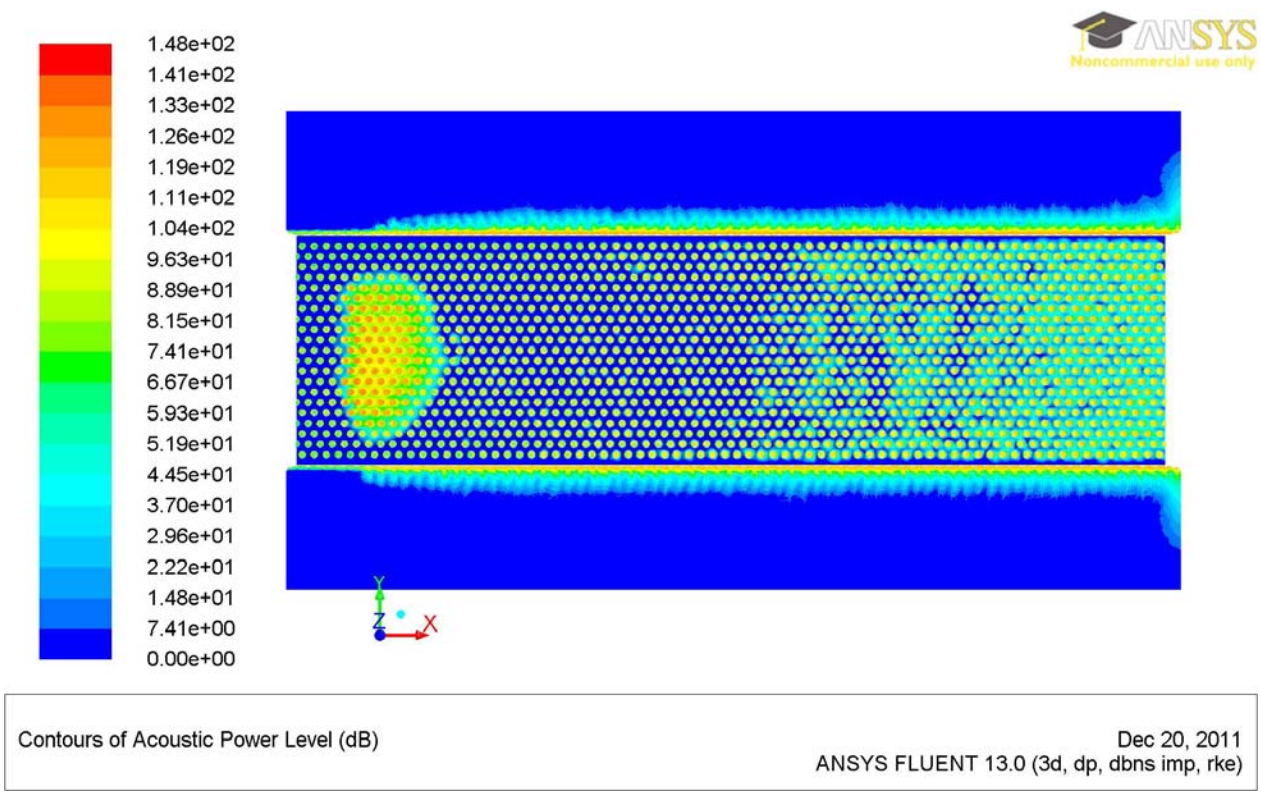

Figure A-10: Acoustic power level contour of silencer with 3" height and glass wool.

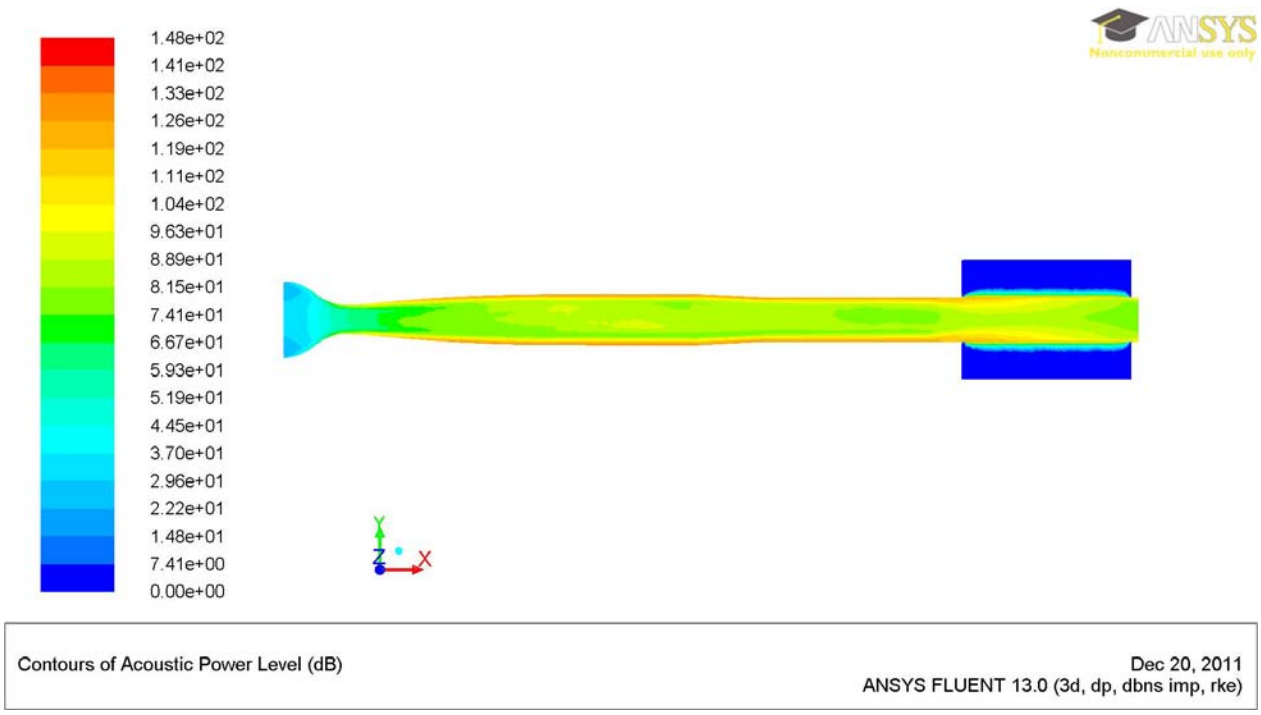

Figure A-11: Acoustic power level contour of tunnel with 5" silencer height and glass wool.

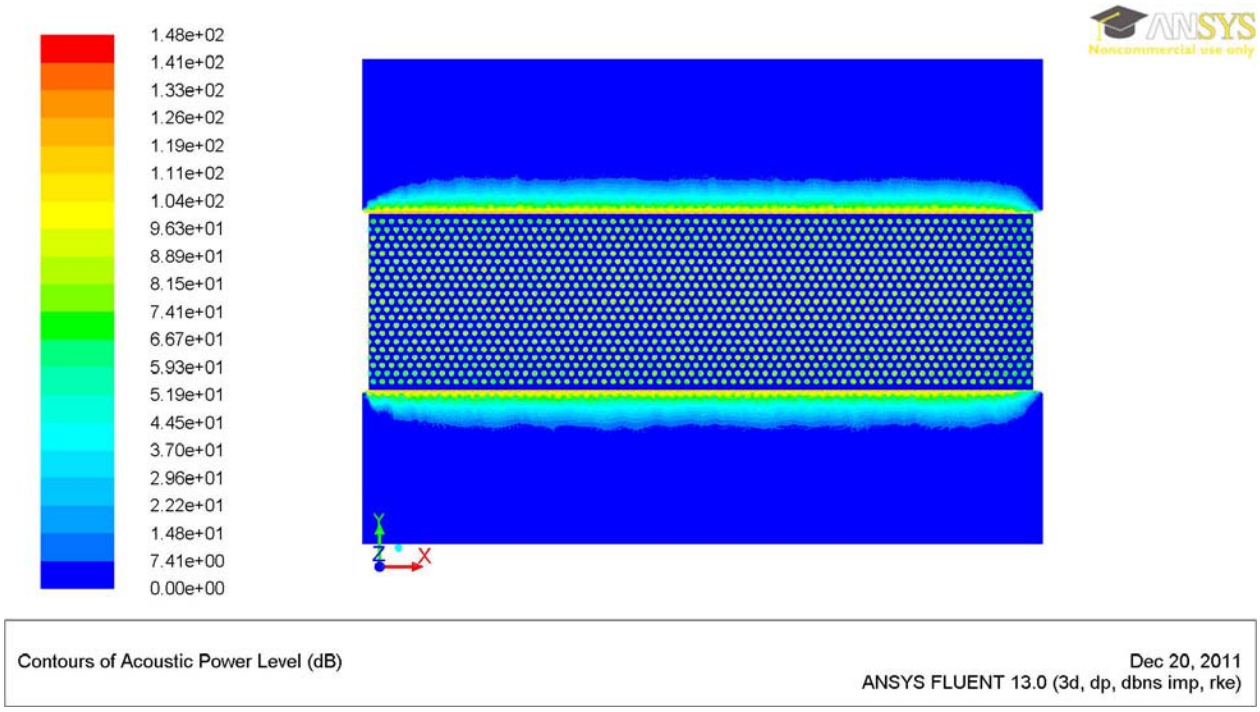

Figure A-12: Acoustic power level contour of silencer with 5" height and glass wool.

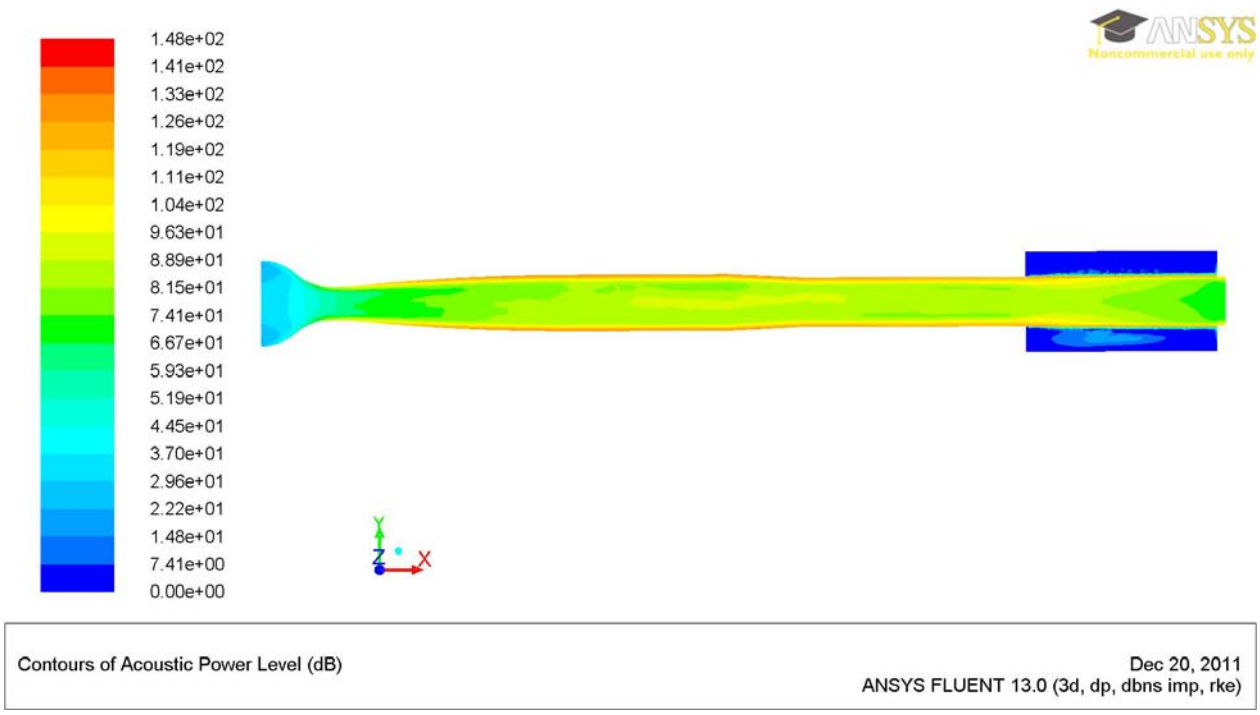

Figure A-13: Acoustic power level contour of tunnel with 3" silencer height and without glass wool.

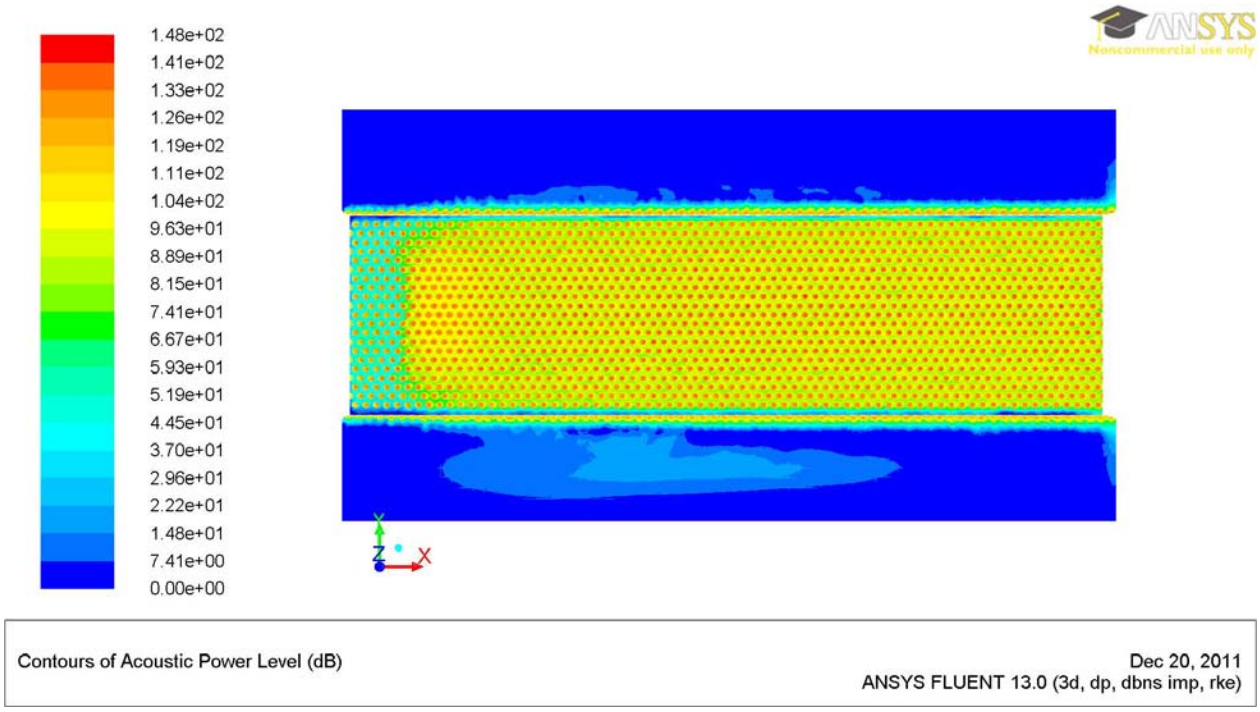

Figure A-14: Acoustic power level contour of silencer with 3" height and without glass wool.

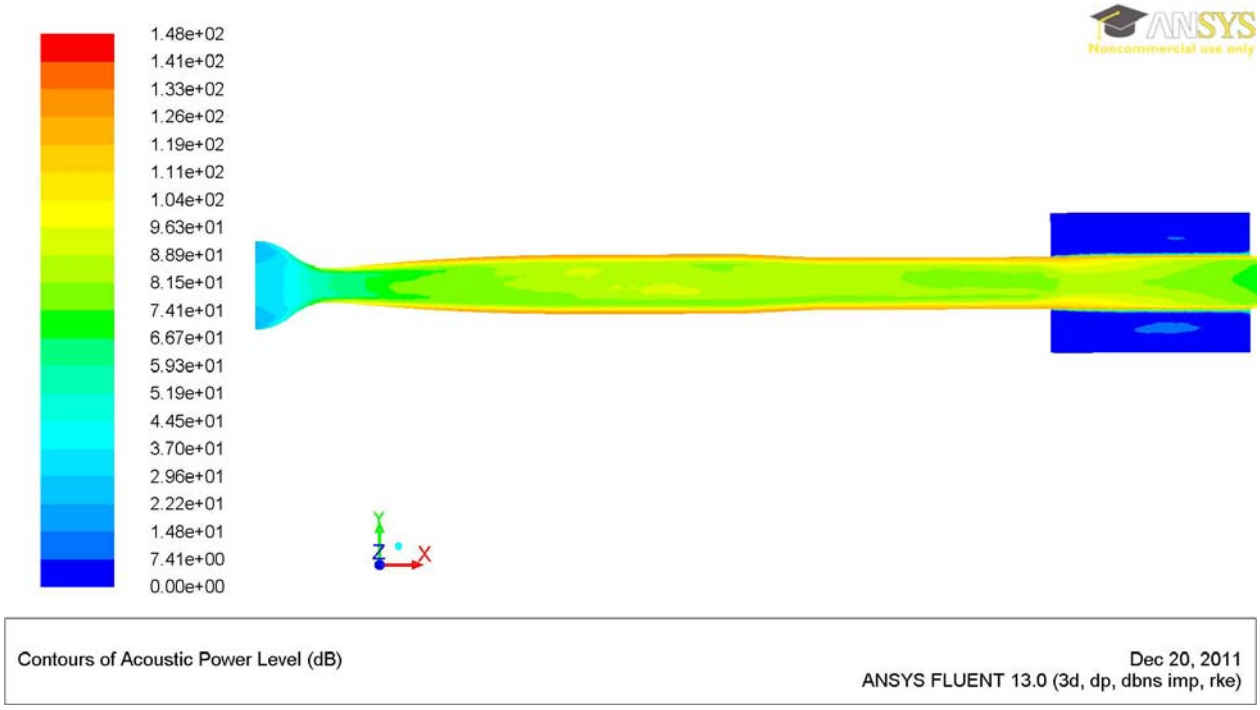

Figure A-15: Acoustic power level contour of tunnel with 5" silencer height and without glass wool.

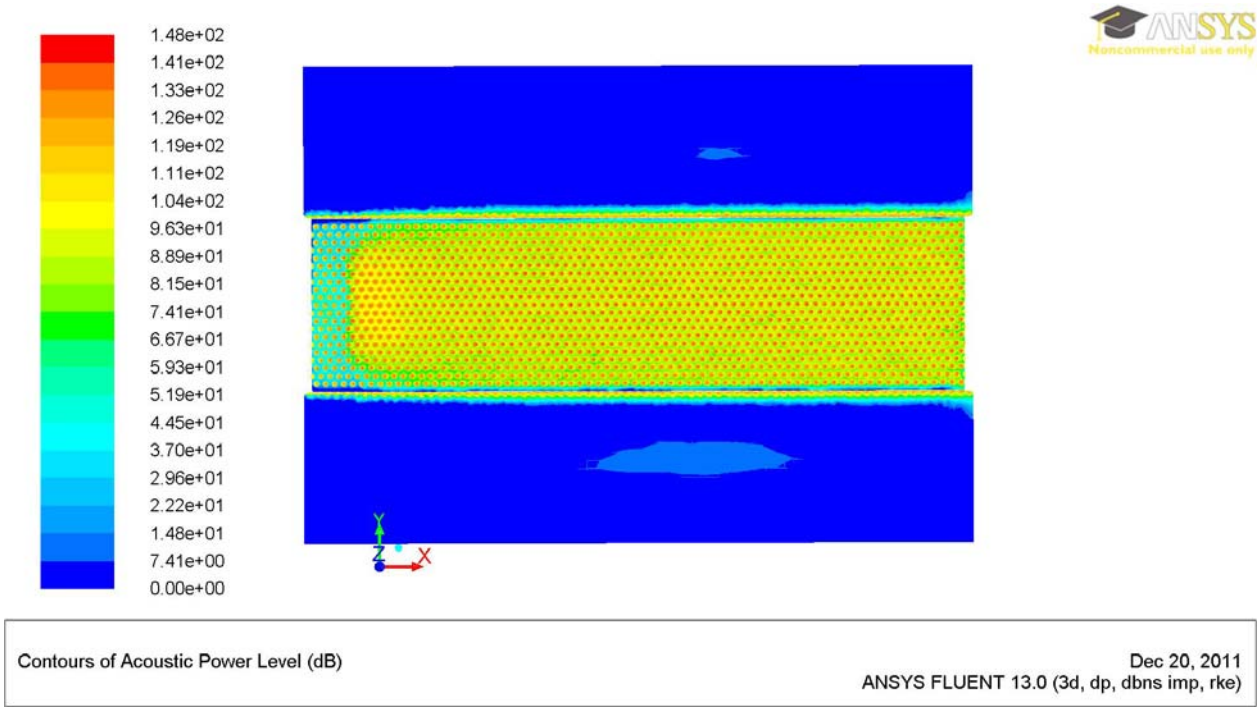

Figure A-16: Acoustic power level contour of silencer with 5" height and without glass wool.

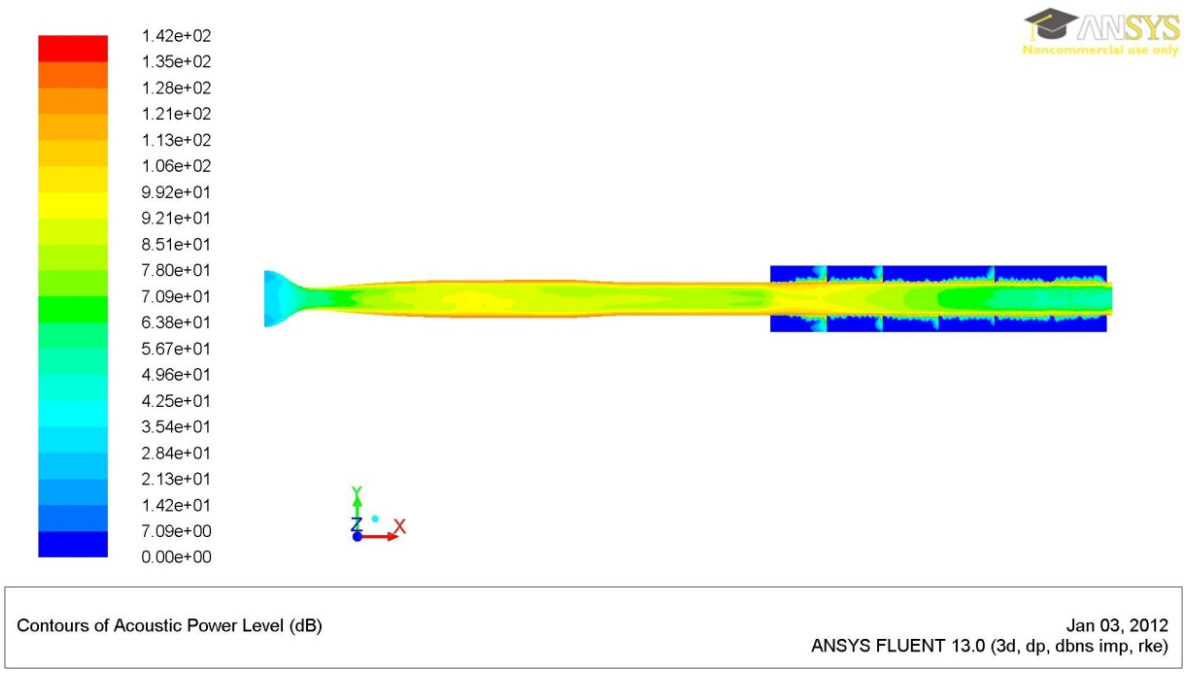

Figure A-17: Acoustic power level contour of wind tunnel with 6-10" silencer.

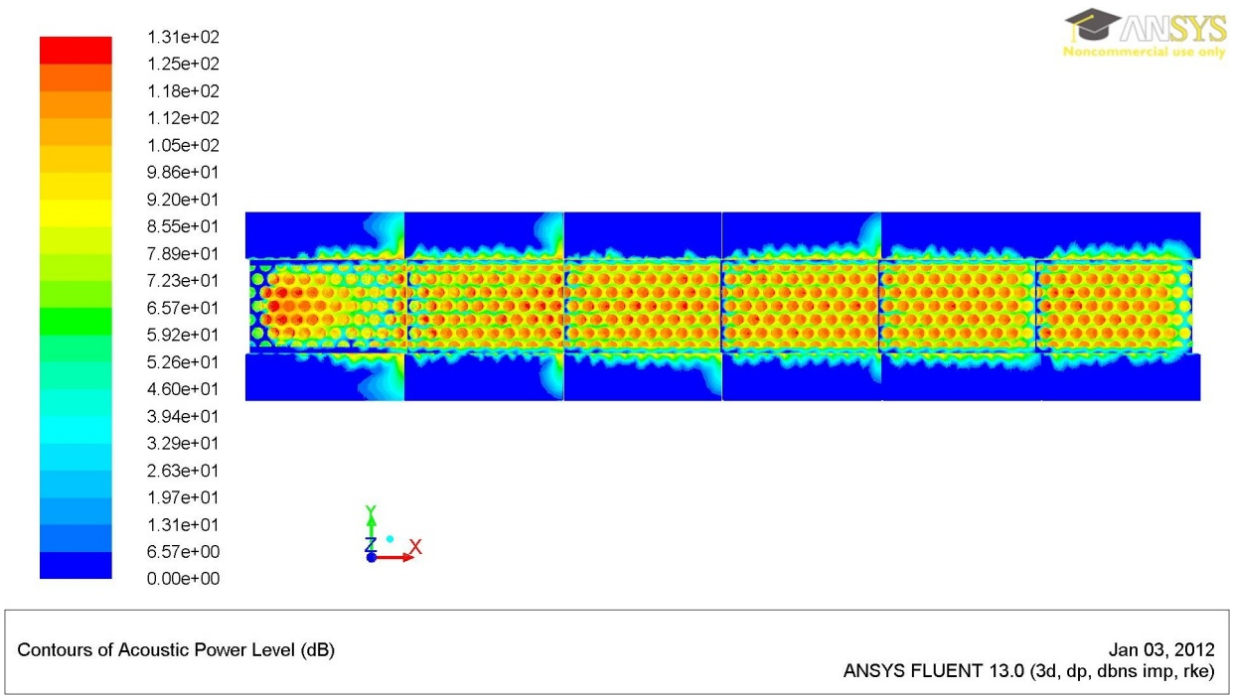

Figure A-18: Acoustic power level contour of 6-10" silencer.

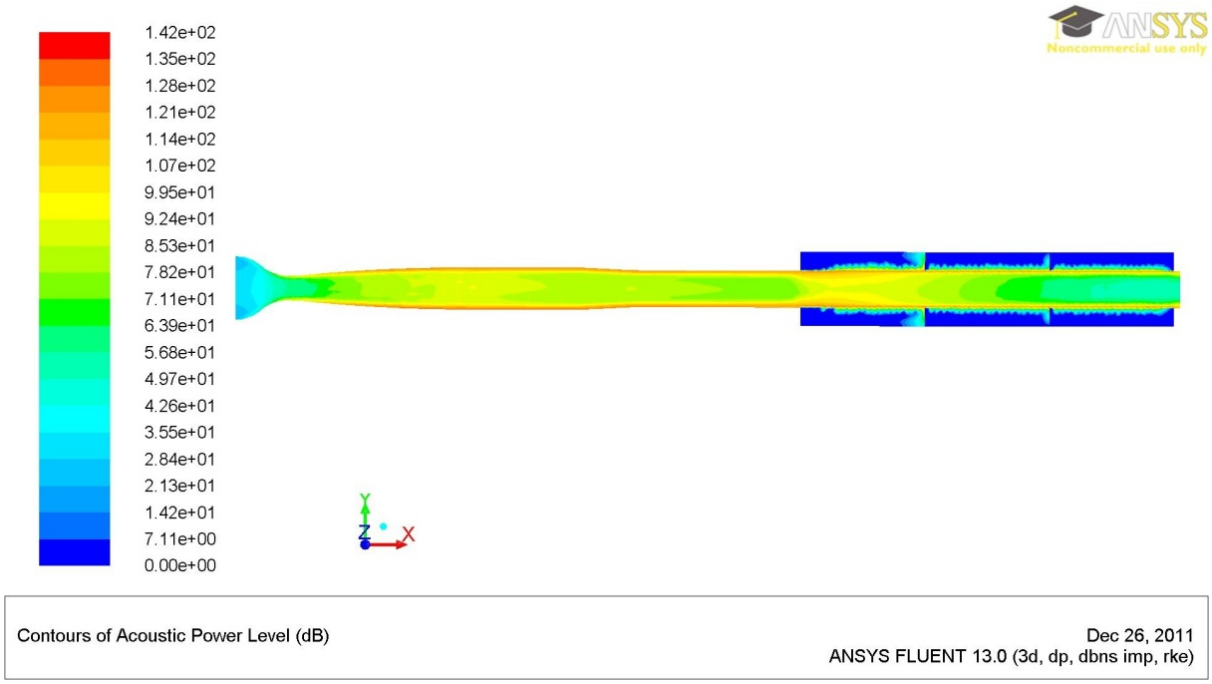

Figure A-19: Acoustic power level contour of wind tunnel with 3-20" silencer.

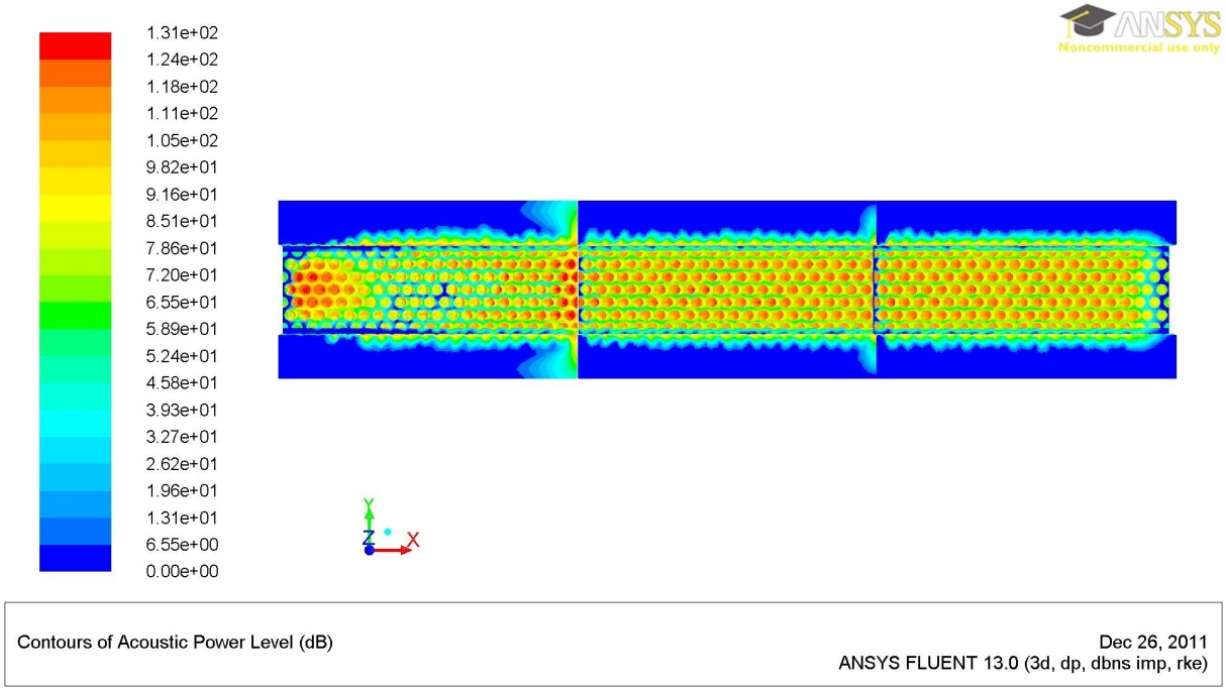

Figure A-20: Acoustic power level contour of 3-20" silencer.

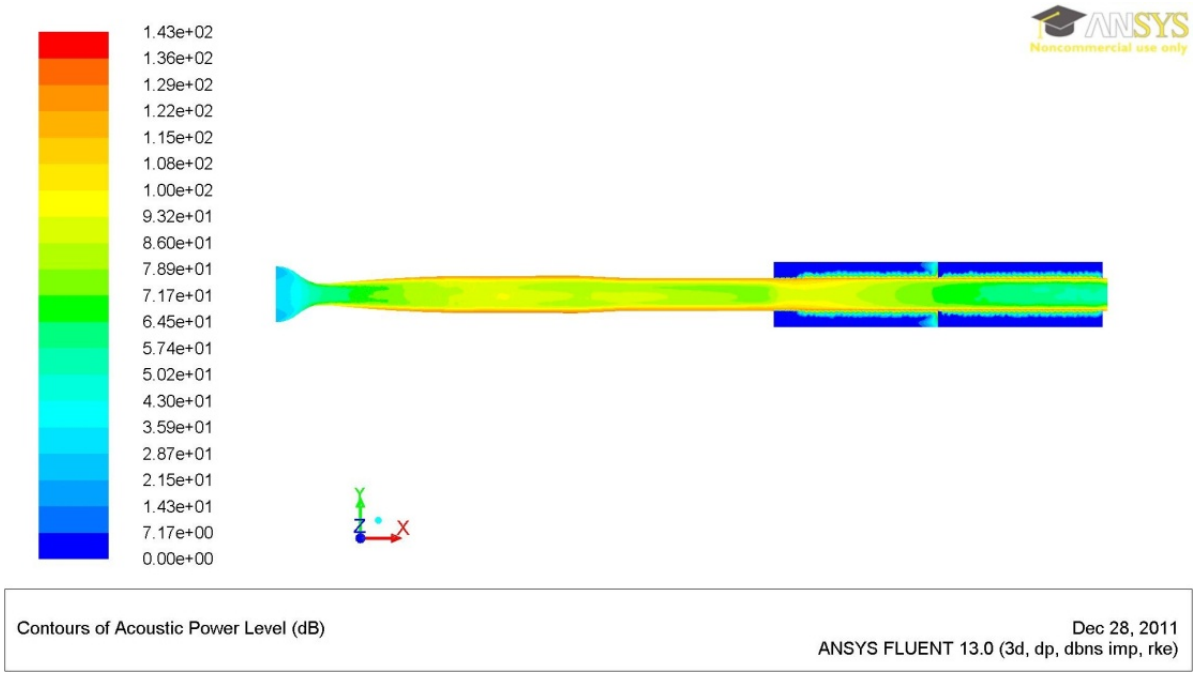

Figure A-21: Acoustic power level contour of wind tunnel with 2-30" silencer.

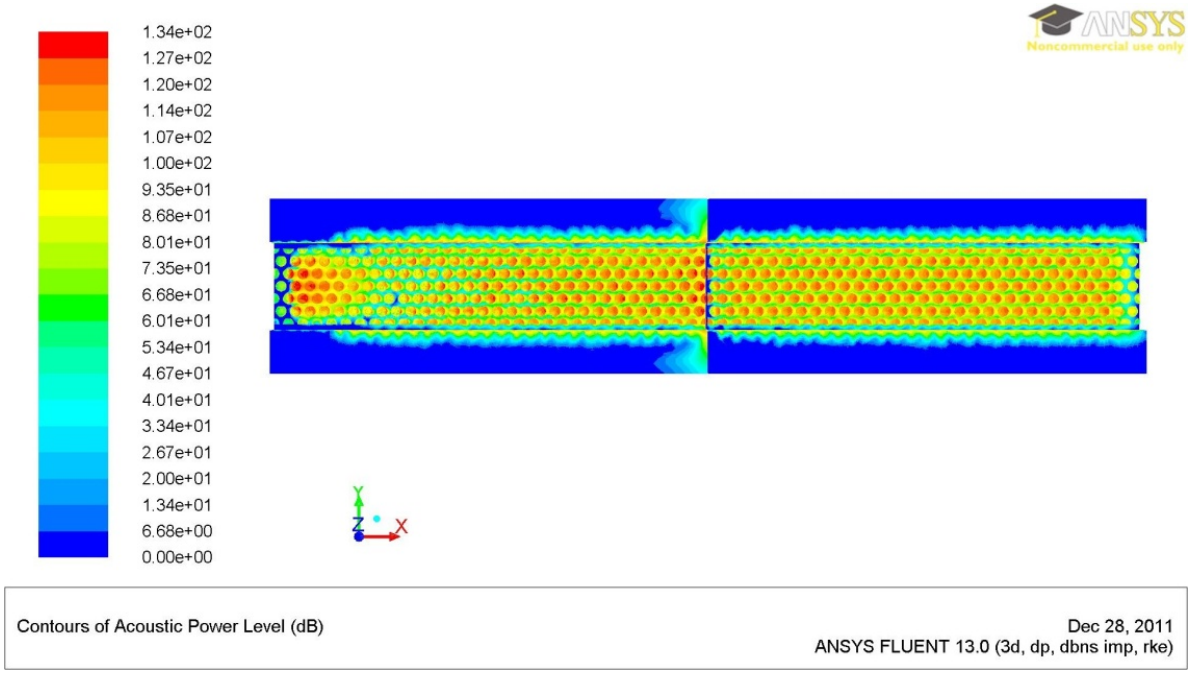

Figure A-22: Acoustic power level contour of 2-30" silencer.

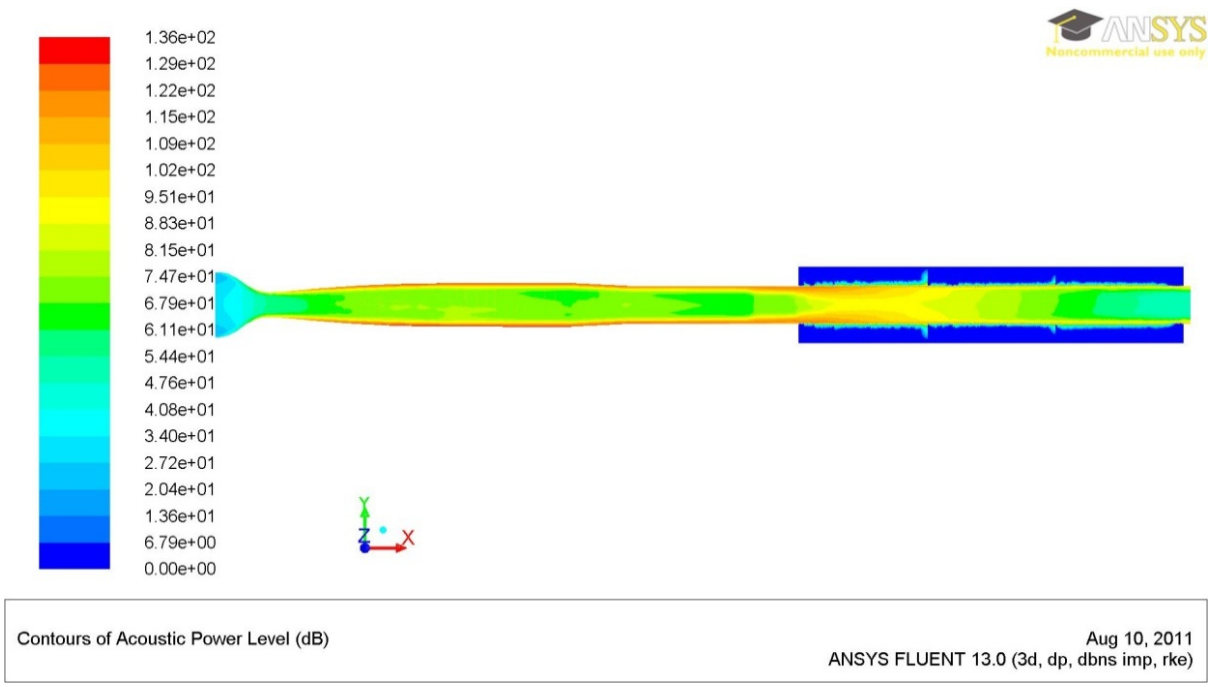

Figure A-23: Acoustic power level of 60" silencer.

Figure A-24: Mach contour of 60" silencer.

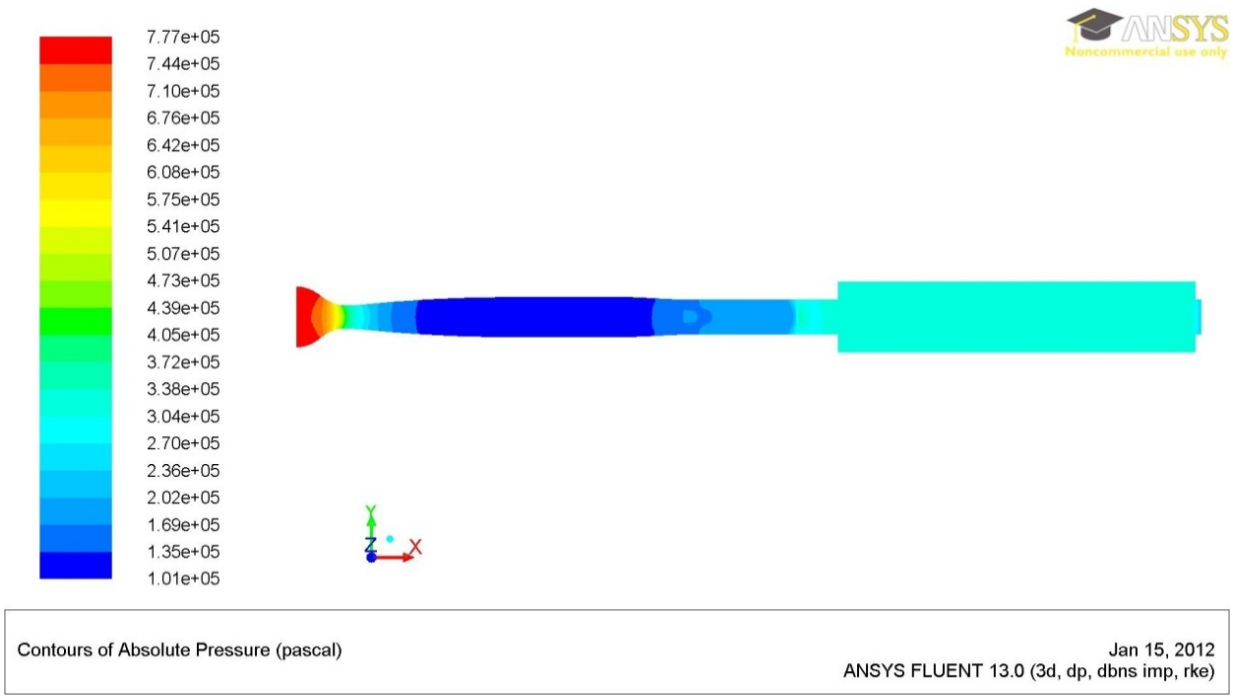

Figure A-25: Pressure contour of 60" silencer.

General		
	Solver	Density Based
Model		
	Energy	On
	Viscous	realizable k-epsilon (steady-state)
		DES realizable k-epsilon (transient)
	Acoustics	Broadband Noise Model (steady-state)
		FW&H (transient)
Material		
	Fluid-air	Density - ideal gas
Boundary Condition		
Zone	Inlet	Pressure - inlet
	Gauge total pressure	691441.8 Pa
	Turbulence - specification method	Intensity and hydraulic diameter
	Intensity	2%
	Hydraulic diameter	0.6096 m
Zone	Outlet	Pressure-outlet
	Turbulence-specification method	Intensity and hydraulic diameter
	Intensity	2%
	Hydraulic diameter	0.089 m
Solution Method		
	Spatial discretization - flow	First order upwind (steady state)
		Second order upwind (transient)
	Transient formulation	Second order implicit
Solution Control		
	Courant number	1
Limits	Maximum absolute pressure	1,500,000 Pa
	Maximum static temperature	1000 K
	Maximum turbulent viscosity ratio	1,000,000

Table A-18: Modified settings used for simulations.

Appendix B - Calculations

Richardson's extrapolation equation (36)

$$R(j,k) = \frac{2^k R(j,k-1) - R(j-1,k-1)}{2^k - 1} \quad \text{(B.1)}$$

At plane 0.1m offset of the outlet

Given from CFD results:

R(0,0) = 91.28521

R(1,0) = 102.0563

R(2,0) = 109.44366

	$O(h^2)$	$O(h^2)$	$O(h^3)$
	R(j,0)	R(j,1)	R(j,2)
0	91.28521	x	x
1	102.0563	112.82739	x
2	109.44366	116.93102	118.16556

At outlet plane

Given from CFD results:

R(0,0) = 88.089211

R(1,0) = 99.033379

R(2,0) = 106.74712

	$O(h^2)$	$O(h^2)$	$O(h^3)$
	R(j,0)	R(j,1)	R(j,2)
0	88.089211	x	x
1	99.033379	109.977547	x
2	106.74712	114.460861	115.955299

Maximum APL

Given from CFD results:

R(0,0) = 141.5895

R(1,0) = 157.6376

R(2,0) = 158.1396

	$O(h^2)$	$O(h^2)$	$O(h^3)$
	R(j,0)	R(j,1)	R(j,2)
0	141.5895	x	x
1	157.6376	173.6857	x
2	158.1396	158.6416	153.6269

Calculation of Head Loss

The pressure loss could be calculated using the following equation (37):

$$\Delta p = \rho g h_f \quad \text{(B.2)}$$

$$h_f = fr \frac{L}{d} \frac{V^2}{2g} \quad \text{(B.3)}$$

Hydraulic diameter

$$d = \frac{4A}{P} \quad \text{(B.4)}$$

$$d = \frac{4 \times 4 \times 2.977 \times 1.2402}{4 \times (2.977 + 1.2402)} = 3.5019\ in = 0.089\ m$$

$$f = fn\ (Re, \frac{\varepsilon}{d})$$

$$for\ aluminum\ \varepsilon = 0.000002\ m$$

$$\frac{\varepsilon}{d} = 0.000025$$

$$from\ CFD\ results\ at\ beginning\ of\ constant\ cross\ section\ in\ diffuser$$

$$V = 444.45\ \frac{m}{s} \quad , T = 313.99\ K \quad , \rho = 2.14\ kg/m^3$$

$$dynamic\ viscosity\ of\ air\ at\ 314\ K = \mu = 0.00002009\ {}^{kg}/_{m\ s}$$

Reynolds number

$$Re = \frac{\rho V d}{\mu} \quad \text{(B.5)}$$

$$Re = \frac{2.14 \times 444.5 \times 0.089}{0.00002009} = 4.21 \times 10^6$$

$$from\ Moody\ chart, fr \approx 0.011$$

To calculate length of diffuser required

$$L = \frac{2\ d\ \Delta p}{\rho\ f\ V^2} \quad \text{(B.6)}$$

$$L = \frac{2 \times 0.089 \times 40354}{2.14 \times 0.011 \times 444.5^2} = 1.54\ m$$

Appendix C – Revised Baseline Wind Tunnel CFD results

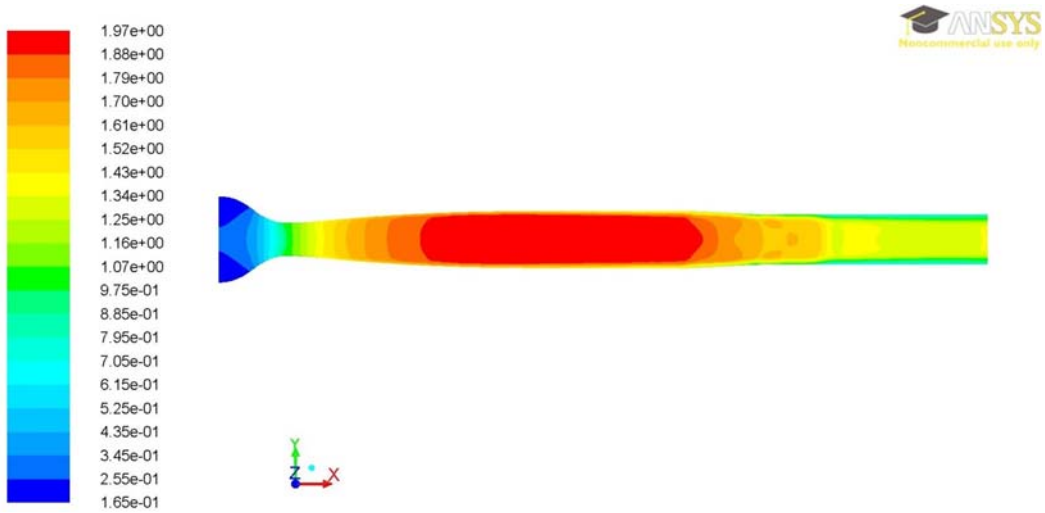

Figure C-1: Mach contour plot of wind tunnel without mixing chamber and silencer.

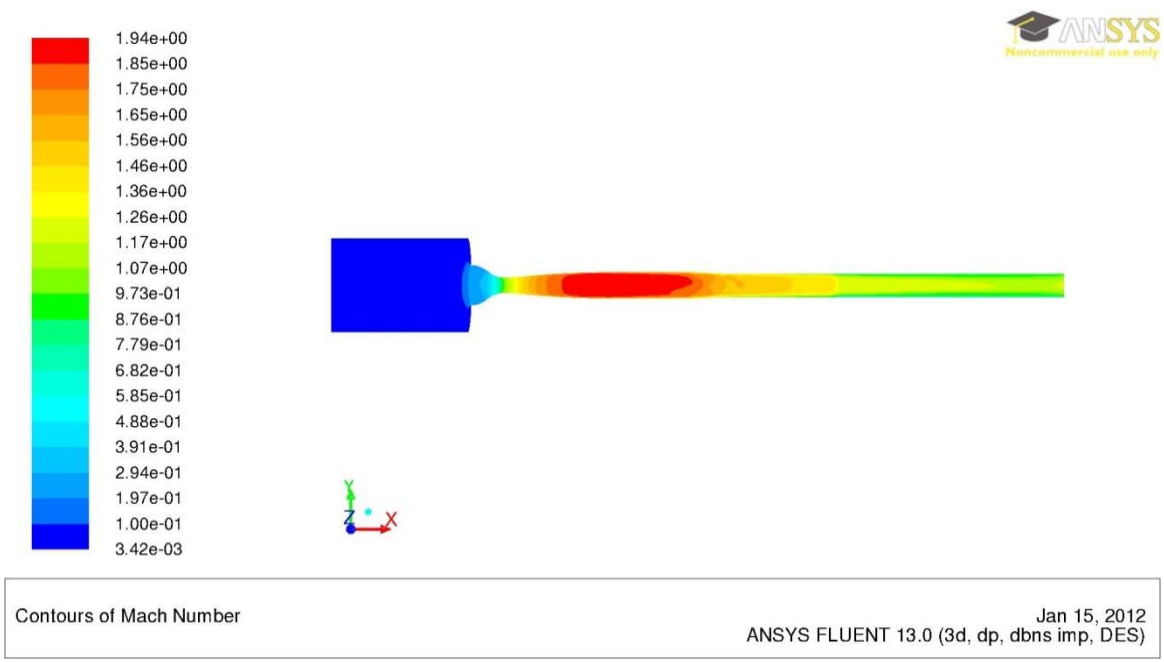

Figure C-2: Existing baseline wind tunnel with 60" extension Mach contour plot.

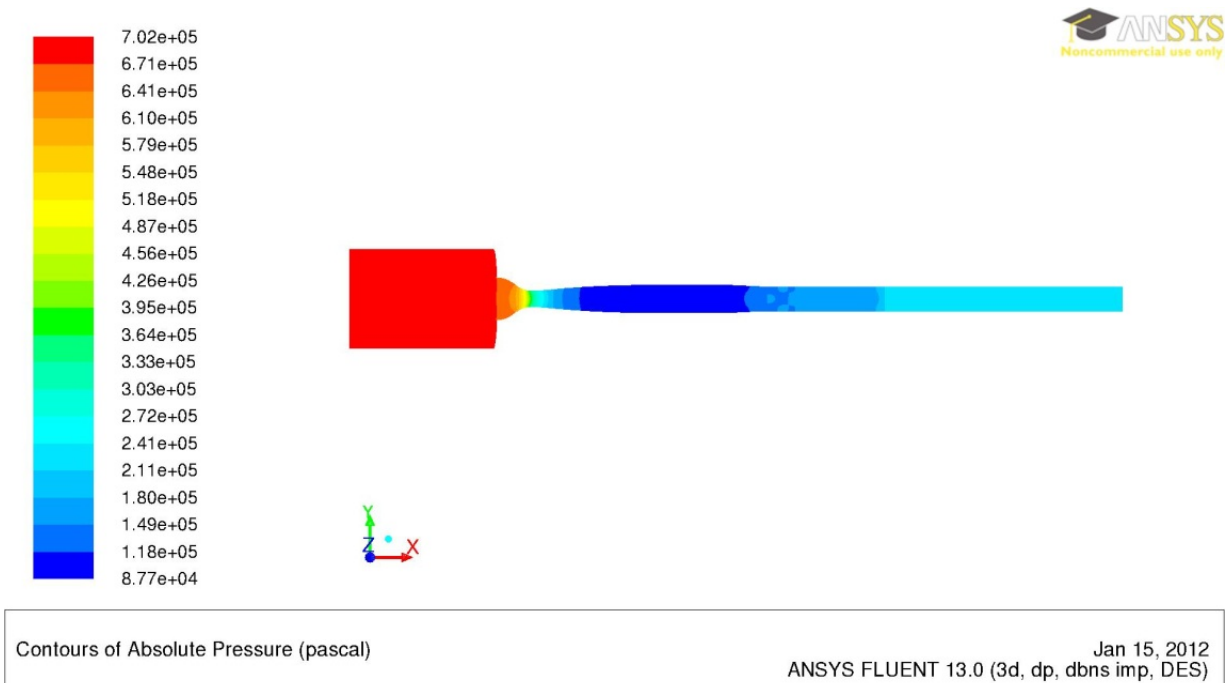

Figure C-3: Existing baseline wind tunnel with 60" extension pressure contour plot.

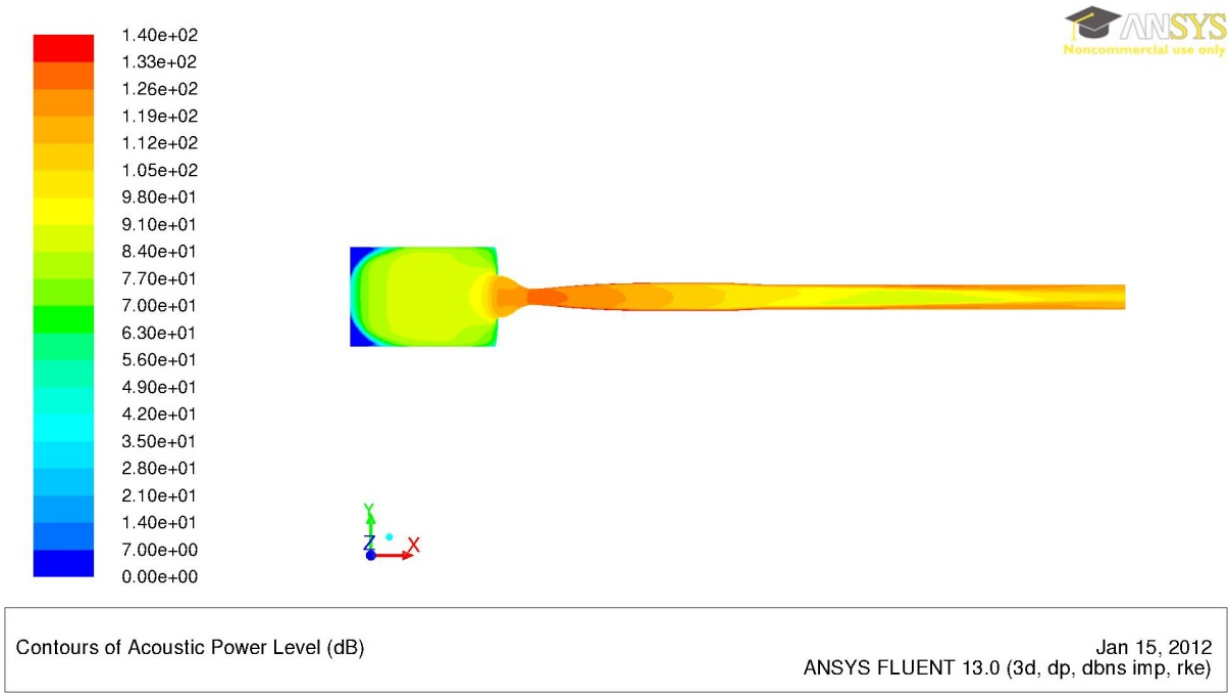

Figure C-4: Existing baseline wind tunnel with 60" extension acoustic power level contour plot.

Figure C-5: Existing baseline wind tunnel with 60" extension acoustic power level contour plot of extended diffuser.

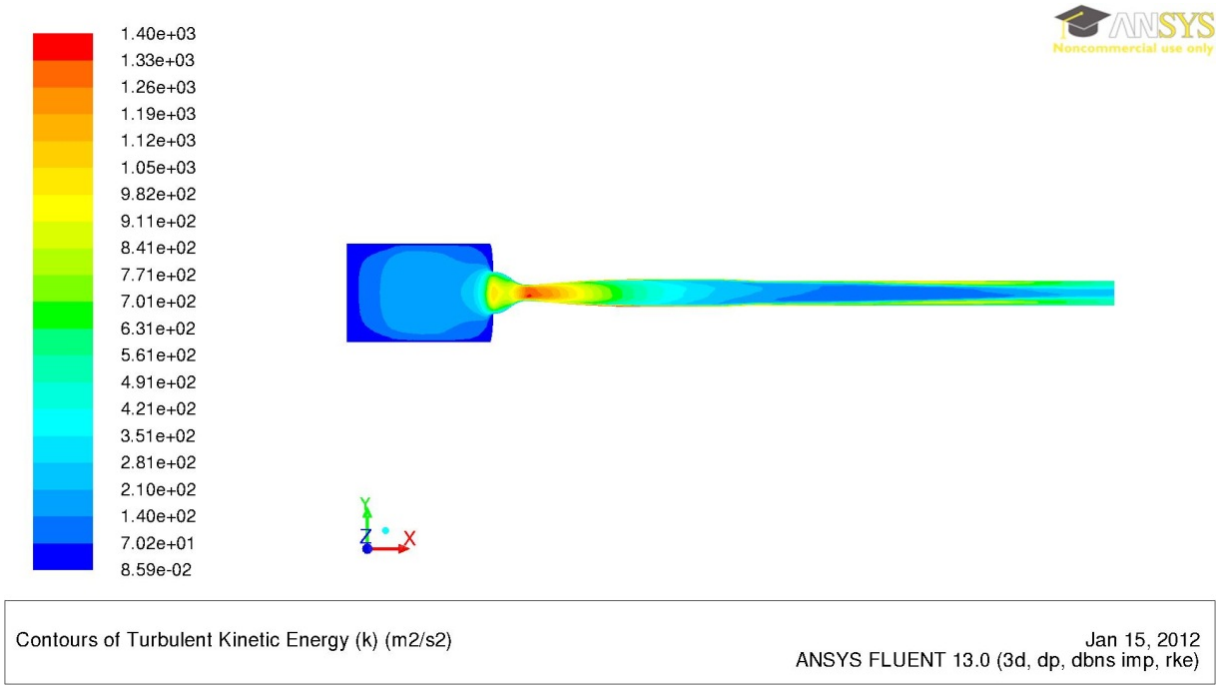

Figure C-6: Existing baseline wind tunnel with 60" extension turbulent kinetic energy contour plot.

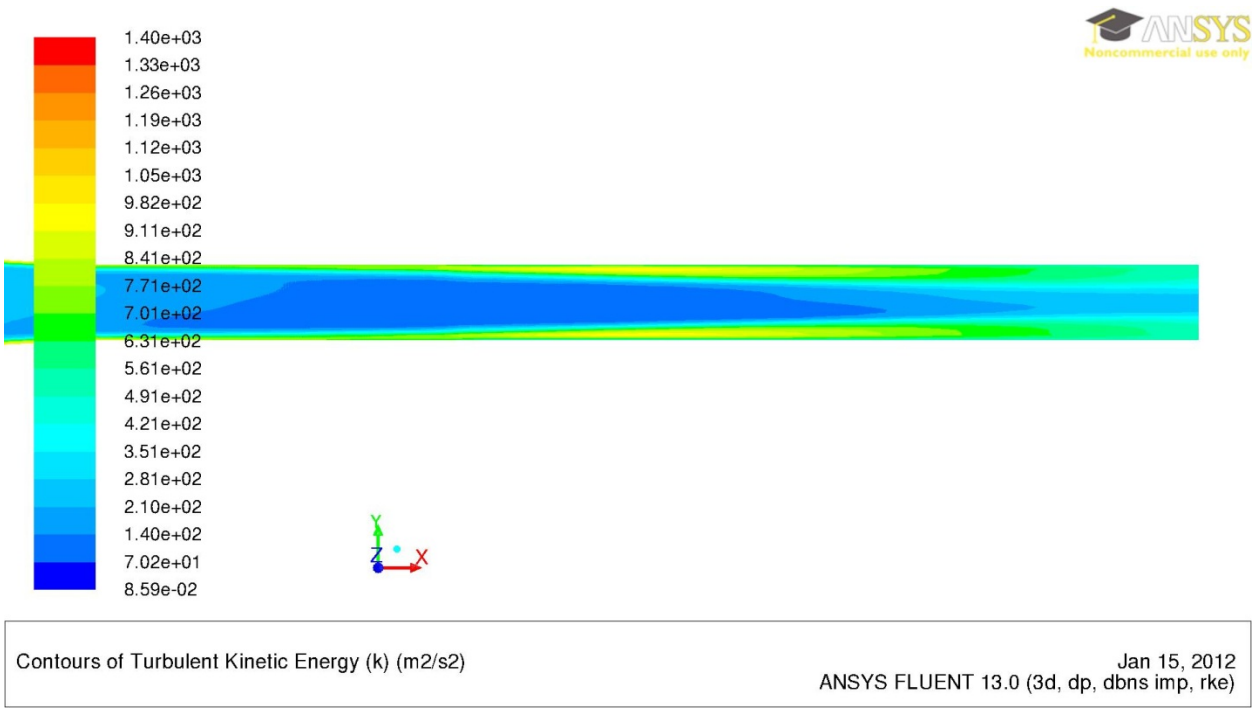

Figure C-7: Existing baseline wind tunnel with 60" extension turbulent kinetic energy contour plot of extended diffuser.

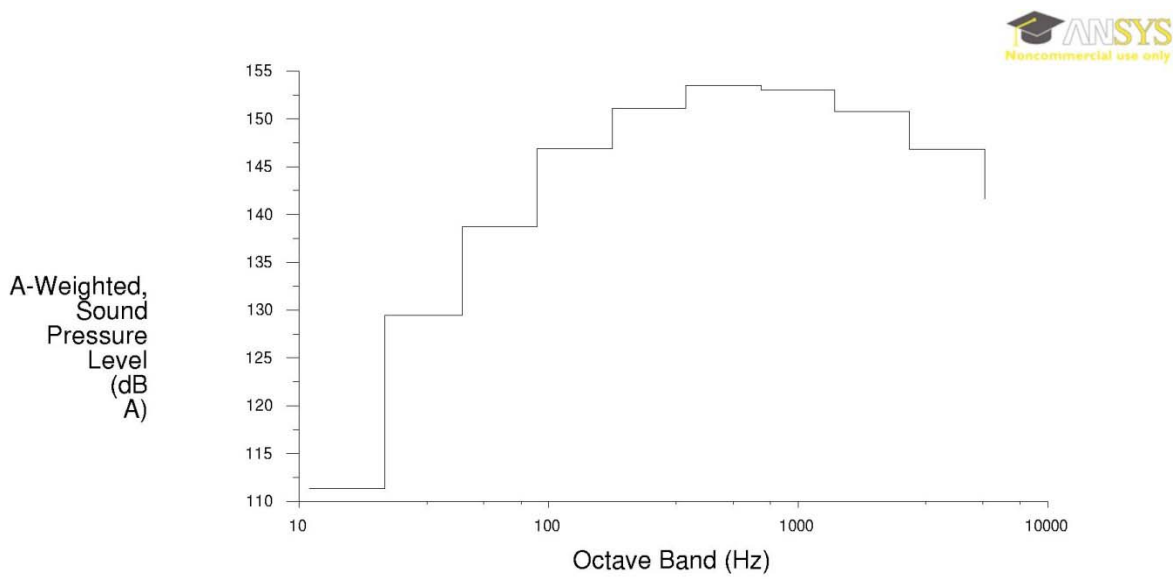

Figure C-8: A-weighted sound pressure level at receiver 1 of baseline wind tunnel with extended diffuser.

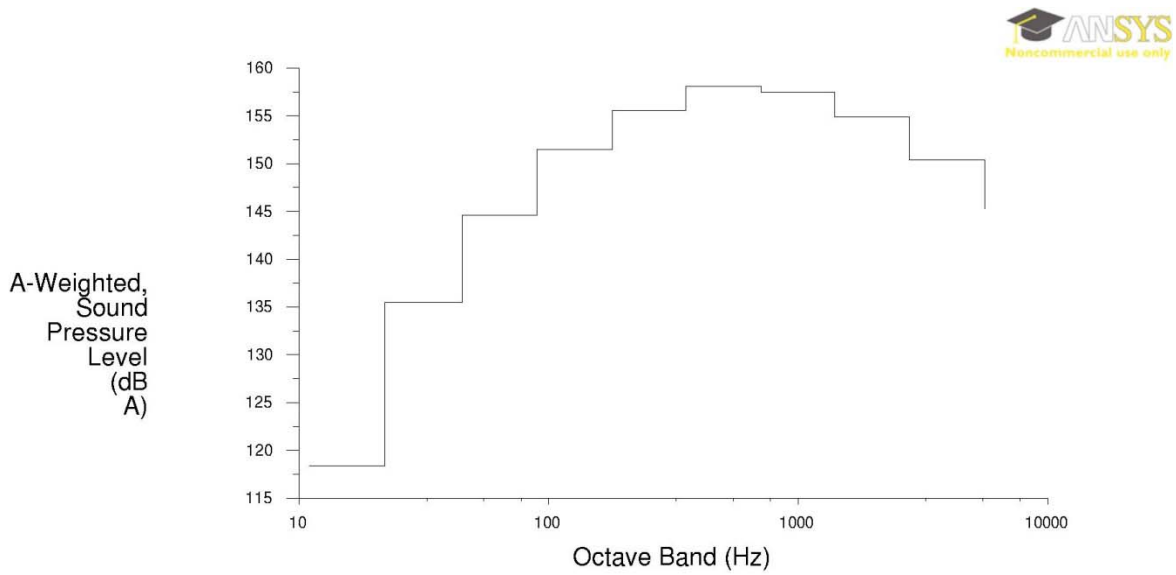

Figure C-9: A-weighted sound pressure level at receiver 2 of baseline wind tunnel with extended diffuser.

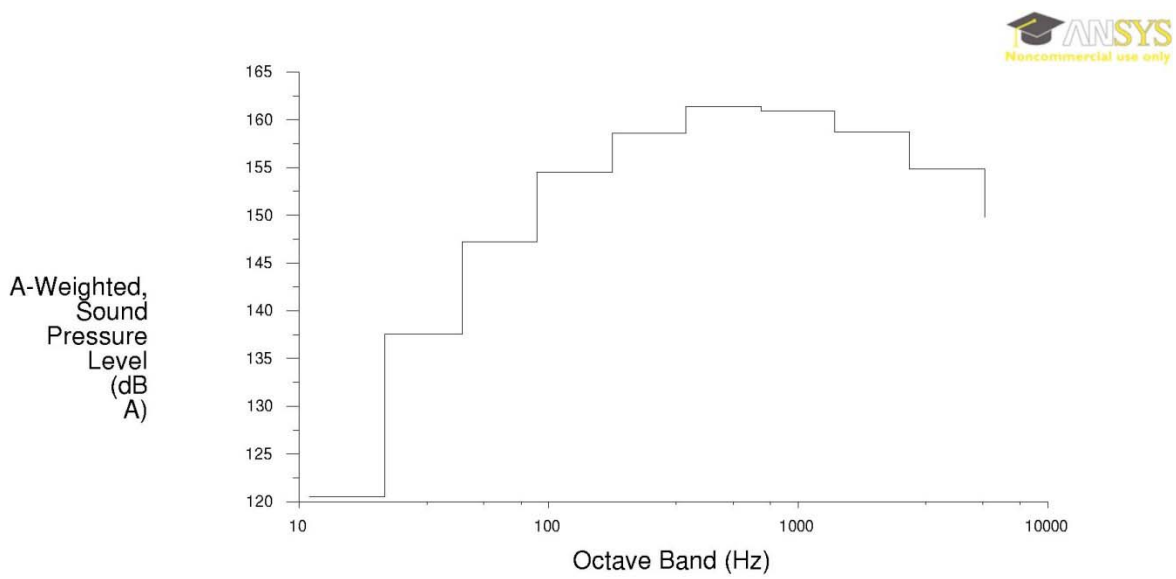

Figure C-10: A-weighted sound pressure level at receiver 3 of baseline wind tunnel with extended diffuser.

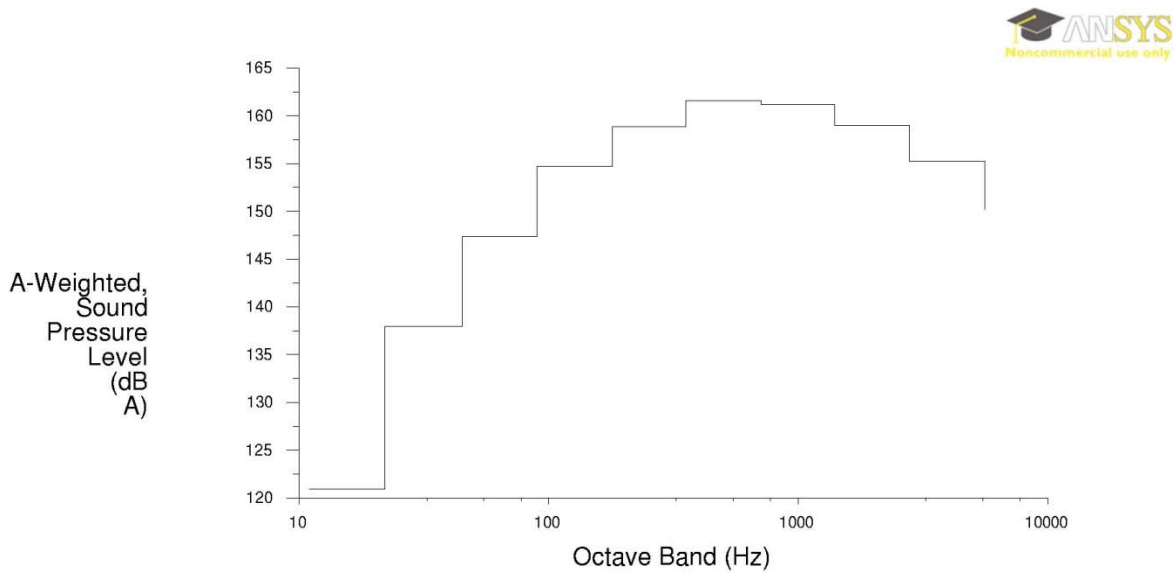

Figure C-11: A-weighted sound pressure level at receiver 4 of baseline wind tunnel with extended diffuser.

Appendix D – Final Design CFD results

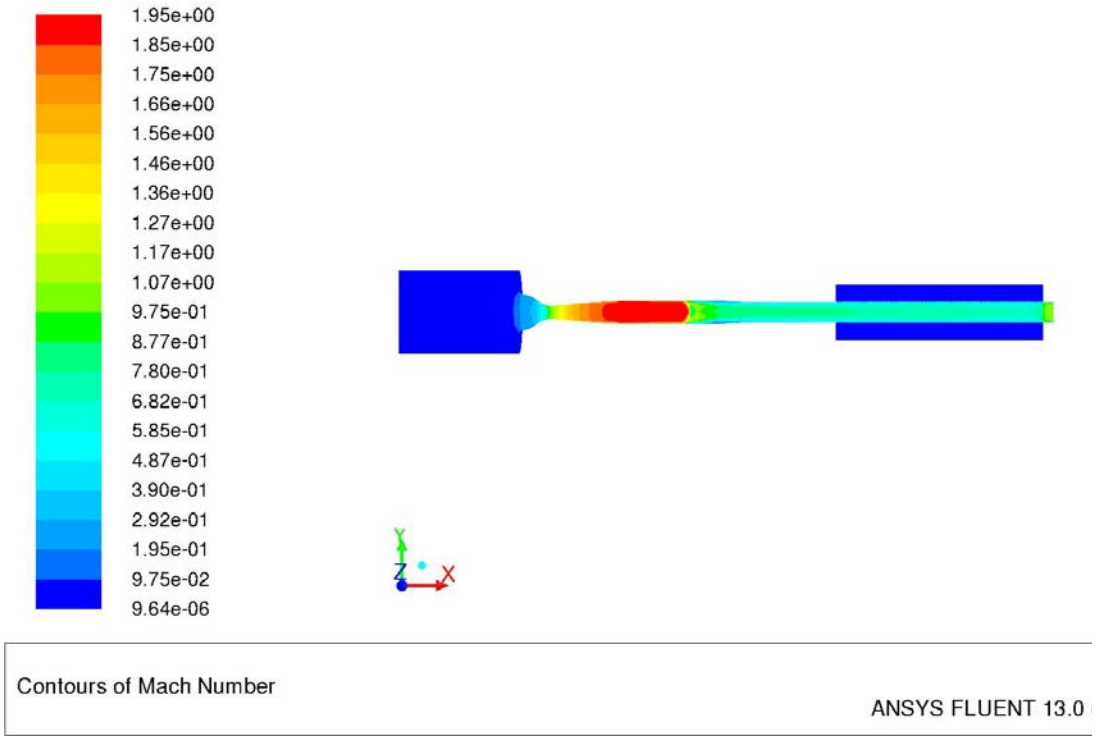

Figure D-1: Mach number contour of wind tunnel and silencer.

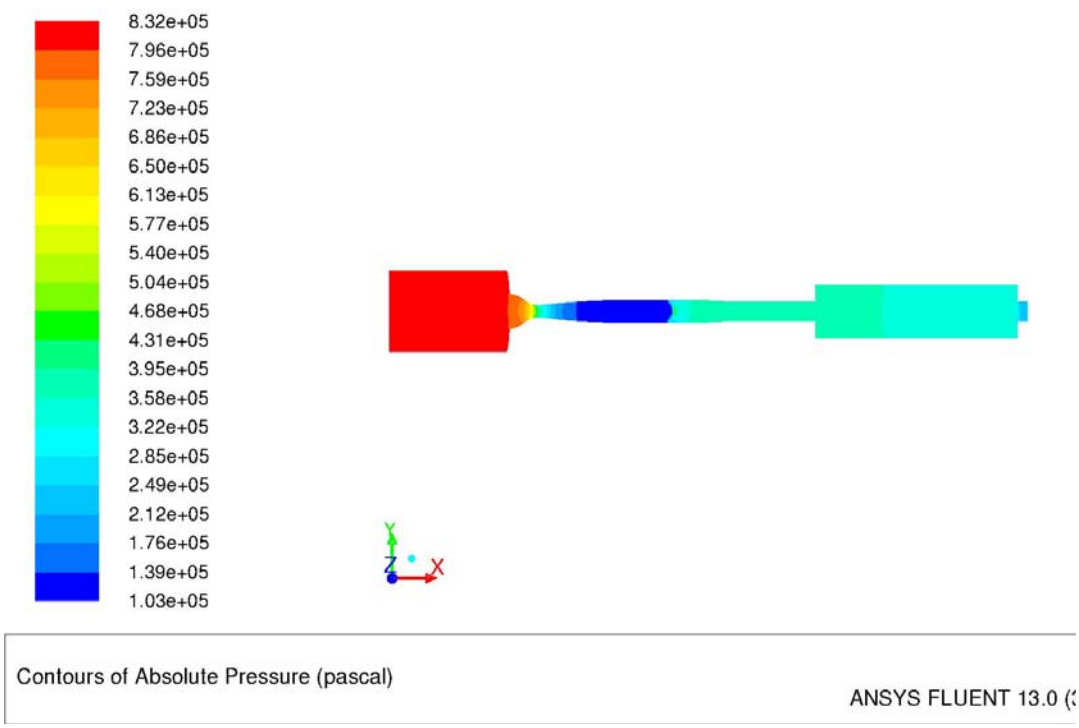

Figure D-2: Absolute pressure contour of wind tunnel and silencer.

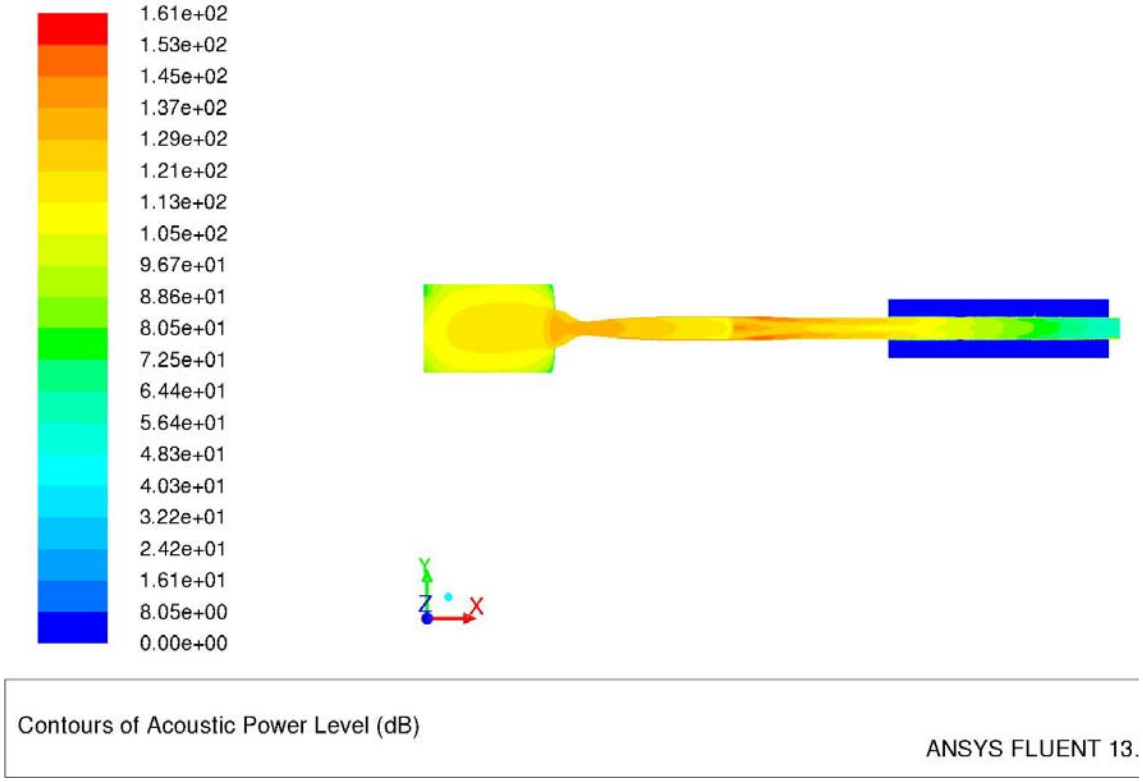

Figure D-3: Acoustic power level contour of wind tunnel and silencer.

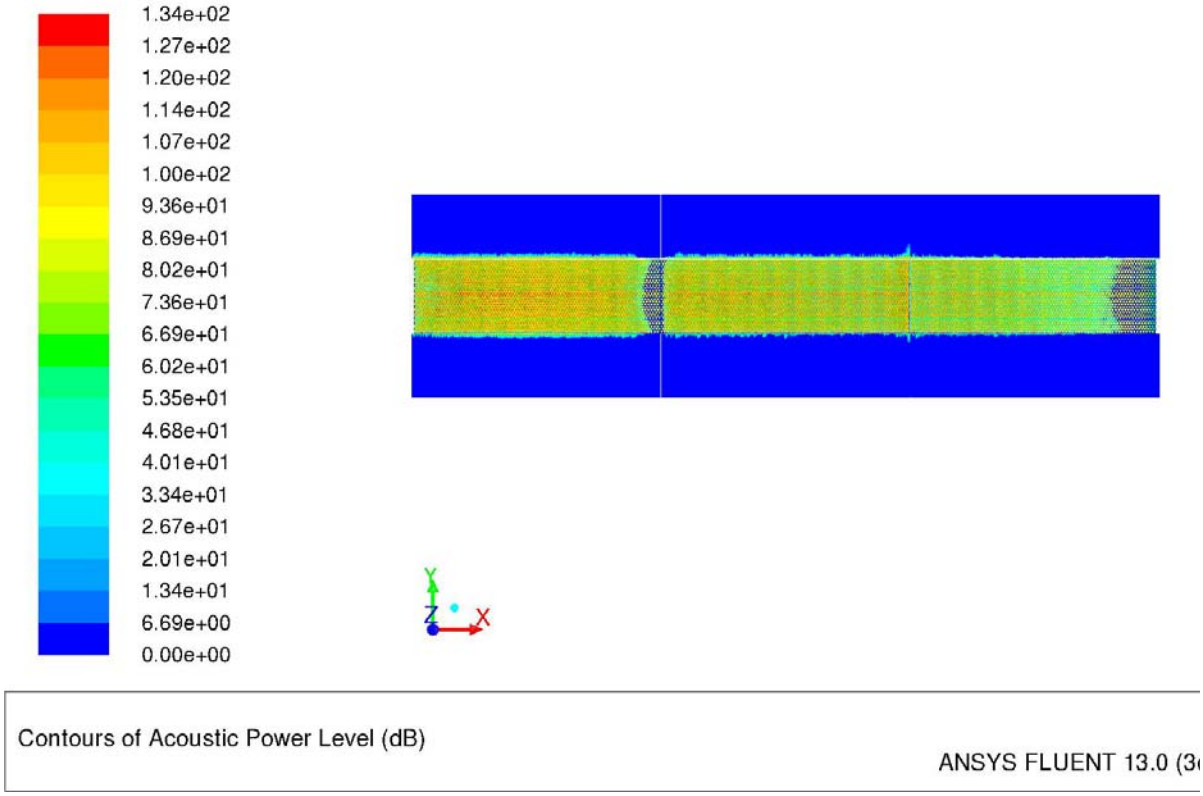

Figure D-4: Acoustic power level contour of silencer.

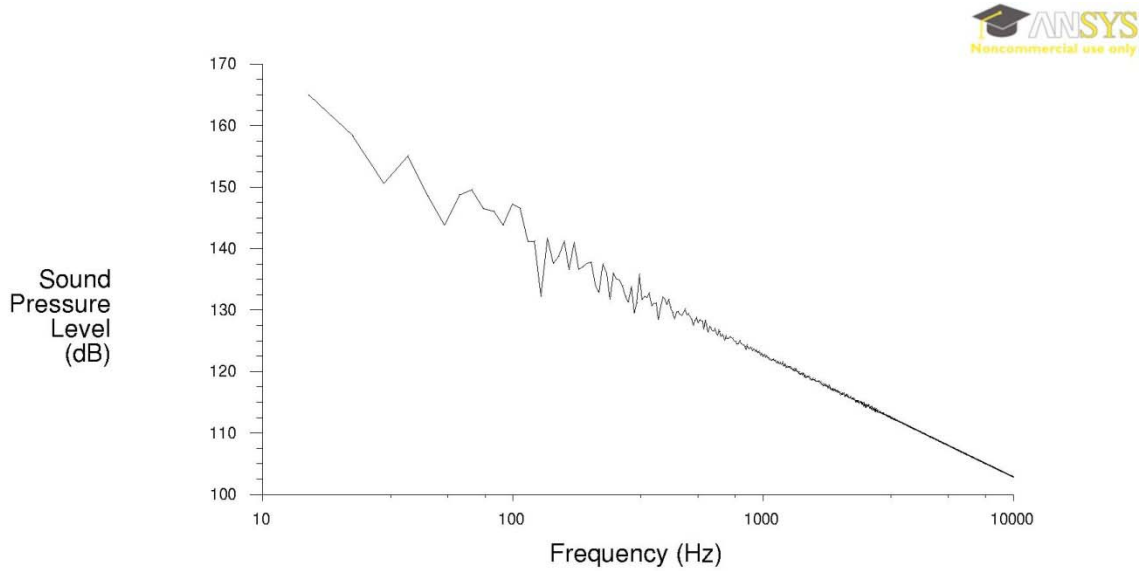

Figure D-5: Sound pressure level at receiver 1 with acoustic treatment.

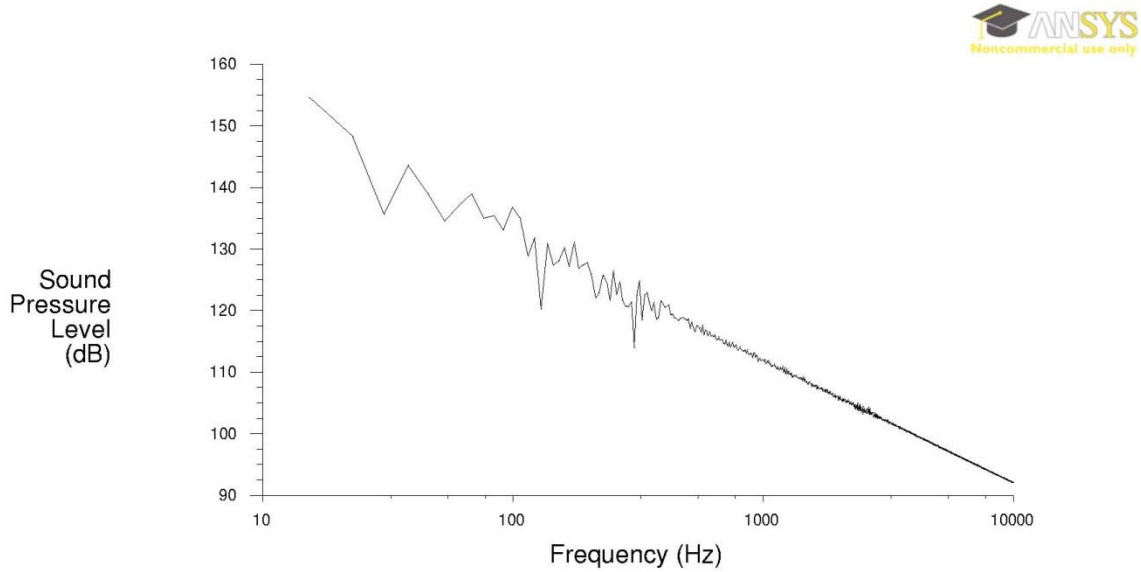

Figure D-6: Sound pressure level at receiver 2 with acoustic treatment.

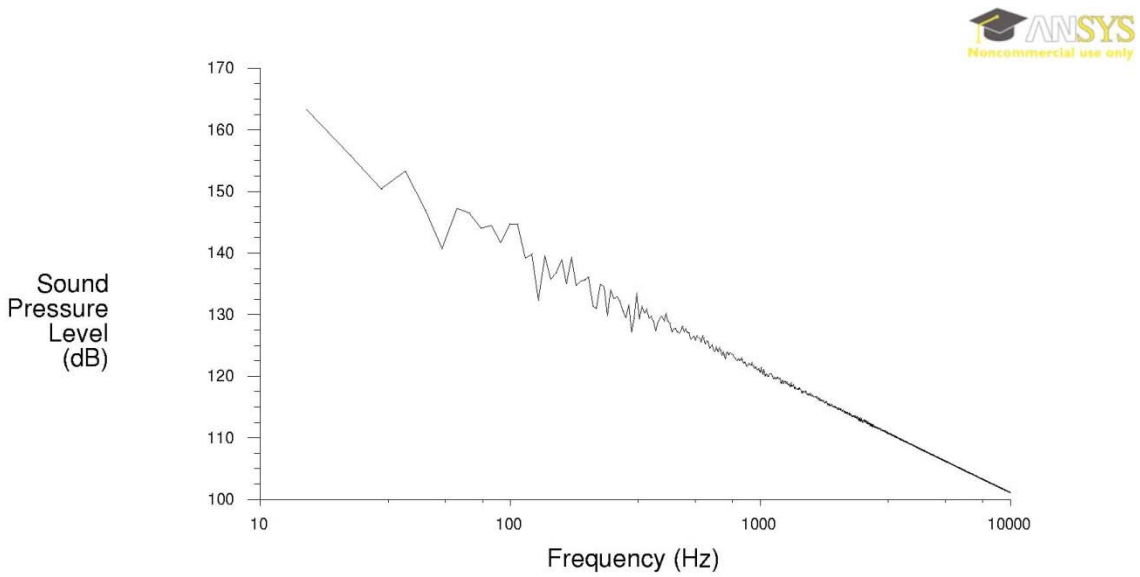

Figure D-7: Sound pressure level at receiver 3 with acoustic treatment.

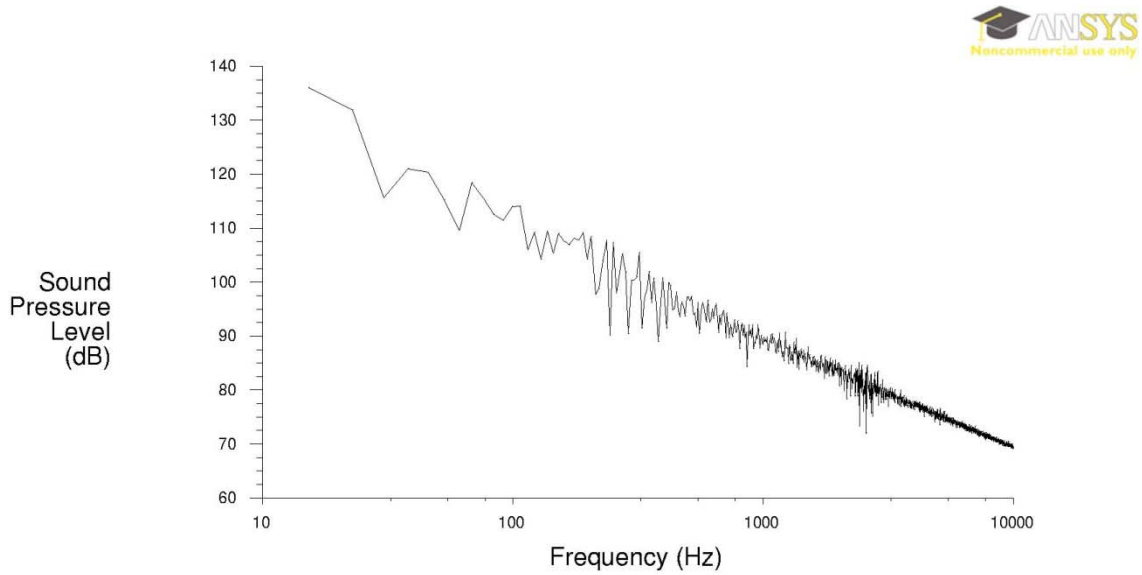

Figure D-8: Sound pressure level at receiver 4 with acoustic treatment.

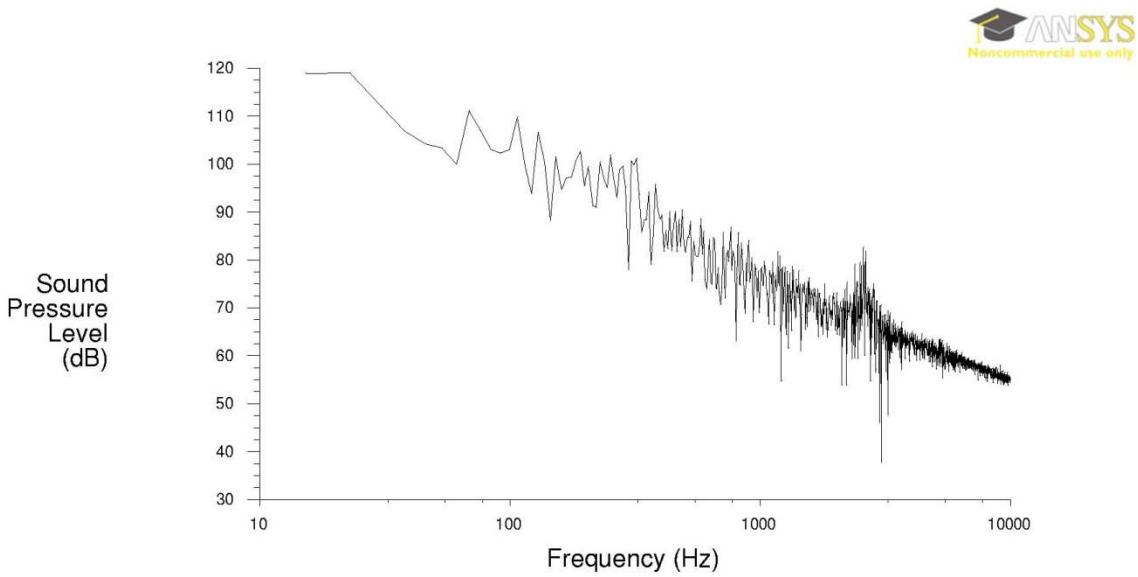

Figure D-9: Sound pressure level at receiver 5 with acoustic treatment.

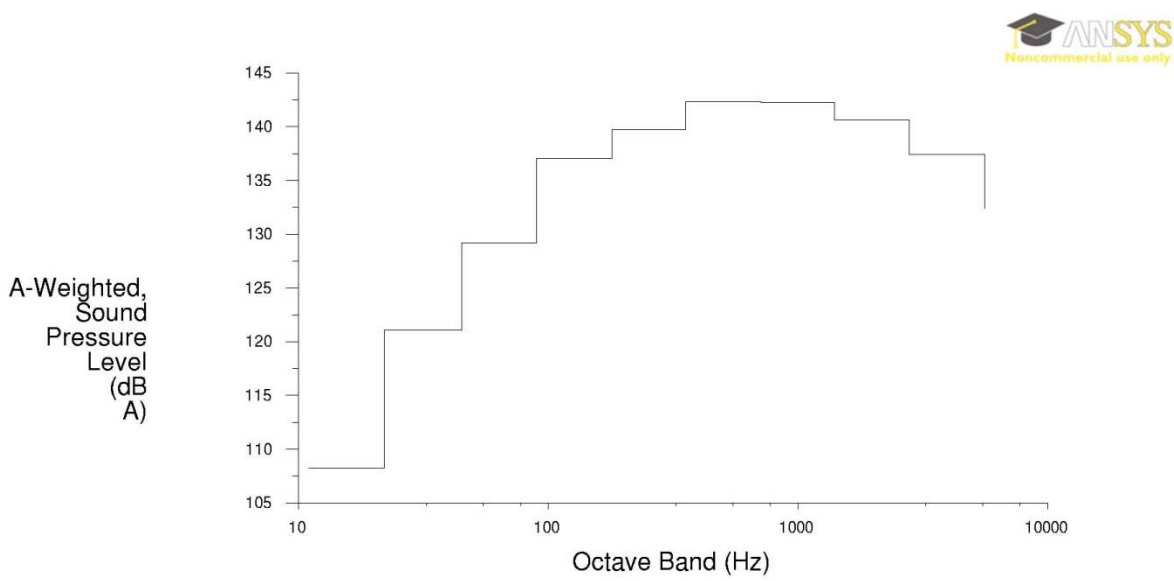

Figure D-10: A-weighted sound pressure level at receiver 1 with acoustic treatment.

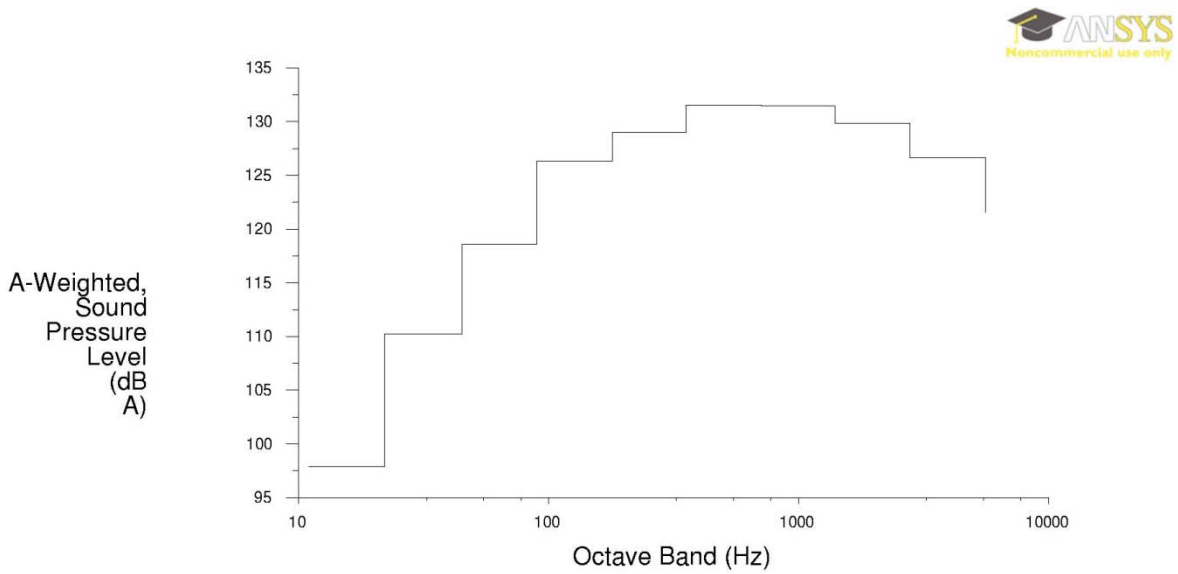

Figure D-11: A-weighted sound pressure level at receiver 2 with acoustic treatment.

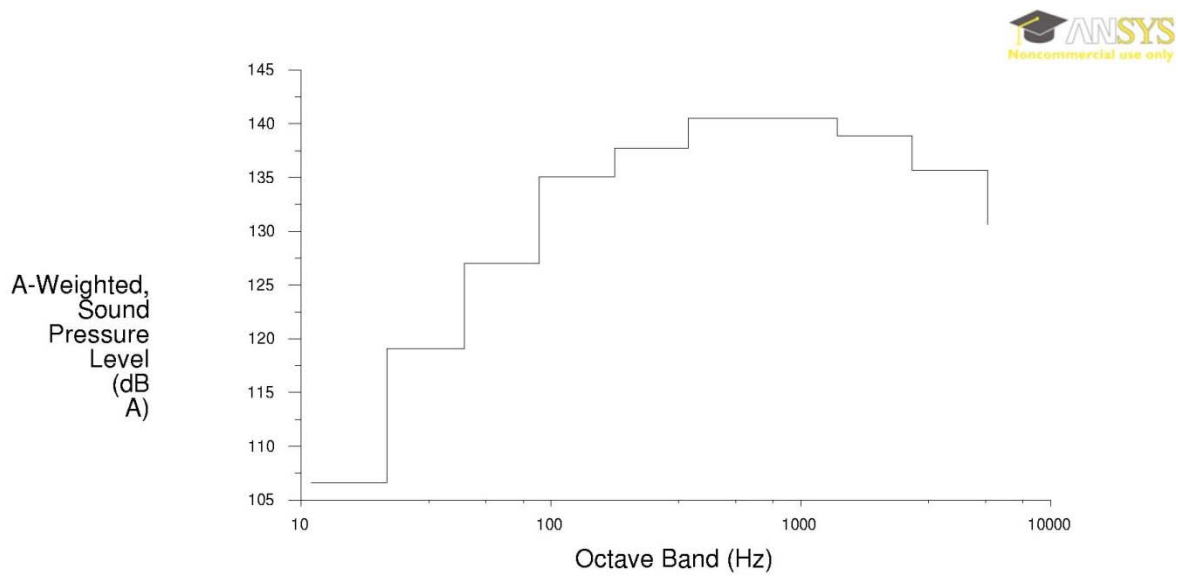

Figure D-12: A-weighted sound pressure level at receiver 3 with acoustic treatment.

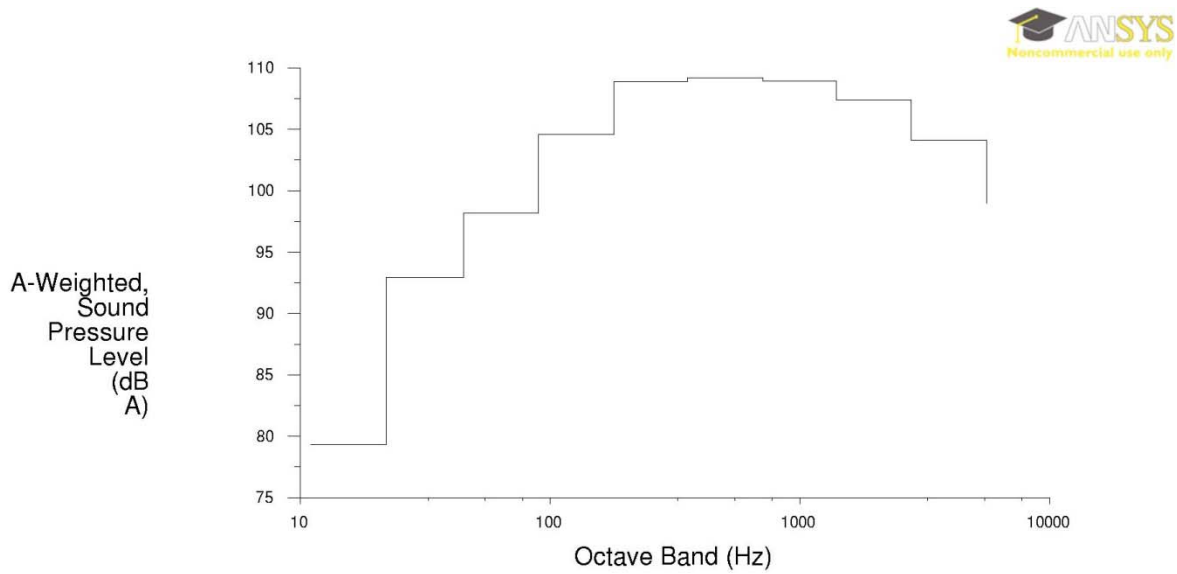

Figure D-13: A-weighted sound pressure level at receiver 4 with acoustic treatment.

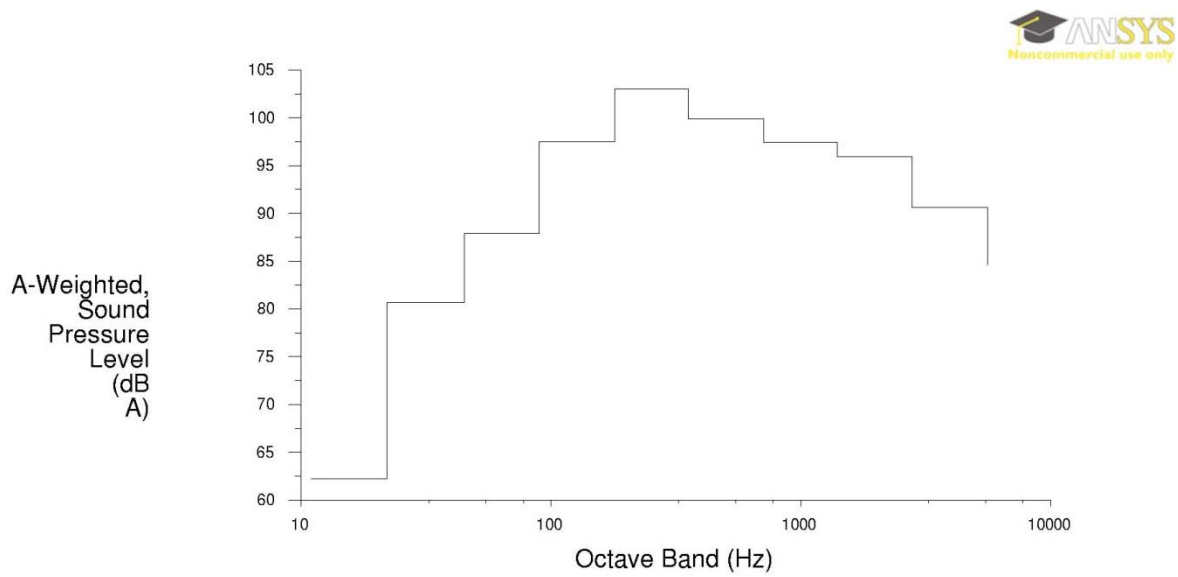

Figure D-14: A-weighted sound pressure level at receiver 5 with acoustic treatment.

List of References

1. **Cox, Trevor J, and D'Antonio, Peter.** *Acoustic Absorbers and Diffusers. Theory, design and application.* 2. Abingdon, Oxon : Taylor & Francis, 2009. pp. 156-160. 0415471745.

2. **Britannica Encyclopedia.** Acoustic impedance (physics). [Online] [Cited: January 22, 2012.] http://www.britannica.com/EBchecked/topic/4005/acoustic-impedance.

3. **Anderson Jr., John D.** *Fundamentals of Aerodynamics.* s.l. : McGraw Hill, 2007. 0071254080.

4. **NDT Resource Center.** Reflection and Transmission. [Online] [Cited: January 22, 2012.] http://www.ndt-ed.org/EducationResources/CommunityCollege/Ultrasonics/Physics/reflectiontransmission.htm.

5. **Simon Fraser University.** Acoustic Impedance. [Online] [Cited: January 22, 2012.] http://www.sfu.ca/sonic-studio/handbook/Acoustic_Impedance.html.

6. **National Aeronautics and Space Administration.** History of Wind Tunnels. [Online] April 1, 2010. [Cited: January 12, 2011.] http://awt.grc.nasa.gov/students_TunnelHistory.aspx.

7. —. Blowdown Wind Tunnel. [Online] May 07, 2009. [Cited: January 11, 2011.] http://www.grc.nasa.gov/WWW/K-12/airplane/tunblow.html.

8. *Fluctuating Distrubances in a mach 5 Wind Tunnel.* **Anders, J.B., et al.** 8, 1977, AIAA Journal, Vol. 15, pp. 1123-1129.

9. *The development of Hypersonic Quiet Tunnels.* **Schneider, Steven P.** 2007, AIAA Fluid Dynamics Conference and Exhibit.

10. *New Technique for Reducing Test Section Noise in Supersonic Wind Tunnels.* **Anders, J. B., Stainback, P. C. and Beckwith, I. E.** 1, 1980, AIAA Journal, Vol. 18, pp. 5-6.

11. Supersonic Flow Characteristics. [Online] 2008. [Cited: September 15, 2010.] www.aerospace.utoronto.ca/pdf_files/supersonic.pdf.

12. **Matsumoto, Joji.** Design and testing of a subscale supersonic aeropropulsion wind tunnel. [Online] May 2000. [Cited: January 9, 2011.] arc.uta.edu/publications/td_files/matsumoto-joji.pdf.

13. *Acoustic Evaluation of the Helmholtz Resonator Treatment in the NASA Lewis 8 by 6 foot Supersonic Wind Tunnel.* **Heidelberg, Laurence J. and Gordon, Elliot B.**

14. *Supersonic and Hypersonic Quiet Tunnel Technology.* **Wilkinson, S.P., Anders, S.G. and Chen, F. J.** 1992, AIAA Journal.

15. *Acoustical Properties of materials and Muffler Configurations for the 80x120 Foot Wind Tunnel.* **Scharton, Terry D. and Sneddon, Matthew D.** 1977, NASA Contract Report.

16. *Active Control of a Mach 0.9 Jet for Noise Mitigation Using Plasma Actuators.* **Samimy, M., et al.** 4, April 2007, AIAA, Vol. 45.

17. *An Investigation of Noise Reduction in a Mach 1.3 Round Jet using Tangential Blowing.* **Luff, Darren S., Ahmad, Arsalan and Cater, John E.** Vancouver : s.n., 2008. 14th AIAA/CEAS Aeroacoustics Conference.

18. *Potential Uses of Vacuum Bubbles in Noise and Vibration Control.* **Ver, Istvan L.** 181829, Cambridge : NASA Contractor Report, 1989.

19. *A two-dimensional computational study of the flow effect on the acoustic behaviour of Helmholtz resonators.* **Iqbal, Asim and Selamet, Ahmet.** 2/3/4, 2010, International Journal Vehicle Noise and Vibration, Vol. 6.

20. *A computational and experimental study of slit resonators.* **Tam, C. K. W., et al.** 2005, Journal of Sound and Vibration, Vol. 284, pp. 947-984.

21. *Improvement of Performance of a Perforated Tube as a Noise Suppressor by Oblique Perforation.* **Khan, Tawhidul Islam, Seto, Kunisato and Xu, Zhixiang.** 3, 2004, JSME International Journal, Vol. 47, pp. 605-611.

22. *On the Mechanism of Choked Jet Noise.* **Powell, A.** 12, 1953, Proceedings of the Physical Society. Section B, Vol. 66.

23. *Computing Jet Screech - A Complex Aeroacoustic Feedback System.* **Loh, Ching Y. and Hultgren, Lennart S.** 2002-211807, August 2002, NASA.

24. *Supersonic Jet Screech Tone Cancellation.* **Nagel, Robert T., Denham, James W. and Papathanasiou, Athanasios G.** 11, November 1983, AIAA, Vol. 21, pp. 1541-1545.

25. *Evolution from 'Tabs' to 'Chevron Technology' - a Review.* **Zaman, K. B. M. Q., Bridges, J. E. and Huff, D. L.** Dhaka, Bangladesh : s.n., December 17-21, 2010, Proceedings of the 13th Asian Congress of Fluid Mechanics.

26. **Fluent Inc.** Lighthill's Acoustic Analogy. [Online] January 24, 2003. [Cited: January 12, 2011.] http://jullio.pe.kr/fluent6.1/help/html/acoustics/node4.htm.

27. **Ansys Fluent.** Predicting Aerodynamically Generated Noise. [Online] September 20, 2006. [Cited: January 3, 2011.] http://my.fit.edu/itresources/manuals/fluent6.3/help/html/ug/node788.htm.

28. *Review of Discretization Error Estimators in Scientific Computing.* **Roy, Christopher J.** s.l. : American Institute of Aeronautics and Astronautics, 2010. 48th AIAA Aerospace Sciences Meeting Including the New Horizons Forum and Aerospace Exposition. AIAA 2010-126-375.

29. *Numerical Simulation of Sidewall Effects on the Acoustic Field in Transonic Cavity.* **Li, Zhisong and Hamed, Awatef.** Cincinnati : American Institute of Aeronautics and Astronautics, 2007, Vols. 2007-1456.

30. *A Computational and Experimental Study of Resonators in Three Dimensions.* **Tam, C.K.W. and Ju, H.** 24, November 22, 2010, Journal of Sound and Vibration, Vol. 329, pp. 5164-5193.

31. *Experiments on the Influence of Flow on Sound Attenuation in Absorbing Ducts.* **Meyer, Erwin, Mechel, Fridolin and Kurtze, Gunther.** 3, March 1958, The Journal of the Acoustical Society of America, Vol. 30.

32. *The Permeability of Fibrous Porous Media.* **Jackson, G. W. and James, D. F.** 3, June 1986, Canadian Journal of Chemical Engineering, Vol. 64, pp. 364-374.

33. **Ansys Fluent.** User Inputs for Porous Media. *Fluent 6.3 User's Guide.* [Online] September 20, 2006. [Cited: June 12, 2011.] https://www.sharcnet.ca/Software/Fluent6/html/ug/node276.htm.

34. Sound Power, Sound Pressure, and Octave Bands Explained. [Online] 2004. [Cited: January 5, 2012.] http://www.docs.hvacpartners.com/idc/groups/public/documents/marketing/gud-04-002.pdf.

35. **Beranek, Leo.** *Noise and Vibration Control.* s.l. : McGraw Hill Inc., 1971. pp. 538-539. 07-004841-X.

36. **Feldman.** Richardson Extrapolation. *University of British Columbia Mathematics Department.* [Online] http://www.math.ubc.ca/~feldman/m256/richard.pdf.

37. **White, Frank M.** *Fluid Mechanics.* s.l. : McGraw Hill, 2006. 0073309206.